Dielectric Non-Linearities of P(VDF-TrFE) Single and Multilayers for Memory Applications

A thesis submitted for the degree of
Dr.-Ing.

Presented by
Danny von Nordheim, M.Sc.

Presented to the
Faculty of Science
Institute of Physics and Astronomy
University of Potsdam

Supervised by
Prof. Dr. Reimund Gerhard
University of Potsdam
and
Prof. Dr. Bernd Ploss
EAH Jena, University of Applied Sciences

"If I have seen further it is by standing on ye sholders of Giants"
Sir Isaac Newton

Potsdam, 12 November 2018

Published online at the
Institutional Repository of the University of Potsdam:
URN urn:nbn:de:kobv:517-opus4-421778
https://nbn-resolving.org/urn:nbn:de:kobv:517-opus4-421778

Abstract Poly(vinylidene fluoride-trifluoroethylene) (P(VDF-TrFE)) ferroelectric thin films of different molar ratio have been studied with regard to data memory applications. Therefore, films with thicknesses of 200 nm and less have been spin coated from solution. Observations gained from single layers have been extended to multilayer capacitors and three terminal transistor devices.

Besides conventional hysteresis measurements, the measurement of dielectric non-linearities has been used as a main tool of characterisation. Being a very sensitive and non-destructive method, non-linearity measurements are well suited for polarisation readout and property studies. Samples have been excited using a high quality, single-frequency sinusoidal voltage with an amplitude significantly smaller than the coercive field of the samples. The response was then measured at the excitation frequency and its higher harmonics. Using the measurement results, the linear and non-linear dielectric permittivities ε_1, ε_2 and ε_3 have been determined. The permittivities have been used to derive the temperature-dependent polarisation behaviour as well as the polarisation state and the order of the phase transitions.

The coercive field in VDF-TrFE copolymers is high if compared to their ceramic competitors. Therefore, the film thickness had to be reduced significantly. Considering a switching voltage of 5 V and a coercive field of 50 MV/m, the film thickness has to be 100 nm and below. If the thickness becomes substantially smaller than the other dimensions, surface and interface layer effects become more pronounced. For thicker films of P(VDF-TrFE) with a molar fraction of 56/44 a second-order phase transition without a thermal hysteresis for an $\varepsilon_1(T)$ temperature cycle has been predicted and observed. This however, could not be confirmed by the measurements of thinner films. A shift of transition temperatures as well as a temperature independent, non-switchable polarisation and a thermal hysteresis for P(VDF-TrFE) 56/44 have been observed. The impact of static electric fields on the polarisation and the phase transition has therefore been studied and simulated, showing that all aforementioned phenomena including a linear temperature dependence of the polarisation might originate from intrinsic electric fields.

In further experiments the knowledge gained from single layer capacitors has been extended to bilayer copolymer thin films of different molar composition. Bilayers have been deposited by succeeding cycles of spin coating from solution. Single layers and their bilayer combination have been studied individually in order to prove the layers stability. The individual layers have been found to be physically stable. But while the bilayers reproduced the main $\varepsilon_1(T)$ properties of the single layers qualitatively, quantitative numbers could not be explained by a simple serial connection of capacitors. Furthermore, a linear behaviour of the polarisation throughout the measured temperature range has been observed. This was found to match the behaviour

predicted considering a constant electric field.

Retention time is an important quantity for memory applications. Hence, the retention behaviour of VDF-TrFE copolymer thin films has been determined using dielectric non-linearities. The polarisation loss in P(VDF-TrFE) poled samples has been found to be less than 20 % if recorded over several days. The loss increases significantly if the samples have been poled with lower amplitudes, causing an unsaturated polarisation. The main loss was attributed to injected charges. Additionally, measurements of dielectric non-linearities have been proven to be a sensitive and non-destructive tool to measure the retention behaviour.

Finally, a ferroelectric field effect transistor using mainly organic materials (FerrO-FET) has been successfully studied. DiNaphtho[2,3-b:2',3'-f]Thieno[3,2-b]Thiophene (DNTT) has proven to be a stable, suitable organic semiconductor to built up ferroelectric memory devices. Furthermore, an oxidised aluminium bottom electrode and additional dielectric layers, i.e. parylene C, have proven to reduce the leakage current and therefore enhance the performance significantly.

Zusammenfassung Ferroelektrika eignen sich generell gut zur Realisierung von Datenspeichern, da einige dieser Materialien bei Raumtemperatur und darüber hinaus eine spontane Polarisation besitzen. Diese lässt sich durch Anlegen einer ausreichend großen Spannung definiert schalten. Die unterschiedlichen Zustände der Polarisation können dann ausgelesen und verschiedenen Speicherzuständen, insbesondere *0* und *1*, zugeordnet werden. Da der Polarisationszustand auch nach Abschaltung der zur Polarisation verwendeten Spannung erhalten bleibt, bezeichnet man diese Speicher als nicht flüchtig, ähnlich wie herkömmliche Flash-Speicher (z.B. USB-Sticks). Bisher wurden vor allem ferroelektrische Speicher aus keramischen Materialien untersucht und implementiert. Ferroelektrische Speicher aus Polymeren bieten u.U. eine größere Freiheit bei der Formgebung. Weiterhin können Polymere einfacher verarbeitet werden.

In der vorliegenden Arbeit wurden dünne Schichten des ferroelektrischen Copolymers VDF-TrFE mit verschiedenen Zusammensetzungen, 56/44 und 70/30 bezogen auf das molare Verhältnis von VDF und TrFE, hinsichtlich ihrer Eigenschaften für die Verwendung in Datenspeichern untersucht. Da die zum Schalten zwischen den Polarisationszuständen benötigte Feldstärke bei den verwendeten Copolymeren sehr hoch ist, musste die Schichtdicke reduziert werden. Auf diese Art und Weise war es möglich, auch mit kleinen, computer-typischen Arbeitsspannungen wie bspw. 5 Volt den Polarisationszustand bzw. Speicherzustand zu ändern. Dazu wurden Schichten mit einer Dicke von 200 Nanometern und weniger durch Aufschleudern einer Lösung (Polymer-Granulat in Lösungsmittel) abgeschieden. Nach der Charakterisierung von Einzelschichten wurden die Untersuchungen auf Doppelschichten und organische Feldeffekttransistoren ausgeweitet.

Aus vorherigen Untersuchungen an dünnen VDF-TrFE Copolymer-Schichten mit einer Dicke von einigen Mikrometern war bereits bekannt, dass die Messung der Nichtlinearitäten ein nützliches Werkzeug zur Charakterisierung dieser Schichten ist. Besonders der bereits erwähnte Schaltzustand lässt sich gut auslesen. Weiterhin können auch das temperatur- und das zeitabhängige Verhalten der Polarisation bestimmt werden. Ersteres ist besonders für den Temperaturbereich ausschlaggebend, in welchem die Speicher eingesetzt werden. Ab einer gewissen Temperatur, der sogenannten Phasenübergangstemperatur, verlieren die Materialien ihre Polarisation und damit jegliche gespeicherte Information. Der zeitliche Verlauf der Polarisation ist für das sogenannte Retentionsverhalten eines nichtflüchtigen Speichers von Bedeutung. Es definiert, wie lange eine gespeicherte Information fehlerfrei erhalten bleibt bzw. ausgelesen werden kann.

Bei der Auswertung der Ergebnisse zeigt sich, dass die hergestellten Schichten selbst bei einer Dicke von 30 Nanometern und weniger eine schaltbare Polarisation

aufwiesen. Es konnte auch beobachtet werden, dass einige Charakteristika, wie z.B. der absolute Wert der Polarisation, die Phasenübergangstemperaturen sowie das Verhalten in der Nähe des Phasenübergangs von denen dickerer Schichten abwichen. Die Polarisation blieb, abhängig von der Zusammensetzung, bis ca. 60 °C bzw. 80 °C stabil. In Bezug auf das Retentionsverhalten der dünnen Schichten konnte festgestellt werden, dass die Polarisation nach einem anfänglichen Verlust auch über mehrere Tage stabil blieb.

Weiterhin wurden Doppelschichten untersucht. Hierzu wurden zwei Schichten unterschiedlicher molarer Zusammensetzung aufeinander abgeschieden. Unter, zwischen und auf den Schichten wurden jeweils Elektroden abgeschieden. Diese wurden so platziert, dass sowohl die Schichten einzeln als auch das Schichtsystem gemessen werden konnten. Bei der Messung der Schichtsysteme und ihrer individuellen Schichten wurde festgestellt, dass Letztere das in vorherigen Messungen an Einzelschichten beobachtete Verhalten aufwiesen. Bei den Schichtsystemen hingegen wurde eine lineare Abhängigkeit der Polarisation von der Temperatur beobachtet.

Abschließend wurden ferroelektrische organische Transistoren (FerrOFET) untersucht. Dabei erwies sich der organische Halbleiter DNTT als geeignetes Material für den leitfähigen Kanal. Weiterhin zeigte sich, dass sich mithilfe von zusätzlich oxidierten Aluminium-Grundelektroden sowie zusätzlichen Schichten von Parylene C die Funktionsfähigkeit der Bauelemente verbessern ließ.

Table of Contents

List of Abbreviations and Symbols

α, γ, δ	Landau parameters
ε_x	Dielectric permittivity of order x
σ	Conductivity
μ_m	Dipole moment of a monomer
ω_0	fundamental frequency ($2\pi f$)
AFM	Atomic Force Microscopy
D	Dielectric displacement
DEC	Diethyl carbonate
DNTT	DiNaphtho[2,3-b:2',3'-f]Thieno[3,2-b]Thiophene
d, L	Film thickness
E	Electric field
E_C	Coercive field
f	Free energy density
F	Free energy
G	Gibbs free energy
$J(t), J_\mathrm{M}(t), j$	Current density
J	Energy difference between (all-)trans and (trans-)gauche bondings
k	Boltzmann constant
mol%	Molar percentage
$\mathrm{N_m}$	Number of monomers per volume
P	Polarisation
$\hat{P}$	Normalised polarisation
P_R	Remanent polarisation
P_S	Spontaneous polarisation
PDMS	Polydimethylsiloxane
PVDF	Polyvinylidene Fluoride
P(VDF-TrFE)	Poly(Vinylidene Fluoride-Trifluoroethylene)
t	Time
T	Temperature
T_0	Transition temperature
T_C	Curie temperature

TGS	Triglycinsulfat
U_{E}	Excitation voltage
$\widehat{U}_{\mathrm{E}}$	Excitation voltage's amplitude
U_{M}	Output voltage
$\widehat{U}_{\mathrm{M}}$	Output voltage's amplitude
V	Volume
wt%	Weight percentage
zA	Interchain interaction energy
Z	Impedance

List of Figures

1 Introduction

The first publication on ferroelectricity is almost a hundred years old. In 1920/21 Valasek published his results revealing a dielectric anomaly in Rochelle salt [1, 77]. He instinctively linked the problem with the observations in ferromagnetic materials, which later lead to the term ferroelectricity. More than four decades and a vast number of publications later, in the 1960s, Kocharyan was the first who published his findings on piezoelectricity in polymers [36]. Another decade later, in 1971 [4], PVDF was the first polymer proven to be pyroelectric. Since that time an unclear number of publications [17, 18] and books [30, 32, 45, 53, 81] has been published on this topic.

Due to their strong ceramic competitors, ferroelectric polymers have tended to be sidelined. But modern problems demand tailor made solutions. Even materials which where presumed dead have attracted attention in the current research on multiferroics, e.g. KDP (Kaliumdihydrogenphosphat). Fluoropolymers can be deposited easily from a solution using substrates of various shapes. Spin coated thin films are transparent, lead-free and chemically stable. Although their figures of merit cannot compete with ceramics, e.g. PZT (lead zirconate titanate), they still win if the aforementioned advantages rather than figures are important.

This work focuses on thin films of the ferroelectric copolymer VDF-TrFE, in particular with regard to memory applications. Single layers, multilayers and transistors, as a special case of multilayers, containing at least one layer of the ferroelectric copolymer have been deposited and characterised using various techniques, i.e. dielectric non-linearities. Those techniques have been used to study two types of devices as potential parts of a working ferroelectric memory. The first device, a simple capacitor, aims at the traditional 1T1C technology. The two possible states

of polarisation, up and down, have been used to define the two states of a memory cell, which are 0 and 1. The second ferroelectric device, a so called FerrOFET, uses the remanent polarisation to permanently open or close the source-drain channel. This enables a simple record of the source-drain current to define the cells state and link it to either 0 or 1.

Dielectric non-linearities are in general a powerful tool to study properties and behaviour of ferroelectric materials [20]. Their main benefit is that the physical quantity under examination, e.g. the remanent polarisation, will not be altered by the measurement. Besides its state-preserving character it is highly sensitive at the same time. Combining both benefits, we are able to measure the remanent polarisation of a ferroelectric material without the additional writing cycle, usually necessary in common memories. Furthermore, we have the possibility to measure even small polarisation values, i.e. in ferroelectric polymers.

A material used for information memory applications has to meet certain requirements. Switching time, fatigue behaviour, temperature stability and retention are some of the key words. The first two points have been extensively discussed elsewhere, e.g. in [83, 21]. The use of non-linearities in this work focuses on transitional behaviour, polarisation state and retention time. The first property is basically of theoretical interest, but could have a significant impact on potential applications as well. The other two are of particular interest for memory applications.

Transitional behaviour might change if the film thickness is reduced below a certain threshold value. The latter depends on the materials in use, deposition techniques and conditions as well as on the general dimensions of the film. Additionally, surfaces and interfaces gain importance if the film thickness is reduced to sizes interesting for memory applications. It is therefore appropriate to extend the considerations by depolarisation effects and an intrinsic variation of the polarisation P [57, 3, 74]. The latter has been discussed in the aforementioned references for both, first-order and second-order transition materials. Depolarisation fields have been studied extensively by Kretschmer and Binder [37]. The theory has been extended to a microscopic level, namely a microscopic mean field theory approach (Ising model in a transverse field - IMTF) by Cottam and co-workers [9] later.

An extra section has been attributed to multilayers of VDF-TrFE copolymer thin films. Experience gained with single layers has therefore been transferred to the multilayered structures. Besides theoretical considerations, actual bilayers and transistors have been deposited and studied. They contain at least one layer of material exhibiting ferroelectric properties. The discussion of the results is based on the knowledge on single layer properties.

Another ferroelectric multilayer device widely studied [2, 40, 51, 78, 79, 84] is the ferroelectric-(organic) field-effect transistor. In contrast to their ceramic competitors, devices completely made of organic materials can be fabricated with less effort. Furthermore, they can be used in combination with flexible, light weight substrates. Basic research has been done in the frame of this work in order to develop such a transistor for memory applications. Therefore, the ferroelectric copolymer VDF-TrFE and the organic semiconductor dinaphtho[2,3-b:2',3'-f]thieno[3,2-b]thiophene (DNTT) have been used as a gate dielectric and channel material, respectively. The devices deposited have been studied with regard to ferroelectric and transistor-related characteristics, i.e. their leakage behaviour and the influence of the properties of the dielectric-semiconductors interface on the mobility of charge carriers in the source-drain channel.

2 Theory and Basic Concepts

2.1 General Theory

As emphasised by Valasek [1] in the early 20s of the past century, the behaviour of ferroelectric materials under investigation is quite similar to those of ferromagnetic nature. While keeping in mind, that the origin of either differs significantly, the similarities in the experimentally observed properties led to the identical prefix *ferro*.

Ferroelectricity is always accompanied by an inherent asymmetry originating from small structural changes or disturbances resulting in a minimum of two orientational polarisation states. The existence and the amplitude of the disturbances strongly depends on temperature. Therefore, the ferroelectric phase is considered being a deviation from the highest symmetric prototype phase, sometimes also referred to as high-temperature phase or non-polar phase. The temperature marking the transition between the ferroelectric and the prototype phase can be of clear observable and singular nature, i.e. for a second-order phase transition, or can be covered by processes involving latent heat, i.e. for first-order phase transitions. The point of transition can be shifted or blurred depending on the materials structure, structural changes and occurring forces, i.e. stress, strain and electric fields. These influencing factors become increasingly important if the film thickness is reduced. In order to understand the origin of deviations in ferroelectric thin films, it is important to study and understand the origin and the impact of each single factor in consideration of all the others appearing at the same time.

2.2 Phenomenological Approach

The most general and common approach to introduce and study the ferroelectrics macroscopically is a thermodynamic function. The function of choice is an expression of the free energy, usually Gibbs free energy (e.g. [7])

$$G = U - TS - X_i x_i \,. \tag{2.1}$$

Starting with the first law of thermodynamics

$$\mathrm{d}U = \mathrm{d}Q + \mathrm{d}W \tag{2.2}$$

$\mathrm{d}Q$ can be substituted by $T\mathrm{d}S$ (second law of thermodynamics) and $\mathrm{d}W$ can be replaced by $X_i\mathrm{d}x_i + E_i\mathrm{d}D_i$. Therefore, the first law of thermodynamics can be rewritten as

$$\mathrm{d}U = T\mathrm{d}S + X_i\mathrm{d}x_i + E_i\mathrm{d}D_i \tag{2.3}$$

from which the dielectric equation of state can be derived

$$E = \left(\frac{\delta U}{\delta D_i}\right)_{S,x} . \tag{2.4}$$

Through the eight possible combinations of the three independent variables (T, S), (X_i, x_i) and (E_i, D_i) with U, Gibbs free energy can be derived as

$$G = U - TS - X_i x_i \tag{2.5}$$

or its differential form as

$$\mathrm{d}G = E_i\mathrm{d}D_i + S\mathrm{d}T - X_i\mathrm{d}x_i \,. \tag{2.6}$$

As pointed out in [45], the most simple approach is to assume that D_i or P_i have a single component oriented along the crystallographic axis. Furthermore, as indexed in the dielectric equation of state, all stresses are zero and the high-temperature

phase is centro-symmetric. Following these restrictions the free energy can be expressed as

$$G = \frac{\alpha}{2}D^2 + \frac{\gamma}{4}D^4 + \frac{\delta}{6}D^6 - ED \tag{2.7}$$

or in the form using the Curie constant and the Curie temperature

$$G = \frac{T - T_\mathrm{C}}{2C}D^2 + \frac{\gamma}{4}D^4 + \frac{\delta}{6}D^6 - ED \tag{2.8}$$

where C is the Curie constant, T_C is the Curie temperature of the material and $D = D(T, E)$ is the dielectric displacement. Usually, the first term $(T - T_\mathrm{C})/2C$ is replaced by $\alpha/2$ or $\beta(T - T_\mathrm{C})/2$ where $\beta = 1/C$. Due to the choice of symbols made in earlier publications, the author will refer to the free energy as F throughout the remaining part of this work. The polynomial representing the free energy can therefore be written as

$$F = \frac{\alpha}{2}D^2 + \frac{\gamma}{4}D^4 + \frac{\delta}{6}D^6 - ED. \tag{2.9}$$

2.2.1 Second-order Phase Transition

Suppose the case γ and δ are positive constants and α depends on the temperature in a linear fashion, i.e. $\alpha = \beta(T - T_0)$, the phase transition is of second order. F as a function of D is plotted in Fig. 2.1 for different values of α.

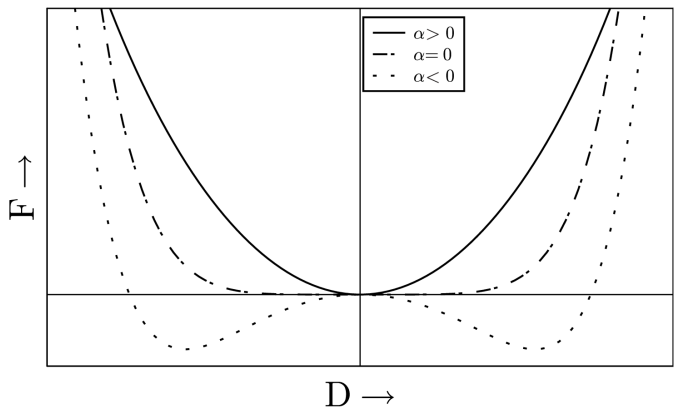

Figure 2.1: Second-order phase transition.

For temperatures above T_C ($\alpha > 0$) the graph has a global minimum at D equal to zero, indicating the paraelectric or high temperature phase. If α is a negative number however, two local minima with non-zero D-values can be observed. Those two values represent the minimum two stable states indicating ferroelectrics. An electric field, large enough to overcome the intrinsic coercive field enables switching between the minimum two states. The field necessary for the polarisation reversal is called coercive field E_C.

Another important quantity for ferroelectrics is the spontaneous polarisation, not to be confused with the remanent polarisation. While the latter is always the result of a measurement, the spontaneous polarisation is of purely theoretical nature. It can be calculated by multiplying the number of dipoles per volume unit with the average dipole moment. The temperature dependence of the spontaneous polarisation can be expressed using the derivative of equation (2.9) which is

$$\left.\frac{\partial F}{\partial D}\right|_{E=0} = \beta(T - T_C)D + \gamma D^3 + \delta D^5 = 0. \tag{2.10}$$

with $D = P_S$. Excluding the trivial solution $P_S = 0$ and neglecting the D^5-term for simplicity, the spontaneous polarisation is

$$P_S^2 = -\frac{\alpha}{\gamma}\,. \tag{2.11}$$

Having a non-zero electric field however, leads to a different behaviour for polarisation versus temperature, as will be shown in the chapter 4.

2.2.2 First-order Phase Transition

Using a negative second Landau parameter γ helps predicting the behaviour which can be observed in most ferroelectrics. If again α linearly depends on the temperature, the free energy F and its derivative are represented by equation (2.12) and equation (2.13).

$$F(D) = \frac{\beta}{2}(T - T_C)D^2 + \frac{1}{4}\gamma D^4 + \frac{1}{6}\delta D^6 - ED. \tag{2.12}$$

$$\left.\frac{\partial F}{\partial D}\right|_{E=0} = \beta(T - T_C)D + \gamma D^3 + \delta D^5. \tag{2.13}$$

A transition between the two states may take place if configurations become thermodynamically equivalent. Figure 2.2 shows F versus D for different values of α. For positive values of α the parabolic shape of the curve becomes more pronounced with positive α and δ dominating the equation.

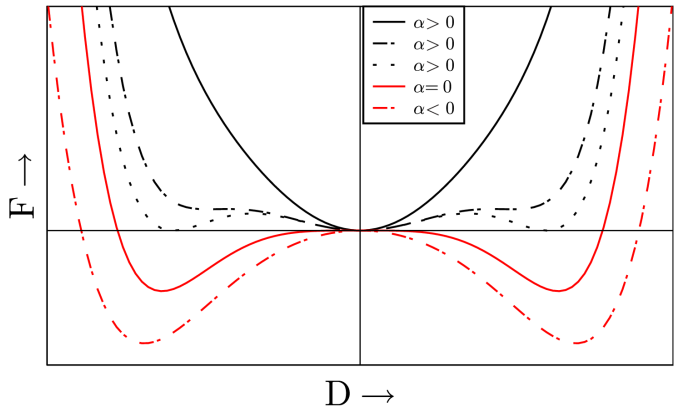

Figure 2.2: First-order phase transition.

The minima can be determined by the derivative of F becoming zero. Therefore, one gets

$$0 = \beta(T - T_0)D + \gamma D^3 + \delta D^5. \tag{2.14}$$

Eliminating the trivial solution $D \neq 0$, the polynomial can be reduced by one order to

$$0 = \beta(T - T_0) + \gamma D^2 + \delta D^4. \tag{2.15}$$

The Curie temperature T_C is defined as the temperature at which F is equal for the polar and the non-polar state, that is $T = T_C$. A solution which satisfies both, equation (2.12) and equation (2.15) is

$$D^2 = -\frac{3}{4}\frac{\gamma}{\delta}. \tag{2.16}$$

For $E = 0$ the dielectric displacement D can be replaced by the spontaneous polarisation

$$P_S^2 = -\frac{3}{4}\frac{\gamma}{\delta}. \tag{2.17}$$

As can be seen in Fig. 2.2, polar and non-polar states become equally favoured if F an its derivative $\partial F/\partial D$ are equally 0 at the same time. A solution meeting this criteria is

$$T = T_C = T_0 + \frac{3}{16}\frac{\gamma^2}{\beta\,\gamma}. \tag{2.18}$$

Equation (2.17) and equation (2.18) display that D changes discontinuously, having a non-zero value at the transition temperature. Furthermore, values for T_C and T_0 are different. Below T_0 only two stable states with a non-zero polarisation exist. For temperatures $T_0 < T < T_C$ the low-temperature phase is still considered a stable state, but a third minimum representing the high-temperature phase arises and exists as a metastable state. If the temperature approaches T_C, the high-temperature phase becomes the thermodynamically favourable and stable phase. At this point, the ferroelectric phase coexists as a metastable state. As a result, the material will have a finite polarisation if it is heated up from a temperature below T_C, whereas it will have a polarisation equal to zero if it is cooled down from a temperature above T_C. This phenomenon is called a thermal hysteresis.

2.2.3 Switching

By definition, a ferroelectric material has minimum two states of polarisation. Switching between those states occurs if an electric field of sufficient value is applied, i.e. $E > E_C$. The impact of the applied electric field is represented by the linear part ED of equation (2.9). The latter adds a linear function with the slope E to the graph representing the ferroelectric phase, e.g. in Fig. 2.1. Figure 2.3 displays the result, with $E_0 = 0$ for zero applied field and E_1 and E_2 representing non-zero electric fields. It can be seen that one of the minima is vanishing in favour of the other

if an electric field of sufficient strength is applied. Therefore, one polarisation state will be preferred. An opposing electric field of sufficient strength will lead to a switch of the polarisation state.

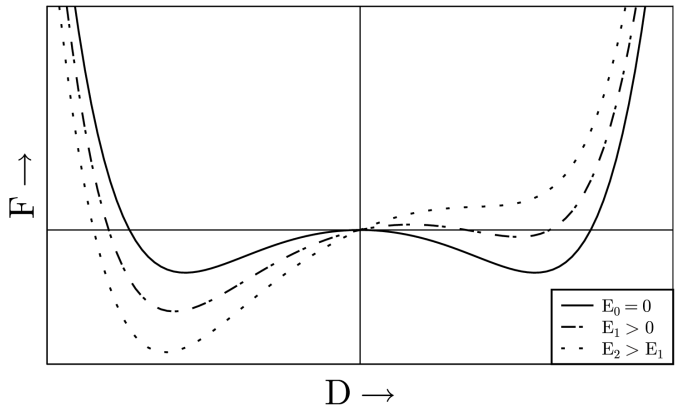

Figure 2.3: Impact of different electric fields on a second-order phase transition.

2.3 Microscopic Approach and Statistical Mechanics

Another way to address a problem in solid state physics is the microscopic approach. Extending this approach to a number of (atomic/molecular) units using the laws of statistical mechanics, creates the link to the phenomenological theory described in the preceding section. In polymer physics it is reasonable to start with a single polymer chain and then extend the considerations to a number of neighbouring chains and study their interaction. These considerations have been made by Odajima and co-workers in [55].

Following the derivation deduced in [55], one can obtain the spontaneous polarisation versus the temperature as

$$P = \frac{N_0 \, \mu \, e^{J/kT} \sinh(F/kT)}{\sqrt{1 + e^{2J/kT} \sinh^2(F/kT)}} \tag{2.19}$$

with

$$F = \frac{Az(N_+ - N_-)}{2N} + \mu E \quad \text{or} \quad F = \frac{AzP}{2\mu N_0} + \mu E, \tag{2.20}$$

furthermore considering

$$P = \mu\nu(2N_+ - N), \quad N = N_+ + N_- \quad and \quad N_0 = \nu \cdot N. \tag{2.21}$$

Inserting equation (2.20) in equation (2.19) one gets

$$P = \frac{N_0\,\mu\,e^{J/kT}\sinh\left(\dfrac{AzP}{2\mu N_0 kT} + \dfrac{\mu E}{kT}\right)}{\sqrt{1 + e^{2J/kT}\sinh^2\left(\dfrac{AzP}{2\mu N_0 kT} + \dfrac{\mu E}{kT}\right)}}\,. \tag{2.22}$$

With the normalised polarisation being

$$\hat{P} = \frac{P}{\mu N_0} \tag{2.23}$$

equation (2.22) can be rearranged as

$$E = \frac{kT}{\mu}\,\mathrm{arcsinh}\left(\frac{\hat{P}}{\sqrt{1-\hat{P}^2}}e^{-J/kT}\right) - \frac{zA}{2\mu}\hat{P}\,. \tag{2.24}$$

For small polarisation values, e.g. close to the ferroelectric transition, the arcsinh can be described using a Taylor series expansion at $P = 0$

$$\mathrm{arcsinh}\left(\frac{\hat{P}}{\sqrt{1-\hat{P}^2}}e^{-J/kT}\right) \approx a\hat{P} - \frac{1}{6}(a(a^2-3))\hat{P}^3 + \frac{1}{40}a(3a^4 - 10a^2 + 15)\hat{P}^5 + ... \tag{2.25}$$

with

$$a = e^{-J/kT}\,. \tag{2.26}$$

As derived earlier

$$E = \alpha P + \gamma P^3 + \delta P^5\,. \tag{2.27}$$

By inserting the right-hand side of equation (2.25) into equation (2.24) and com-

paring the coefficients with equation (2.27) Landau's parameters can be derived as shown in [62]

$$\begin{aligned}\alpha &= \left(\frac{kT}{\mu}e^{-J/kT} - \frac{zA}{2\mu}\right)/N\mu \\ \gamma &= \frac{kT}{\mu}e^{-J/kT}\frac{1}{2}\left(1 - \frac{1}{3}e^{-2J/kT}\right)/(N\mu)^3 \\ \delta &= \frac{kT}{\mu}e^{-J/kT}\frac{3}{4}\left(\frac{1}{2} - \frac{1}{3}e^{-2J/kT} + \frac{1}{10}e^{-4J/kT}\right)/(N\mu)^5 .\end{aligned} \tag{2.28}$$

Following this approach, all parameters become temperature-dependent in a non-linear fashion. As has been shown in [62], it is more likely for Landau parameters of higher order to be a function of temperature as well. Further implications on the advantage of temperature-dependent parameters will be derived in section 4.4.2.

2.4 P(VDF-TrFE) Thin Films - Properties and Material

2.4.1 Depolarisation Effects in Ferroelectric Thin Films

Because of their dimensions, thin layers exhibit properties different from those of thick layers or bulk material. This difference can be mainly subjected to interface phenomena, which gain importance if the interface layer's thickness becomes relevant. Focusing on ferroelectric materials, it is has been suggested in [76] that the interface layers adjacent to the electrodes exhibit deviating polarisation values and transition temperatures if compared to the bulk material.

For multilayer structures built up with different ferroelectric materials exclusively, different layers will show different transition temperatures as well. Furthermore, a thin boundary layer attached to the electrodes is subjected to stress, originating from the deposition process as well as from different thermal expansion coefficients of the two adjacent materials. Postulating a continuous change in polarisation within the film, one is able to derive a polarisation profile as will be shown in section 2.4.2.

There exist different ansatzes and models to include and describe interface phe-

nomena and the resulting polarisation profile within the phenomenological theory. Most of them include an extension of the well known Landau-Devonshire and Landau-Ginzburg Theory, respectively. Tilley and Zeks introduced the extrapolation length to describe polarisation profiles and the impact of their shape on the transition behaviour. Levanyuk and Sannikov [41], however, managed to describe a multi-transition material (Rochelle salt) on a single basis using a smaller number of constants. The idea is to describe phases of lower symmetry as a distortion of a single, more symmetric phase.

Having a closer look on the interface phenomena one can discriminate between two major classes: mechanical and electronic phenomena. Both are always present in real films, but depending on the system under observation either of them is more or less pronounced. A mechanical impact changing film properties could be strain. Strain can be inbuilt from a substrate to thin film lattice parameter mismatch. Conducting measurements including a change in temperature will influence the strain, because of material-dependent thermal expansion coefficients.

Electronic conditions influencing or changing thin film properties can originate from the compensation charge distribution within the electrodes or adjacent materials, e.g. semiconductors in thin film ferroelectric field effect transistor devices. Apart from ideal conditions, where compensation charges are placed directly at the metal-ferroelectric interface, charges in a real electrode are distributed over a finite volume within the electrode. Such distributions combined with a lack of free charges, e.g. in an ideally insulating ferroelectric thin film, will cause strong depolarisation fields with an impact inverse proportional to the film thickness [10]. An incomplete compensation or screening of the depolarisation fields can be suppressed by the formations of domains of opposite polarisation. Examining the polarisation profile perpendicular to the electrode surface the shape can be assumed to be asymmetric. This is due to the sequence of deposition, deposition conditions and the materials used. The main compensation effects for a depolarisation field have been graphically summarised in Fig. 2.4 [58].

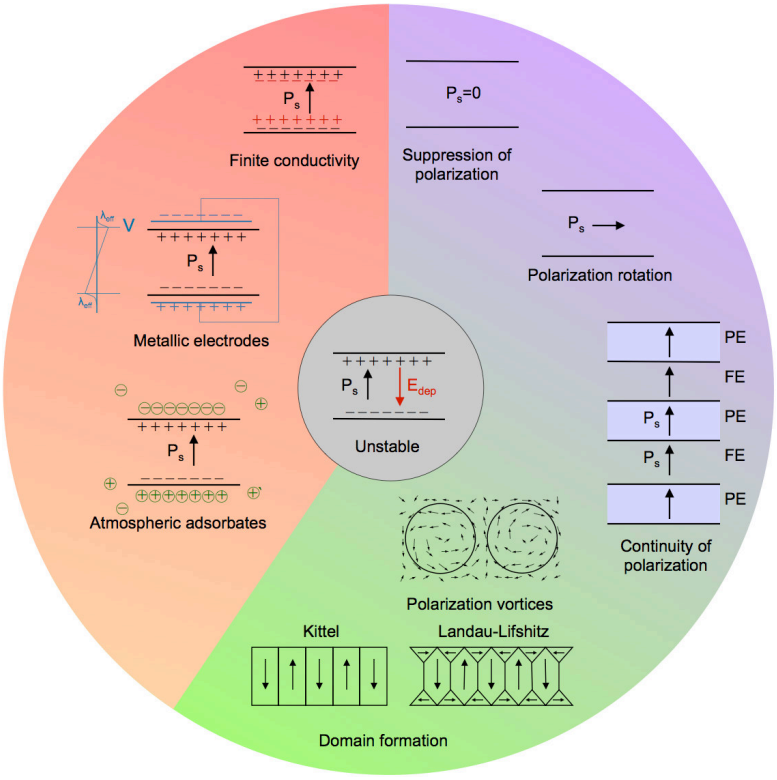

Figure 2.4: Effects of the depolarizing field in ferroelectric thin films. The left side of the diagram illustrates different mechanisms for screening of the surface bound charges, allowing the ferroelectric state to be uniformly maintained throughout the sample. If the screening is insufficient, the ferroelectric state can be preserved through the formation of domains or rotation of the polarization vector, as shown on the right side of the diagram. If all else fails, the polarization is suppressed [58].

2.4.2 Polarisation Profiles - The Tilley-Zeks Model

The principle of extrapolation length and its contribution to the transition behaviour are straightforward to derive [56]. In order to follow the publication and avoid confusion with the derivative, L will be used instead of d to indicate the thickness. Taking a thin ferroelectric layer of thickness L with its center at $L = 0$, the polarisation at the surface can attain three values. It can be either higher than, lower than or equal to the polarisation of the bulk. Hence, considering δ being the slope of the polarisation from the surface towards the bulk, it can be either positive, negative or infinite as depicted in Fig. 2.5.

The free energy of a thin film at thermodynamic equilibrium has been described

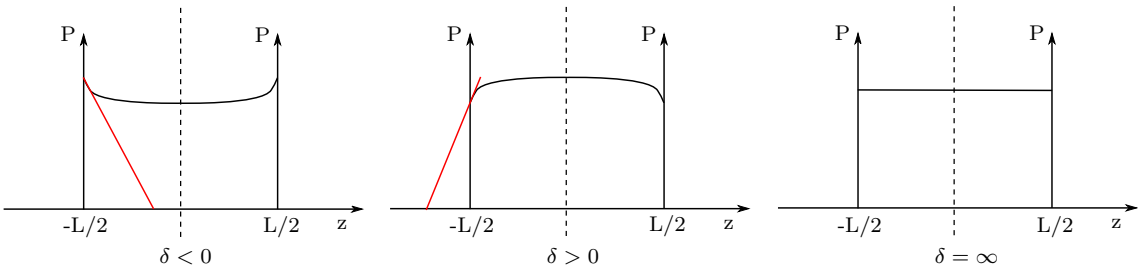

Figure 2.5: Principle of extrapolation length δ.

as [76]

$$F/A = \int_{-L/2}^{L/2} dz \left\{ \frac{1}{2}\alpha P^2 + \frac{1}{4}\gamma P^4 + \frac{1}{2}\kappa \left(\frac{dP}{dz}\right)^2 \right\} + \frac{1}{2}\kappa\delta^{-1}\left(P_-^2 + P_+^2\right) \tag{2.29}$$

where F/A is the free energy per surface area, $\alpha \lessgtr 0$ for $T \lessgtr T_\mathrm{C}$ and linearly temperature-dependent ($\alpha = \beta\left(T - T_\mathrm{C}\right), \beta > 0$ and constant), $\gamma < 0$ for a first-order phase transition and $\gamma > 0$ for a second-order phase transition, $\kappa > 0$ and constant. The surface polarisation $P(z)$ is given by $P(-L/2) = P_-$ and $P(L/2) = P_+$. In order to obtain the energy minima for a system with a non-homogeneous order parameter (dP/dz) preferred by the system, the Euler-Lagrange differential equation

$$\kappa\frac{\mathrm{d}^2P}{\mathrm{d}z^2} - \alpha P - \gamma P^3 = 0 \tag{2.30}$$

has to be introduced. If boundary conditions with δ as extrapolation length are considered

$$dP/dz \pm \delta^{-1}P = 0 \quad \text{at} \quad z = \pm L/2, \tag{2.31}$$

then

$$P = P_\mathrm{max} = P(L/2) = P(-L/2) \quad \text{if} \quad \delta < 0 \tag{2.32}$$

and

$$P = P_{\min} = P(L/2) = P(-L/2) \quad \text{if} \quad \delta > 0. \tag{2.33}$$

As derived in [76], there is a single phase transition temperature for $delta > 0$, indicating a second-order phase transition. Furthermore, a positive δ indicates a polarisation value declining towards the electrodes, which has been derived in the equations (2.33) above and which is displayed in Fig. 2.5. A negative value of δ however, is defined by a polarisation increasing towards the electrodes. A material showing this polarisation profile will exhibit two transition temperatures, typical for a first-order phase transition. Although in this case, the existence of a thermal hysteresis can not (solely) be attributed to latent heat originating from domain wall motion. It rather originates in the polarisation profile itself, with different layers of the film having different transition temperatures. This will be discussed later in section 4.4.

2.4.3 Dielectric Non-Linearities and Landau Parameters

For the following derivation the more general relation between the free energy F and the polarisation P being expressed in equation (2.9) has been used. Therefore, assuming a homogeneous distribution of the polarisation, as it is general the case in thick films, is necessary. The free energy as a function if the dielectric displacement D and the temperature T can be written as

$$F(D,T) = \frac{1}{2}\alpha D^2 + \frac{1}{4}\gamma D^4 + \frac{1}{6}\delta D^6 - ED\,, \tag{2.34}$$

with $\alpha = \beta(T - T_{\mathrm{C}})$. The relation between D and E can be found using the first derivative of F with respect to D which is

$$E = \frac{\partial F(D,T)}{\partial D} = \alpha\, D + \gamma\, D^3 + \delta\, D^5. \tag{2.35}$$

The same non-linear relation is, of course, also true for the inverse function D versus E, with $D = P_S$ at $E = 0$

$$D(E,T) = P_S + \varepsilon_0\varepsilon_1 E + \varepsilon_0\varepsilon_2 E^2 + \varepsilon_0\varepsilon_3 E^3. \tag{2.36}$$

Therefore, the higher order dielectric coefficients can be derived using the n-th partial derivative of $D(E,T)$ at $E = 0$

$$\varepsilon_0\varepsilon_n = \frac{1}{n!}\left(\frac{\partial^n D}{\partial E^n}\right)_{E=0}. \tag{2.37}$$

In order to relate permittivities with the Landau parameters, one can use the recursion formula

$$f_1(D) = \frac{\partial D}{\partial E} = 1/\frac{\partial E}{\partial D} = \frac{1}{\alpha + 3\gamma D^2 + 5\delta D^4} \tag{2.38}$$

or more general

$$f_n(D) = \frac{1}{n!}\frac{\partial^n D}{\partial E^n} = \frac{1}{n} f_1(D) \frac{\partial f_{n-1}}{\partial D} \tag{2.39}$$

and

$$\varepsilon_0\varepsilon_n = f_n(P_S). \tag{2.40}$$

The coefficients most interesting for characterising the ferroelectric copolymers used in this work, namely ε_1, ε_2 and ε_3, can now be calculated using

$$\begin{aligned}
\varepsilon_0\varepsilon_1 &= 1/\left(\alpha + 3\gamma P_S^2 + 5\delta P_S^4\right),\\
\varepsilon_0\varepsilon_2 &= -P_S(\varepsilon_0\varepsilon_1)^3(3\gamma + 10\delta P_S^2),\\
\varepsilon_0\varepsilon_3 &= (\varepsilon_0\varepsilon_1)^5(-\alpha\gamma - 5(2\alpha\delta - 3\gamma^2)P_S^2 + 85\delta\gamma P_S^4 + 150\delta^2 P_S^6).
\end{aligned} \tag{2.41}$$

It is now appropriate to take a look at the ferroelectric ($P_S \neq 0$) and the paraelectric ($P_S = 0$) phase. As can be seen from equation (2.41), the permittivities of odd order do not depend on the sign of the polarisation. Considering the paraelectric case with

$P_S = 0$, the permittivities can be calculated by

$$\begin{aligned} \varepsilon_0\varepsilon_1 &= 1/\alpha, \\ \varepsilon_0\varepsilon_3 &= -\gamma/\alpha^4, \\ \varepsilon_0\varepsilon_5 &= (3\gamma^2 - \alpha\delta)/\alpha^7. \end{aligned} \tag{2.42}$$

Due to the inversion symmetry associated with the paraelectric phase, permittivities of even order vanish above the ferroelectric to paraelectric phase transition temperature. But below this temperature, in the ferroelectric phase, they do depend on the sign of polarisation and are therefore proportional to the remanent polarisation P_R

$$\varepsilon_0\varepsilon_2 = -P_R(\varepsilon_0\varepsilon_1)^3(3\gamma + 10\delta P_S^2). \tag{2.43}$$

If γ and δ are considered to be temperature-independent in the low symmetry ferroelectric phase, then

$$\varepsilon_0\varepsilon_2 \propto -P_R(\varepsilon_0\varepsilon_1)^3 \quad \text{and} \quad P_R \propto -\frac{\varepsilon_0\varepsilon_2}{(\varepsilon_0\varepsilon_1)^3}\,. \tag{2.44}$$

The latter can be used to describe the polarisation as a function of temperature or time. Furthermore, the states of polarisation, up or down, can be described by using the sign of ε_2.

2.4.4 Displacive and Order-Disorder Transitions

Ferroelectric phase transitions have been traditionally divided in two general classes: displacive and order-disorder. While most of the well-known ferroelectric materials like $BaTiO_3$ can be assigned to group one, others, i.e. P(VDF-TrFE), show a transition of an ordering-disordering nature. As displayed in Fig. 2.6, the lattice spacing in P(VDF-TrFE) is a function of temperature. It can be seen, that an increasing temperature induces a structural change from the polar and ferroelectric all-trans conformation to the non-polar trans-gauche conformation. While during lower tem-

peratures a lattice spacing assigned to the ferroelectric all-trans phase is dominating the diffraction pattern, elevated temperatures cause a shift to lower diffraction angles. The latter are assigned to the high-temperature, non-polar trans-gauche phase.

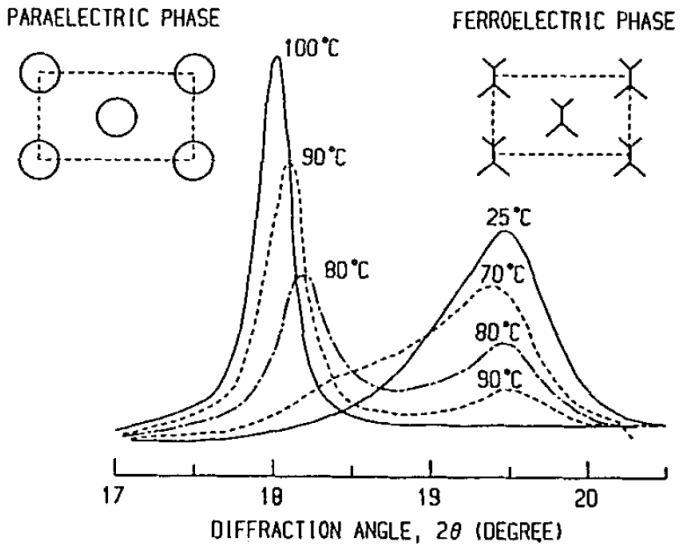

Figure 2.6: The X-Ray pattern of P(VDF-TrFE) 65/35 as a function of temperature [19].

2.4.5 P(VDF-TrFE) Ferroelectric Copolymer

A major part of the well studied and commercially used ferroelectrics are inorganic materials, namely ceramics. Therefore, ferroelectric polymers are unique in some ways. Among ferroelectric polymers, PVDF and its copolymers remain the most used and studied since decades. PVDF has four crystalline polymorphs, as shown in Fig. 2.7 (left). The naturally favoured, but from a ferroelectric viewpoint less interesting phase is the non-polar α-phase. Polymorphs can be transformed into each other, as depicted in Fig. 2.7 (right). The effort spend on a transformation can be very high. Some of them lead to a phase which is neither favourable nor stable and all of them include an additional work step. Therefore, Lando and Doll [39] suggested adding defined amounts of TrFE or TeFE. The expectation was, that a copolymer synthesised in this way would show a melt crystallisation similar to the β-phase of PVDF. The β-phase is ferroelectric and therefore the favoured polymorph for potential applications.

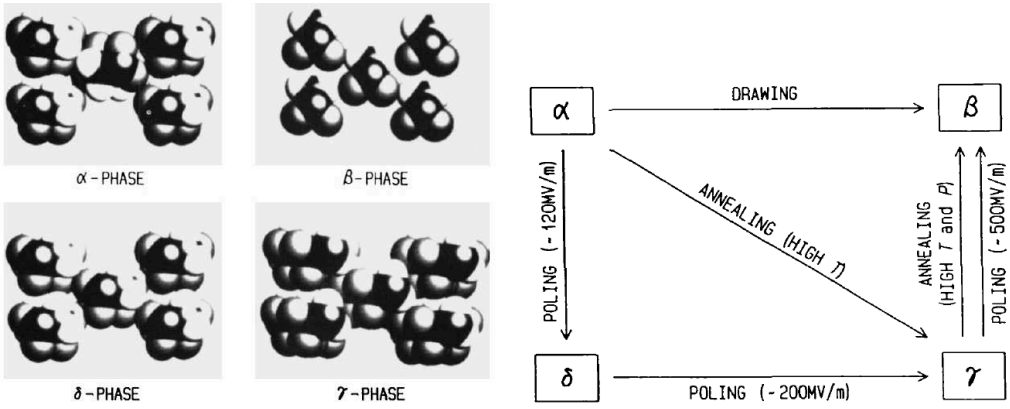

(a) Polymorphs (b) Transformations

Figure 2.7: (a) Crystalline Polymorphs of PVDF [18]. (b) Transformations among Crystalline Polymorphs of PVDF [18].

The structure of P(VDF-TrFE) is characterised by randomly distributed VDF and TrFE units resulting in a molecular chain, as shown in Fig. 2.8. According to [18] copolymers with a PVDF fraction of 50 mol%−80 mol% are of special interest, due to their clear indication of a Curie point. By annealing the material at a temperature in-between the Curie temperature and the melting point, crystallinity can be improved notably. While PVDF has an average crystallinity of about 50 %, its copolymers can show values of up to 90 %, depending on the VDF content. Figure 2.9 displays the remanent polarisation P_R as a function of the VDF content. Two things can be seen. At first, from a VDF content of 50 % up to 80 % the remanent polarisation increases remarkably, due to the higher dipole moment of VDF. If the content reaches 80 % however, P_R goes down, caused by a decreasing crystallinity.

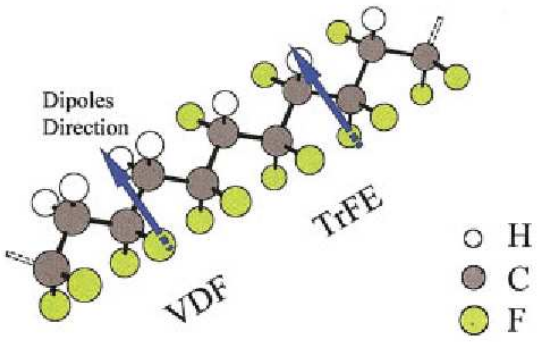

Figure 2.8: Structure of P(VDF-TrFE) [14].

The VDF content is also important for the paraelectric to ferroelectric phase

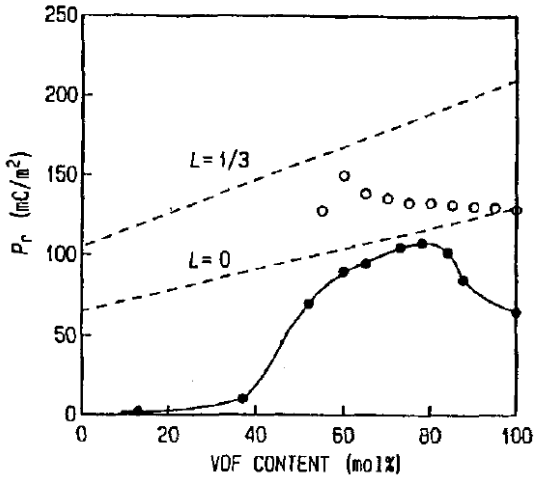

Figure 2.9: Remanent polarisation as a function of VDF content [18].

transition, i.e. the order of the transition and the phase transition temperatures. Odajima [55] calculated that P(VDF-TrFE) copolymers with a high amount of VDF undergo a first-order phase transition, while a lower VDF content is tied to a second-order phase transition.

VDF-TrFE copolymers give us the possibility to deposit materials with piezo-, pyro- and ferroelectric properties directly from the solution. This is very important for technical applications. It is therefore highly desirable to understand the physics of these materials, which will help us to further improve the properties important for potential applications.

2.5 Physics of Ferroelectric Multilayer Thin Films

2.5.1 General Phenomenology

Inorganic multilayers have been described extensively in the respective literature. The intend of this work is to extend the knowledge to polymeric multilayers. Although main properties, namely polarisation versus temperature and the resulting transition behaviour are similar, the intermixing in spin-coated multilayers is much stronger and cannot be neglected.

There are two main ansatzes to describe multilayer systems. The most obvious and most common ansatz involves the description of each single layer by a set of

carefully chosen parameters. Equations representing these single systems will then be combined to a set of functions modelling the multilayer properties. The free energy of a system of n layers possessing $m = n - 1$ interfaces can then be expressed as

$$\begin{aligned} F = &\sum_{i=1}^{n} \left[\frac{\alpha_i}{2} D_i^2 + \frac{\gamma_i}{4} D_i^4 + \frac{\delta_i}{6} D_i^6 + f_{\mathrm{PE},i} - E_i D_i \right] V_i \\ &+ \sum_{j=1}^{m} \left(f_{\mathrm{I},j} - E_{\mathrm{I},j} D_{\mathrm{I},j} \right) V_{\mathrm{I},j} \end{aligned} \tag{2.45}$$

where f_{I} is the free energy density of the appropriate interface layer, E_{I}, D_{I} and V_{I} are its electric field, its dielectric displacement and its volume, respectively. It is important to notify that the present ansatz uses the energy density instead of the gradient. Using the latter draws a clearer picture of the conditions, namely the polarisation distribution within the film, but becomes rather unimportant if the number of layers is increased.

A second, quite different ansatz is to consider the whole multilayer as an improper ferroelectric [42]. The system will then be described by a minimum two-component order parameter transforming according to irreducible two-dimensional representations. In this case, the single-component polarisation is not the primary effect in the phase transition, but the secondary instead. Using this approach, Levanyuk and Sannikov have predicted a linear dependence if the polarisation P is plotted as a function of the temperature T, as depicted in Fig. 2.10 (left). Despite the interesting approach and the similarities with results obtained for multilayers in this work, i.e. the linear dependence of the polarisation as a function of temperature, there are many open questions. As can be seen in Fig. 2.10 (right), the susceptibility is rather independent of the temperature. This is not true for multilayers measured for this work. Nevertheless, it seems worth mentioning the approach and suggesting further studies, especially with regard to multilayer systems. Those implicate a set of parameters, with each parameter assigned to an individual layer.

Following approach one and considering the free energy F of the layer system being the sum of the free energies of each single layer and the dielectric displacement D

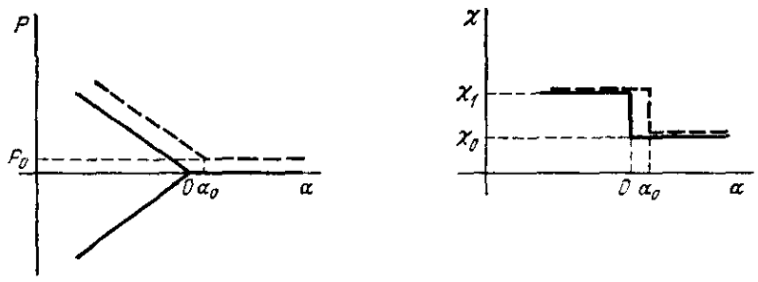

Figure 2.10: The dependence of P and χ on $T(\alpha = \tilde{\alpha}(T - \Theta))$ for the second-order ($\beta_1 > 0$) phase transition $0 \leftrightarrow 1$. The dashed lines represent the dependences for $E \neq 0$, $\alpha_0 = |e|$, $P_0 = |E|/\kappa_0$, $\chi = 1/\kappa$, $\chi_1 = [1 + (\Delta/\beta_1)/\kappa]$ [42].

of the layer system being equal to the dielectric displacement of each single layer, equation (2.45) can be simplified to

$$\begin{aligned} F = &\sum_{i=1}^{n} \left(\frac{\alpha_i}{2} D^2 + \frac{\gamma_i}{4} D^4 + \frac{\delta_i}{6} D^6 + f_{\mathrm{PE},i} - E_i D \right) V_i \\ &+ \sum_{j=1}^{m} \left(f_{\mathrm{I},j} - E_{\mathrm{I},j} D \right) V_{\mathrm{I},j}. \end{aligned} \tag{2.46}$$

From equation (2.46) main properties of a layer system and the impact of an interface layer can be derived. Assuming an equal area A for the main and the interface layers, the volume can be replaced by the thickness studying the impact of the latter. Having a thickness much smaller than the main layers, the interface layer's impact (sum) will be reduced by a smaller factor $V_{\mathrm{I},j}$ as well as by a higher electric field $E_{\mathrm{I},j}$. Assuming a non-ferroelectric dead layer(s), the term representing the interface layer(s) would simplify to $f_{\mathrm{I},j} \cdot V_{\mathrm{I},j}$.

Considering the free energy of all layers being the sum of the related polynoms excluding the interface part, it is inevitable to assume a shift of the minima in $F(D)$ as well. Therefore, the location of the layer system's spontaneous polarisation will be shifted as well. The temperature dependence of the polarisation of a bilayer system without the interface layer can be calculated using the first part of equation (2.46). The result of this calculation is displayed in Fig. 2.11. It can be seen, that for the sum of both functions the values for spontaneous polarisation at $dF/dD = 0$ are shifted to values in-between $P_{\mathrm{S},1}$ and $P_{\mathrm{S},2}$ (Fig. 2.11, top). Calculating and plotting the derivative (Fig. 2.11, center and bottom) it becomes apparent that the remanent

polarisation (intersection with E-axis, center and bottom) takes values in-between the values of the single layers. The values for the coercive field ($\mathrm{d}^2(F_1+F_2)/\mathrm{d}D^2 = 0$) will also be in-between the single layer values if both functions F are added. This theoretical results will be compared to the measurements in section 4.6.1.

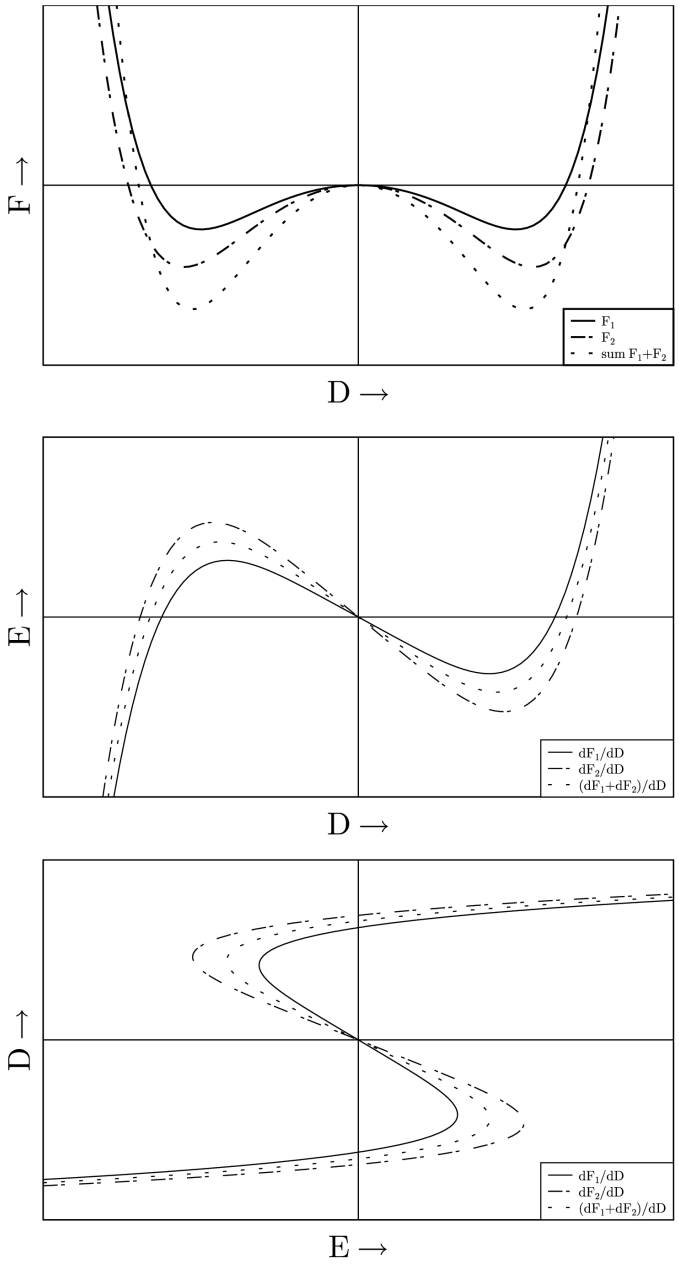

Figure 2.11: Sum of two functions representing the phenomenological approach discussed in 2.2 (top). Derivative of single functions F_1 and F_2 as well as the sum showing a medium polarisation (center) and an increased coercive field for $F_1 + F_2$.

2.5.2 Polarisation Profile in Multilayers

It is well known (e.g. [45]) that DC electric fields present in ferroelectric thin films induce a polarisation at temperatures slightly above but close to the transition temperature. This, in fact, is a shift of the ferroelectric to paraelectric phase transition towards higher temperatures. According to soft mode theory, the electric field removes the centre of symmetry causing a first-order Raman effect, with the scattering intensity being proportional to the field applied.

The origin of the DC electric field can be of different nature, as discussed in section 2.4.1. The main source is the stress induced asymmetry created by the necessity to deposit the film on a substrate. It can be amplified by the use of different electrodes [21] and the native oxide layer adjacent to the bottom electrode, i.e. if aluminium is used as an electrode material. A further source discussed in earlier publications [87] is a non-switchable polarisation present throughout the whole temperature range measured. This temperature-independent polarisation might be found in an interface layer, since it has not been measured in thicker films of the same material. Nevertheless, a temperature-independent polarisation can be induced in thicker films of P(VDF-TrFE) if the as-deposited film has been poled prior annealing. The sign of the non-switchable polarisation will then depend on the direction of the electric field applied for poling. An appearance without an intended poling might indicate an intrinsic field, caused by the sources named above [62].

Another source of DC fields can be introduced by combining layers having different polarisation properties, i.e. a combination of a paraelectric and a ferroelectric layer. A similar effect can be achieved by pairing two ferroelectric materials having different transition temperatures. Profiles of bilayer and multilayer systems have been discussed in [44]. Despite the polarisation profile within a layer as discussed in 2.4.2, the interface coupling between a ferroelectric and a paraelectric layer has been calculated.

3 Preparation and Characterisation

3.1 Preparation of Single and Multilayer Thin Film Devices

3.1.1 Deposition of P(VDF-TrFE) Thin Films

The amount of VDF strongly determines the properties of P(VDF-TrFE) [18]. Therefore, samples containing different molar percentages of VDF have been deposited (Tab. 3.1). All copolymers were provided in form of granules from Solvay. Because of a good solubility and a low hydrophilicity, diethyl carbonate (DEC) was used as a solvent as shown in Tab. 3.1. One has to remark, that the polymer solution has to be heated up to 80°C and stirred for at least two hours in order to dissolve the copolymer granules completely.

VDF/TrFE in mol%	P(VDF-TrFE)/solvent in wt%	solvent
56/44	1, 2.5, 5	DEC
70/30	1, 2.5, 5	DEC
80/20	1, 2.5, 5	DEC

Table 3.1: Solutions.

Deposition of the copolymer thin films has been done by spin coating, which is a well controlled process with reproducible results. A diagram of film thickness versus spinning speed for different solutions is shown in Fig. 3.1. Although values shown in Fig. 3.1 do not exactly reflect our results, since the substrates and the solvent used in our experiments were different, they display the general behaviour of a thin film's thickness as a function of the spinning speed the solution's composition.

All parameters were chosen based experiences gained in earlier experiments. The amount of P(VDF-TrFE) was chosen to be 1 wt% to yield ultra thin films, 2.5 wt% and 5 wt% to yield thin films of about 20 nm, 60 nm and 200 nm, respectively. The copolymer solution has been trickled onto the substrate using a syringe with a PTFE made filter. The filters used had a pore size of 2 µm. The value for the spinning speed has been chosen to be 2000 rpm in order to achieve smooth, homogeneous layers of the copolymer.

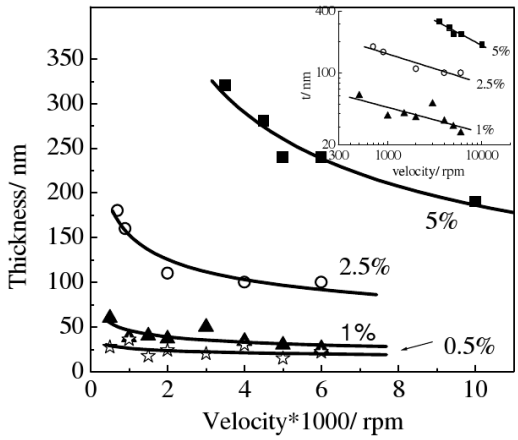

Figure 3.1: Layer thickness vs rotation speed [49].

Microscope slides were used as substrates. It is important that the edges of the slide are not ground, because during the process of grinding small splinters of glass fall onto the substrate. Since their temperature is usually high, they tend to be burned-in and form a rather rough surface. Substrates were cleaned in four steps. For every step a bath-type sonicator was used. First of all, the glass slides were put into ethanol. The sonic was applied for five minutes. That time was not changed for the following processes. The liquids were exchanged from ethanol to acetone, then to ethanol again. Finally some deionised water was used to remove the residues. All cleaning steps as well as the polymer deposition have been carried out in a cleanroom.

After the cleaning procedure, the bottom electrodes where thermally evaporated onto the clean substrates, followed by the copolymer and the top electrodes. The copolymer was deposited as mentioned above. Furthermore, an annealing step was added to increase the crystallinity of the copolymer. Annealing is described in the

appropriate section.

Deposition of the Electrodes

The material used for the electrodes has an impact which cannot be neglected [21]. Especially the use of top and bottom electrodes made of different materials can cause unwanted, asymmetry related effects. For availability reasons aluminium has been used. The thin layers of the electrode material have been thermally evaporated. Despite the low costs, aluminium increases the break-down voltage of the thin film due to its native oxide layer. On the other hand, the oxide poses an additional layer, causing asymmetry and increasing the electric field needed for polarisation reversal.

A sketch containing both, bottom and top electrode for a single layer thin film device is shown in Fig. 3.2. The section, in which two electrodes overlap constitutes a capacitor, which has been used to characterise the properties of interest. Each sample provides 14 capacitors initially. For contacting the electrodes a standard aluminium foil was used. It was cut into small stripes, which were then attached to the electrodes with the help of conductive silver (commercially available solution).

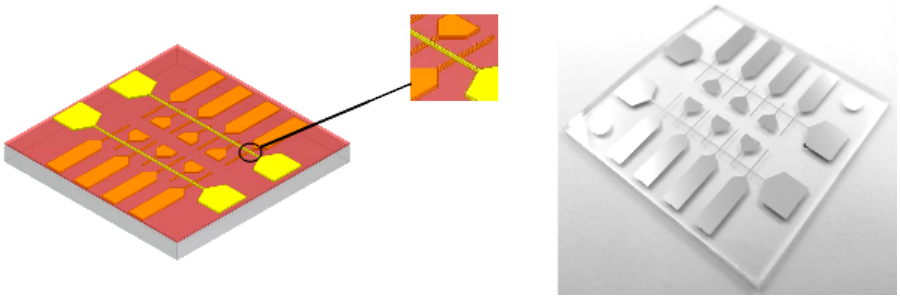

Figure 3.2: Sketch (top electrodes yellow) and photograph of a capacitor-type sample.

To prevent the solvent being trapped below the top electrode material, annealing was conducted before the final deposition step. Aluminium electrodes were non-transparent and reflective with a thickness of approximately 50 nm. Using silver as an electrode material led to devices showing a poor performance caused by a higher conductivity.

Annealing Conditions

Annealing is a process of multiple functionality. In a first step, while increasing the temperature at an appropriate rate, the solvent will be evaporated (almost) completely. After reaching a value well above the transition to the prototype phase but fairly below melting, the temperature is kept constant for about two hours as displayed in Fig. 3.3. Finally, the sample has to be cooled down slowly to support crystallisation [18]. Parameters chosen for different film thicknesses are listed in Tab. 3.2.

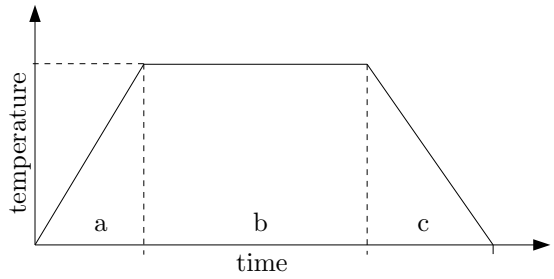

Figure 3.3: Temperature regime for annealing (a-heat up, b-annealing, c-cool down).

Thickness of film in nm	Annealing temperature in °C	Heating/cooling rate in °C/min
below 100	120	2/2
above 100	140	2/2

Table 3.2: Annealing parameters.

In order to reach the temperature wanted, the furnace has to be well controlled. Especially overheating has to be avoided, since the annealing temperature is close to the melting point. This can be done by increasing the temperature stepwise. The same attention has to be paid during the cooling. A slow cooling rate is important for crystallisation. We have chosen both, heating and cooling rate, to be 2°C/min.

3.1.2 Deposition of P(VDF-TrFE) Multilayer Thin Films

The experimental details have been already described in [95] VDF-TrFE copolymer thin films of different molar ratios have been spin coated onto a glass

substrate covered with aluminium electrodes. After the deposition and subsequent annealing, a second copolymer thin film of the same or a different molar ratio has been deposited on top of the first. The so built bilayer was then completed by an annealing step and the deposition of top electrodes. Furthermore, an intermediate electrode for single layer characterisation has been deposited at distinct positions in the sample (Fig. 3.4).

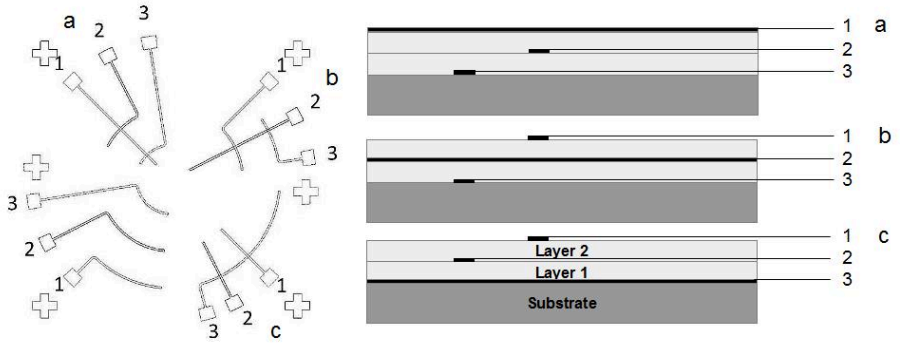

Figure 3.4: Electrode design for the characterisation of bilayer samples. Each sample is equipped which three sets of the pattern in which the electrodes are placed as given in the sketch. In total, the electric properties of the two single films as well as of the bilayer can be measured [95] ©2016 IEEE.

Thickness measurements have been conducted with the capacitive method (LCR-meter), profilometer and atomic force microscopy (AFM) as described in section 3.2. It has been shown, that the thickness sums up nearly linear if several layers were deposited subsequently under identical conditions. Another indicator for the first layer being stable is the stability of the electrodes on top of it. However, a small amount of material on top of the previous layer might be solved creating an intermixed layer, especially at parts of the film not covered by an intermediate electrode.

As described in [95] and shown in Fig. 3.4, electrode patterns (a3, b3, c3), (a2, b2, c2) and (a1, b1, c1) have been deposited on the substrate, on top of the bottom layer and on top of the upper layer, respectively. Pattern *b* can be used to measure the individual layers (bottom, top), while in pattern *a* and *c* the bilayer and the top layer or the bilayer and the bottom layer can be characterised.

3.1.3 Preparation of P(VDF-TrFE)-DNTT FerrOFET Devices

For the bottom gate design, VDF-TrFE copolymer thin films with a composition of 70/30 mol% and different thicknesses were deposited on a glass substrate covered with anodised aluminium electrodes. If intended, the copolymer layer was then annealed at temperatures appropriate to the film thickness (Tab. 3.2) for two hours before the organic semiconductor was evaporated on top of it. The samples were finalised by silver source/drain top electrodes. For the top gate design, the deposition order has to be reversed. The deposition of the consecutive layers was done using different techniques appropriate for the material in use. The techniques will be described in the following sections.

Different methods have been applied to control the surface morphology. Besides imprint techniques (embossing) and the deposition of a thin parylene layer on top of the copolymer, the question has been raised if the annealing step is generally necessary. As has been observed in experiments earlier, a ferroelectric hysteresis can be recorded even for a pristine thin film after running a few poling cycles.

Deposition of the Gate Electrode

In a first step, if the bottom-up design has been used, an aluminium bottom gate electrode was deposited. In order to prevent or minimise the leakage current, an anodisation of the gate electrode is advisable. The procedure to achieve an aluminium-oxide of appropriate thickness and structure (blocking) is as follows.

1. Evaporation of aluminium gate electrode, deposition rate 40 Å per second, thickness equal to 100 nm

2. For 0.02 mol/l stir 1.5 g trisodium citrate dihydrate (linear formula, Sigma Aldrich: $HOC(COONa)(CH_2COONa)_2 \cdot 2H_2O$, molecular weight: 294.1) in 250 ml of deionised water

3. Place the sample in the solution, connect the sample to positive (+) and the platinum electrode to ground

4. Choose a voltage and a current appropriate for the thickness and the type of oxide layer [13, 28, 34] wanted

The anodising ratio was measured to be 1.3 nm/V. So the source current and the compliance have been chosen to be 50 µA and 15 V, respectively, in order to get a barrier-type oxide layer with a thickness of approximately 20 nm. The thickness is mainly determined by the type, the concentration and the temperature of the electrolyte used for anodisation [13, 28]. In order to make sure that the aluminium oxide film is of barrier type, it was necessary to record the ionic current during the film growth. For the barrier-type layer the current density has to show a continuous drop, as depicted in Fig. 3.5.

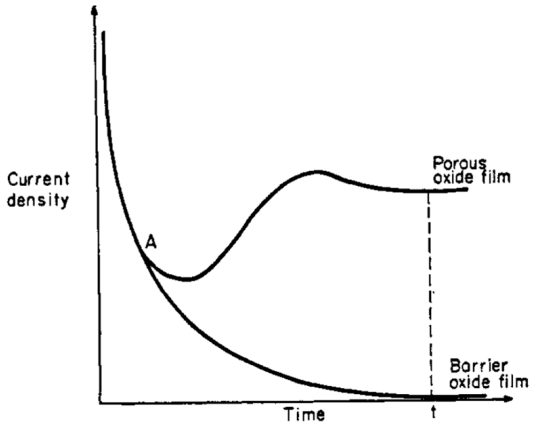

Figure 3.5: Current density-time transients for the formation of a barrier-type and a porous-type anodic film on aluminium. Point A represents the point at which divergence of the two curves occurs, and hence may be related to pore initiation phenomenon. Time t is typically 25 sec for a 15-V step application to aluminium in 15% sulphuric acid [13, 28].

Deposition of the P(VDF-TrFE) Gate Dielectric

The ferroelectric copolymer VDF-TrFE has been deposited as described in section 3.1.1. Deposited films have been annealed at 120°C for 2 hours to increase the crystallinity and therefore the remanent polarisation. The device under design forms a surface inversion channel built up at the dielectric-semiconductor interface. This type of channel can be characterised as a two-dimensional sheet and has usually a thickness in the order of some nanometres [72]. The surface roughness largely depends on the surface morphology of the material used as gate dielectric. P(VDF-TrFE) usually shows a surface roughness limited to some nanometres (arithmetic

average of absolute values), which is sufficient for most of the applications. But being used as a base for the conducting channel, each additional nanometre in roughness means a loss in mobility. In order to avoid or decrease the surface roughness, several details or techniques can be changed or varied, respectively:

- Additional imprinting or embossing after the deposition
- Decreasing the annealing temperature below 120°C
- Skip annealing completely
- Top gate design instead of bottom gate design
- Deposition of two layers of P(VDF-TrFE), only the first layer will be annealed
- Deposition of a second layer of another smoothing and/or insulating material, e.g. parylene C.

Some of these ideas have been tried, others have been discarded, due the materials in use or to the deposition conditions. The influence of different details on the device performance will be discussed in section 4.6.2.

Deposition of DNTT Organic Semiconductor

The centrepiece of each MISFET is the layer containing the channel, either conductive or non-conductive, depending on the type (enhancement, depletion) and on the voltage applied. Typically used organic semiconductors, e.g. pentacene and DNTT, can be either deposited by evaporation or spin coating. Although the latter is preferable because of the simplicity of the process, the evaporation method has been used to deposit semiconductor thin films, i.e. 40 nm films of DNTT.

Deposition of the Silver Top Electrode

The top electrode has been deposited evaporating a 50 nm layer of silver at 2 nm/s.

3.2 Characterisation Techniques

3.2.1 Thickness and Roughness Measurements

Mainly capacity measurements were used to measure the samples thickness. The thickness can be accessed by using the simple formula

$$C = \varepsilon \frac{A}{d}. \tag{3.1}$$

The area size of the electrodes has been measured under a classical Zeiss® microscope using the supplied software. The capacity was determined using an LCR meter, with a voltage and frequency appropriate ($V < E_C/10; f = 1\text{kHz}$). The relative permittivities of P(VDF-TrFE) with molar fractions of 56/44 and 70/30 were supposed to be 19 and 10.25, as can be found in [18] and [54]. To avoid misleading assumptions, AFM measurements were conducted in order to prove the thickness. It can be seen, that the sample's thickness measured with the AFM is usually about 10% lower than the one determined using the capacitive method. The reason could be of a dimorphic nature. As shown in [54], the total permittivity of a polymeric system containing crystalline and amorphic parts can be calculated using

$$\bar{\varepsilon} = X_C^{2/3} \frac{1}{X_C^{1/3}/\varepsilon_K + \left(1 - X_C^{1/3}\right)/\bar{\varepsilon}_A} + \left(1 - X_C^{2/3}\right) \bar{\varepsilon}_A \,. \tag{3.2}$$

From the equation it can be seen, that the permittivity of the copolymer strongly depends on its crystallinity. The amorphous parts have a lower permittivity of $\varepsilon_A = 8$ and $\varepsilon_A = 9.3$ for P(VDF-TrFE) 56/44 and P(VDF-TrFE) 70/30, respectively [62]. Having a relative permittivity ε_A smaller than the relative permittivity of the crystalline material ε_K, which is 19 for P(VDF-TrFE) 56/44 and 10.25 for P(VDF-TrFE) 70/30, the overall permittivity of the mixed system ε_M can be considered to be $\varepsilon_A < \varepsilon_M < \varepsilon_K$. For the calculation of the film thickness the relation $d = \varepsilon_0 \varepsilon_M A/C$ was used. It can be seen, that assuming a perfect crystal and using ε_K for the calculation of the thickness, the calculated thickness value might exceed the real thickness by the factor given in equation (3.2).

The second reason for a deviation can be attributed to the measurement techniques itself. While the AFM uses a rather small force while touching the surface, other techniques or instruments, i.e. the DecTak profilometer, might scratch the surface resulting in a measured thickness smaller than the actual film thickness. But using the AFM for thickness measurements, a sharp edge has to be created in order to separate film and substrate. This was done by scratching the film with tweezers. In order to use the results of this measurement, one has to postulate that using the scratching method all polymer material has been removed. Furthermore, the substrate material should remain unharmed. The AFM has also been used to measure the roughness of the copolymer thin films.

Additionally a DecTak profilometer was used to determine the thickness. A decreased contact pressure in combination with the rigidity of the annealed P(VDF-TrFE) thin film made it possible to conduct most of the contact measurements without harming the thin film significantly. Since we were mostly interested in the qualitative temperature-dependent behaviour of the permittivity, a small deviation of the latter is acceptable. Hence, a small deviation in thickness is acceptable as well.

3.2.2 Hysteresis Measurements

The hysteresis measurements have been conducted using a principle well known since the late 1920s [67]. If not specified otherwise, loops were recorded at a frequency of 1 kHz. For all measurements that involve a temperature variation, the sample was placed in a vacuum chamber in order to stabilise the temperature. Fatigue behaviour was limited using a triangular shaped signal instead of a sinusoidal function as suggested in [83]. The capacity C_{R} of the reference capacitor for the hysteresis measurements was chosen to be large compared to the sample's capacity C_{S}, e.g. $C_{\mathrm{S}}/C_{\mathrm{R}} < 0.01$.

3.2.3 Dielectric Non-Linearities

The set-up (Fig. 3.6) used to measure the non-linearities of the ferroelectric samples is a serial connection of the sample and a resistor of known size. An ideal resistor is known to have a linear *I-U* characteristic and an impedance solely real. The impedance of the resistor | Z_R | was chosen to be small compared to that of the sample | Z_S |, e.g. | Z_R |/| Z_S |< 0.01. In this way, the main voltage drop can be accounted to the sample. For measurements based on varying temperatures the sample was placed in a vacuum chamber to stabilise temperature through limiting convection.

The response of a dielectric sample to an harmonic electric field $E_\mathrm{E}(t)$ contains higher harmonics of the applied electric field's frequency. In other words, the response is non-linear. The amplitude of the electric field $\widehat{U}_\mathrm{E}$ must be chosen small enough, e.g. $\widehat{U}_\mathrm{E}/\widehat{U}_\mathrm{C} < 0.1$, to avoid orientational polarisation, but high enough to pronounce the non-linear behaviour.

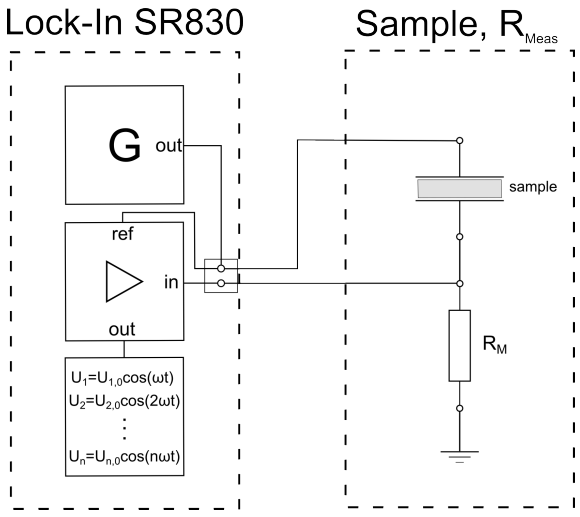

Figure 3.6: Sketch of a measurement set-up using an analogue lock-in amplifier.

As derived in appendix A.1 the dielectric displacement D can be described using the harmonic excitation voltage $U_\mathrm{E}(t)$ as

$$D(t) = \varepsilon_0\varepsilon_1\frac{\widehat{U}_\mathrm{E}}{d}\cos(\omega_0 t) + \varepsilon_0\varepsilon_2\left(\frac{\widehat{U}_\mathrm{E}}{d}\cos(\omega_0 t)\right)^2 + \varepsilon_0\varepsilon_3\left(\frac{\widehat{U}_\mathrm{E}}{d}\cos(\omega_0 t)\right)^3 . \quad (3.3)$$

A change in the dielectric displacement D with respect to the time t is equal to the

current density $J(t) = dD/dt$. Considering Ohm's law, the geometry of the sample, i.e. the surface A and the thickness d, and the resistor used for the measurements, the complex permittivities ε_1 and ε_1 can be determined as

$$\varepsilon_1' - i\varepsilon_1'' = \frac{d}{\omega_0 \varepsilon_0 A R_\mathrm{M} \widehat{U}_\mathrm{E}} \left(U_{\mathrm{M},1}'' - iU_{\mathrm{M},1}'\right) \tag{3.4}$$

and

$$\varepsilon_2' - i\varepsilon_2'' = \frac{d^2}{\omega_0 \varepsilon_0 A R_\mathrm{M} \widehat{U}_\mathrm{E}^2} \left(U_{\mathrm{M},2}'' - iU_{\mathrm{M},2}'\right) \tag{3.5}$$

Assuming an ideal insulator with no loss, the imaginary parts of the permittivities can be neglected and the real parts can be written as

$$\varepsilon_1' = \frac{d}{\omega_0 \varepsilon_0 A R_\mathrm{M} \widehat{U}_\mathrm{E}} U_{\mathrm{M},1}'' \quad \text{and} \quad \varepsilon_2' = \frac{d^2}{\omega_0 \varepsilon_0 A R_\mathrm{M} \widehat{U}_\mathrm{E}^2} U_{\mathrm{M},2}'' \,. \tag{3.6}$$

As derived in equation (2.44), the permittivities can be related to the remanent polarisation as $P_\mathrm{R} \propto -(\varepsilon_0\varepsilon_2)/(\varepsilon_0\varepsilon_1)^3$. Hence, the factor proportional to the remanent polarisation can be determined by

$$P_\mathrm{R} \propto -\frac{\omega^2 A^2 R_\mathrm{M}^2 \widehat{U}_\mathrm{E}}{d} \frac{U_{\mathrm{M},2}''}{(U_{\mathrm{M},1}'')^3} \,. \tag{3.7}$$

If the amplitude $\widehat{U}_\mathrm{E}$ and $U_{\mathrm{M},1}'' \propto \varepsilon_1'$ are positive numbers, the state of polarisation, up or down, can be derived solely from the sign of U_2''.

3.2.4 Measurements using a Software-Based Lock-In

In order to simplify the set-up towards commercialisation, the lock-in amplifier has to be replaced or digitalised, respectively. That can be done using a set-up displayed in Fig. 3.7.

The left element of the drawn set-up consists of a PC running Matlab. The PC basically has to replace three devices. The first device, marked with a G and sometimes also part of the second device is a function generator. Despite being able to provide the desired wave forms of wanted frequency, whereby the latter

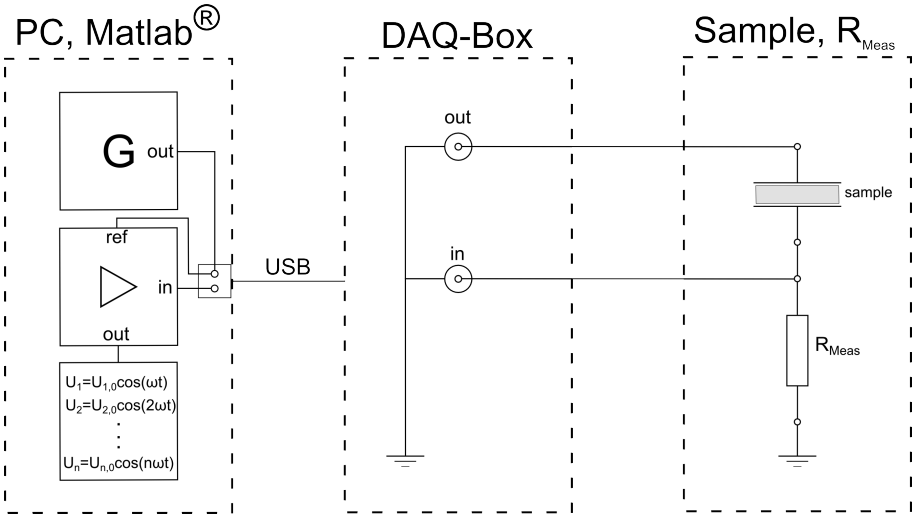

Figure 3.7: Sketch of a measurement set-up using a software-based lock-in amplifier.

will be usually limited by the DAQ box, the function generator has to assure a single mode excitation signal. The absence of higher harmonics is mandatory. The second and key part of element one is a software-based lock-in amplifier, which can be programmed using the simple mathematics underlying the lock-in principle. In order to catch signals of lower amplitude generated by higher-order harmonics, the digital set-up might have to be completed by an analogue amplifier. The third device replaced by the PC is the evaluation unit.

The center element is a common DAQ box, e.g. NI USB-6251 used for data collection. The right element consists of the sample and a reference resistor. The latter has to be significantly smaller in resistance in order to allow a main part of the voltage drop over the sample, as described before. A rule of thumb is a factor of 100. For temperature spectra measurements the resistor is placed outside the vacuum chamber, subjected to ambient temperature and can be used to measure the sample's response at a constant, temperature-independent value of resistance.

Within the scope of a Master's thesis first measurements using a software-based lock-in set-up have been conducted. The aim was to measure the permittivities ε_1 and ε_2 in order to calculate and record $\varepsilon_2/\varepsilon_1$ over time to quantify retention. It has been shown, that measuring samples without a physical, but with a digital lock-in amplifier instead yields promising results. The results have proven, that not only the sign and therefore the state of the polarisation can be measured. It has also been

shown, that interesting properties, i.e. the retention behaviour can be determined through software-based lock-in measurements.

3.2.5 Piezoresponse Force Microscopy (PFM)

PFM has become a common tool to investigate piezo- or ferroelectric properties of ferroelectric thin films. Besides studying the domain growth, domain dynamics and structures in ferroelectric thin films, simple polarisation patterns written into the film can be used to prove a films ferroelectricity. PFM measurements were especially helpful to study ferroelectric ultra-thin films of VDF-TrFE copolymer. While using classical hysteresis measurements would lead to an electrical breakdown of the material, PFM measurements using moderate voltages are able to display switching properties at a very high resolution. Measurements have been carried out with a conducting tip serving as a top electrode.

For further reading on the PFM principle and applications, the PFM Application Note on *Asylum Research's* homepage can be highly recommended.

4 Results and Discussion

4.1 General Remarks

The following sections will sum up the results, their evaluation and the discussion of the same. They have been gathered for different theoretical aspects and with regard to different potential applications. Theoretical aspects have been discussed in several papers published since 2011 (Contributions). The more practical aspects and the use in applications, i.e. in (organic) ferroelectric field-effect transistors, arose from several co-operations with universities in Hong Kong, i.e. *The Polytechnic University of Hong Kong* and the *University of Hong Kong*, and Malaysia, i.e. the *University of Malaya*. It seems advisable to mention, that although great care was taken to avoid using original text from earlier publications, i.e. [87] ©2012 IEEE, [90], [93] ©2013 IEEE, [95] ©2016 IEEE, repetitions were inevitable at some point. The text used in previous publications was formulated with great care.

As has been shown in publications earlier (Contributions), dielectric non-linearities are a powerful tool to describe properties of a ferroelectric material, such as polarisation state, ferroelectric to paraelectric phase transition order, retention time and depolarising fields. Despite being a multi-use tool, the measurement of the dielectric non-linearities is very sensitive and non-destructive. Both properties are especially interesting for memory applications using ferroelectric polymers.

The conducted measurements and therefore the following chapter focus on VDF-TrFE copolymer thin films with two different molar fractions of VDF, namely 56 % and 70 %, and with different thicknesses. The film thickness of single layers will not exceed 200 nm. Films with thicknesses deceeding 50 nm will usually be referred to as ultra-thin films. The thickness range chosen might be interesting for applications

using voltages common in (micro-) computer technology, usually not exceeding several volts. Since the coercive field of PVDF and its copolymers is generally high if compared to inorganic ferroelectrics, the thickness has to be reduced in order to achieve switching with a voltage as low as 5 V. Depending on film properties, i.e. the film thickness, the coercive field of P(VDF-TrFE) thin films is 50 MV/m (e.g. [18]) or higher. If considering a field of 50 MV/m and a switching voltage of 5V, the thickness of a P(VDF-TrFE) ferroelectric thin film must be as low as 100 nm. Following the linear equation $d = U/E$, half of the thickness would require half of the switching voltage. For thin films with a thickness deceeding 100 nm however, the field might increase by a factor of 2 or higher (e.g.[10]). The same applies, if one intends to increase the switching speed. Therefore, further decreasing the thickness might contradict the purpose of decreasing the switching voltage, if the sample's set-up (electrode material, substrate, etc.) remains unchanged.

While thicknesses below 100 nm can be easily produced using spin coating, a process which is well studied because of its extensive use in semiconductor industry, the properties of the thin films deposited become even more complex. Surface effects become more pronounced and bulk properties are blurred or even altered. Although some of these properties seem to be of a pure theoretical interest, they are important to be understood in order to get a full picture of an ultra-thin film's behaviour. Some will be helpful for potential applications, i.e. a shift of the transition temperature to lower or higher values.

4.2 Dielectric Non-Linearities in P(VDF-TrFE) Ferroelectric Thin Films

As discussed in [86], studying the dielectric non-linearities in P(VDF-TrFE) thin films is a powerful tool to gain information on the thin film properties. The small-signal measurements conducted are sensitive enough to collect data on the thin film properties, but avoid major impact on the same. The technique has already been used in [27] to measure P(VDF-TrFE) thin films with thicknesses of several µm. It will be shown, that reducing the film thickness to 200 nm and below has a major

impact on some thin film properties, while others remain unchanged. The properties of interest are derived using absolute and temperature dependent values of ε_1, ε_2 and ε_3, with the term *absolute* referring to the algebraic sign. Theoretical aspects and the measurement principle have been discussed in chapter 2 and chapter 3.2.

As can be seen from Fig. 4.1, values for permittivities calculated from results at the measurement frequency of 1 kHz and at a field significantly smaller than the coercive field E_C, can be gathered at a good quality, even for thicknesses below 30 nm. Although the signal measured throughout different temperatures becomes smaller with decreasing thickness and therefore the change in ε_1 becomes less pronounced, main properties like transition temperatures and thermal hysteresis are clearly observable. Nevertheless, if possible measurements were always backed by recording a ferroelectric hysteresis curve. In order to do so, one has to assure that the ferroelectric hysteresis measured shows key features as humorously emphasised in [70], i.e. saturation at high electric field and inflection points at E_C (Fig. 4.4).

During the measurements, often hysteresis loops lacking all key features have been recorded. This is partially due to the finite resistance observed in P(VDF-TrFE) thin films, leading to a finite conductivity which cannot be suppressed in ultra-thin films of P(VDF-TrFE). The resistance of the samples measured is usually in the two-digit MΩ region, so that measurement resistors have been chosen to be $10 - 100\,\mathrm{k\Omega}$. Using the relation $\sigma = i\omega\varepsilon_0\varepsilon$ derived in section 4.4.1, conductivity can also be observed while measuring the non-linearities. Therefore, the imaginary part of the permittivity ε_n'' has to be assigned to the real part of the conductivity σ_n'. P(VDF-TrFE) thin films usually displayed permittivities having an imaginary part ε_n''. Figure 4.1 displays the real and imaginary parts of P(VDF-TrFE) thin films. It can be seen, that the imaginary part accounts for up to 10 % of the real part ε_1' for the ultra-thin film with a thickness of 25 nm. The imaginary contribution decreases to approximately 5 % if the film thickness is increased to 64 nm.

As can be seen in Fig. 4.2, the right hysteresis curve, recorded for a 175 nm P(VDF-TrFE) thin film, shows all properties or features pointing at a material having ferroelectric properties. There is a clear tendency to saturation at higher electric fields. Furthermore, there are inflection points at zero dielectric displacement indicating a

maximum slope associated with the coercive field E_C.

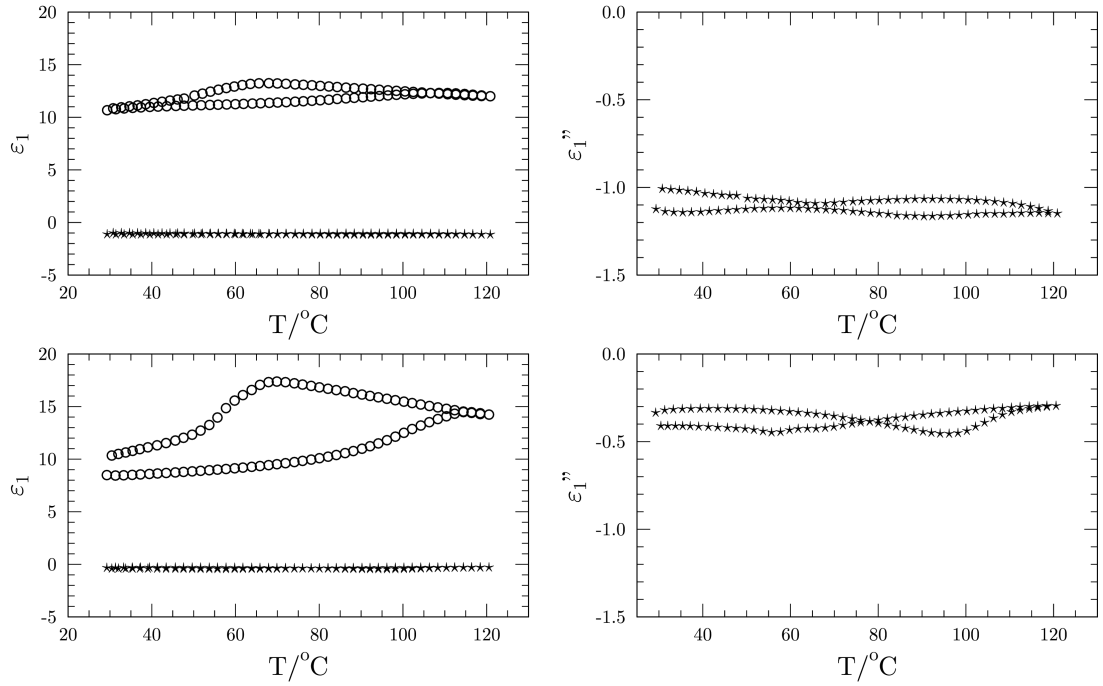

Figure 4.1: Real (ε_1', $\circ$) and imaginary (ε_1'', $\star$) part of the permittivity ε_1 of a 25 nm (upper line) and 64 nm (lower line) P(VDF-TrFE) 70/30 mol% thin film.

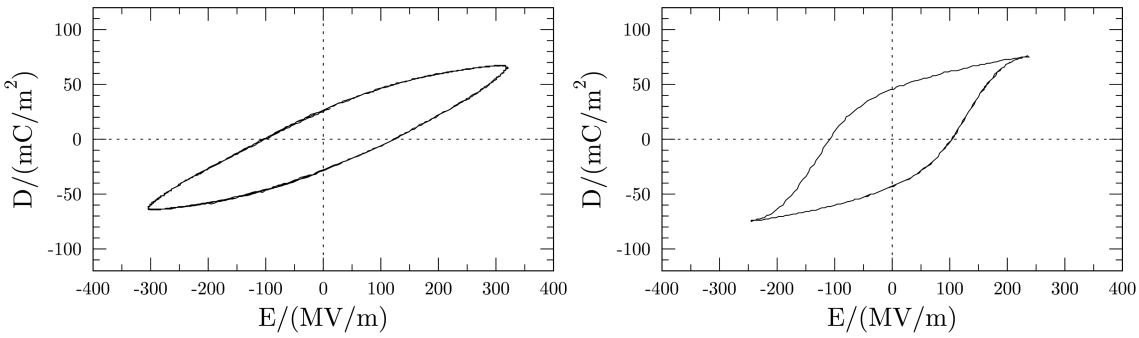

Figure 4.2: Ferroelectric hysteresis curves of P(VDF-TrFE) 70/30 mol% thin films, 64 nm (left, [87] ©2012 IEEE) and approximately 180 nm (right).

The left hysteresis curve, recorded for 64 nm P(VDF-TrFE) thin film appears to lack all properties mentioned in the paragraph above. There is no clear sign of saturation. The slope at zero dielectric displacement shows no inflection points. The appearance could lead to the assumption that the material under observation is not ferroelectric, but rather of a lossy capacitor type. Thin films of P(VDF-TrFE) are lossy indeed, especially if subjected to high electric fields as applied during a hysteresis measurement. Nonetheless, the graphs drawn for the same thin film

and for ε_1 and the remanent polarisation in Fig. 4.3 clearly indicate a ferroelectric material. If in doubt, plotting the derivative of the hysteresis as shown in Fig. 4.4 is also useful if other measurement techniques are not available. The inflection points can be easily recognised as a local maxima of the permittivity, while in the saturation region the permittivity approaches zero. Due to the finite resistance of the samples, a full saturation could never be recorded. If desired, all parts not representing the ferroelectric polarisation could be excluded mathematically.

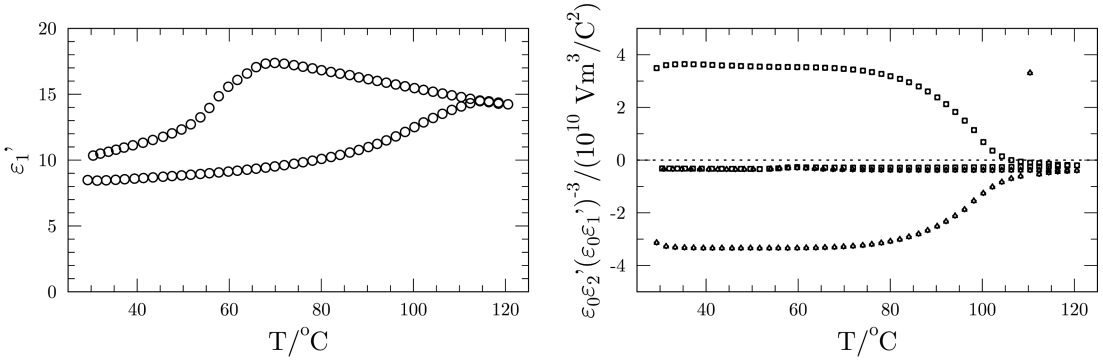

Figure 4.3: Real part of the permittivity ε_1' and polarisation (both directions) for a 64 nm ferroelectric thin film of P(VDF-TrFE) 70/30 mol% (similarly published in [90]).

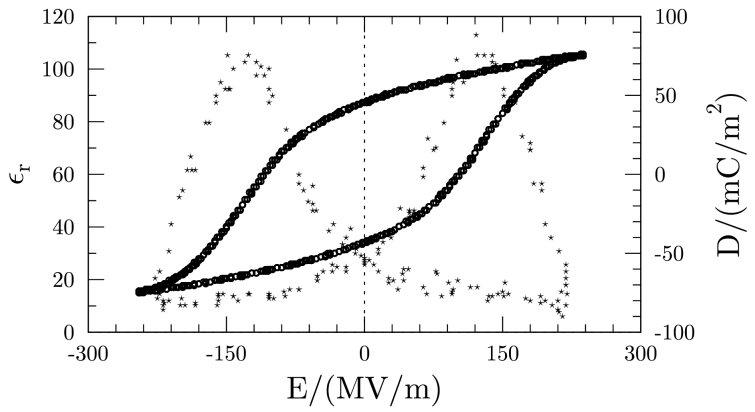

Figure 4.4: Hysteresis curve $(D, \circ)$ and its derivative dD/dE $(\varepsilon_r, \star)$ of a 200 nm ferroelectric thin film of P(VDF-TrFE) 56/44 mol%.

Polarisations as displayed in Fig. 4.3 (right) have been calculated using the linear permittivity ε_1 and the non-linear permittivity ε_2. As derived in [86], ε_2 is related to the spontaneous polarisation through

$$\varepsilon_0\varepsilon_2 = -P_R(\varepsilon_0\varepsilon_1)^3(3\gamma + 10\delta P_S^2), \tag{4.1}$$

with the term $(3\gamma + 10\delta P_S^2)$ assumed to be temperature-independent. Assuming a positive ε_1, the state of polarisation in memory applications can be determined using the sign of ε_2 only. Figure 4.5 displays ε_2 of a P(VDF-TrFE) thin film recorded for cooling and heating as well as for both possible directions of poling. Since an unpolarised material should behave as an ideal capacitor, permittivity with even indices should be zero for small-signal measurements. As can be clearly seen from Fig. 4.5, ε_2 is rather non-zero above the upper transition temperature and while cooling. That could indicate a non-vanishing polarisation, favouring one direction. Further details will be discussed in 4.5.1.

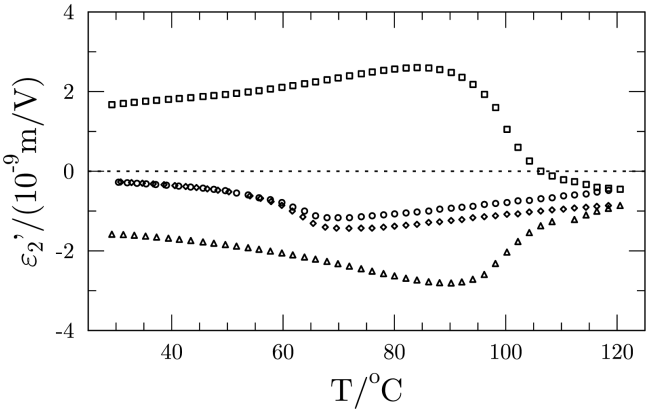

Figure 4.5: Real part of the non-linear permittivity ε_2' for a P(VDF-TrFE) 70/30 mol% ferroelectric thin film. The permittivity was recorded for both poling directions (up and down), for heating and cooling [87] ©2012 IEEE.

4.3 Thermal Hysteresis and Phase Transition Order in P(VDF-TrFE) 56/44 Thin Films

P(VDF-TrFE) with a molar fraction of 56/44 is known to undergo a ferroelectric to paraelectric phase transition of second order, e.g. [54] and Fig. 4.6 (right). If the VDF fraction is increased, the transition order will change to the first order, allowing metastable states and displaying a thermal hysteresis if the permittivity ε_1 versus temperature is plotted. An example is P(VDF-TrFE) with a molar fraction of 70/30 as depicted in Fig. 4.6 (left). Increasing the molar content of PVDF means, at the same time, increasing the crystallinity of the material and consequently the

size of crystallites pervading the semi-crystalline material.

As stated in [54], a semi-crystalline material like (thin) films of PVDF and its copolymers allows two mechanisms of realising zero remanent polarisation, as commonly displayed by unpoled films. One is to give the dipoles arranged in chains a random orientation, meaning the net dipole moment is zero. The second one is to decompose into domains, regions showing a uniform orientation. The domain structure is not to be confused with the crystalline structure. A polycrystalline material indeed allows single domain properties. Nevertheless, existence and size of the domains strongly depends on the size of the crystallites. As the temperature decreases below the transition point, domains start to grow and energy will be dissipated in order to move domain walls. The existence of latent heat in ferroelectric material is linked to the domain growth. Since larger domains will exist in films having a higher crystallinity ([63]), the latent heat, and therefore the size of the thermal hysteresis, will grow with crystallinity and VDF content until a limit is reached (Fig. 2.9).

These mechanisms are certainly true for thick films, when the thickness of the film significantly exceeds the thickness of the contact layer. They might be influenced by other phenomena if the film's thickness decreases significantly and approaches the size of the dead-, interface- or metal layer, with the latter representing the electrodes sandwiching the thin film(s). A clear sign of such phenomena superimposing bulk material mechanisms can be observed by studying the non-linear dielectric permittivities. In order to compare thick film properties with those exhibited by thin films, results published earlier in a PhD-thesis [62] have been used. For the experiments published in [62] not only the same materials, but also the same batches of copolymer were used.

For comparison only the first-order linear, or as it is sometimes called the 0th-order non-linear permittivity ε_1 will be considered. Regarding the shift of the transition temperatures and the appearance of a thermal hysteresis, the third-order non-linear permittivity ε_3 will follow the behaviour of other permittivities having odd indices, i.e. ε_1. As can be seen from the comparison of Fig. 4.6 upper part and Fig. 4.7, transition temperatures for the heating cycles are shifted by approximately 5°C. While the shift in P(VDF-TrFE) 70/30 (Fig. 4.7, left) might partially originate from

a pre-polarisation visible from the different start- and end values, as reported in [62], the shift in P(VDF-TrFE) 56/44 (Fig. 4.7, right) also appears in an unpoled sample. The result of the shift for one direction of the cycle, i.e. the heating cycle, introduces a thermal hysteresis. Since the appearance of the same is considered to be a sign for a first-order phase transition, the type of transition must have been changed for thin films, as suggested by Qu and co-workers in [65]. Ong and co-workers [57] where not convinced of Qu's argument. They have shown, that equations and therefore solutions for supercooling and superheating temperatures are equal, clearly indicating a second-order phase transition. The thermal hysteresis recorded for heating and cooling cycles might therefore not originate from latent heat, caused by domain wall motion.

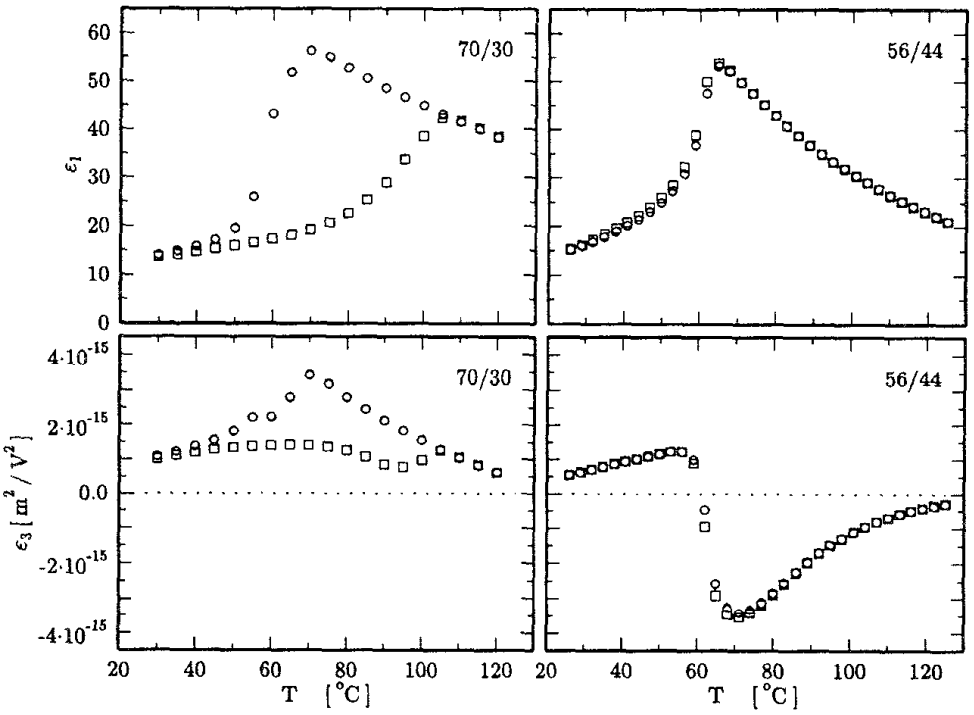

Figure 4.6: First- and third-order permittivity of a 70/30 mol% (left column) and a 56/44 mol% (right column) P(VDF-TrFE) thick film (thickness a few μm). The film was measured in a heating (□) and in a cooling (○) cycle [27].

As derived in 2.4.3, the third-order non-linear permittivity ε_3 in the paraelectric phase is directly connected to the second Landau parameter γ by

$$\varepsilon_0\varepsilon_3 = -\gamma/\alpha^4 \tag{4.2}$$

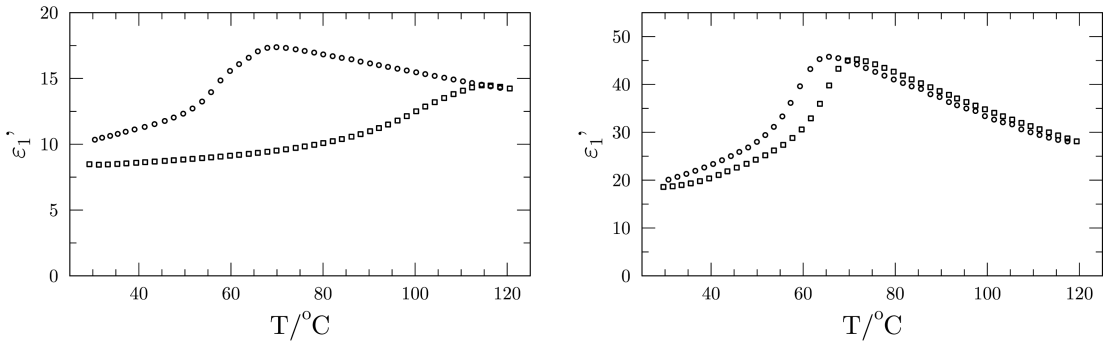

Figure 4.7: Real part of ε_1 as a function of temperature of a 175 nm thick 70/30 mol% (left) and a 200 nm thick 56/44 mol% (right) P(VDF-TrFE) thin film in a heating (□) and cooling (○) cycle (similarly published in [90]).

where γ and ε_0 are considered to be temperature-independent values. Since the vacuum permittivity ε_0 and any number with an exponent x being an even integer are always positive, the signs of γ and ε_3 are directly related to each other. Furthermore, one knows from theory that the free energy F of a second-order phase transition can be described by equation (2.9) with a positive γ. The third-order non-linear permittivity ε_3 should therefore be negative in the paraelectric phase. For a first-order phase transition the opposite is true, γ will be negative and ε_3 will be positive. According to the pre-conditions used in chapter 2, all this is true for the paraelectric phase.

Comparing the results for thicker films with the results of the measurements conducted for this work for ε_1 and ε_3 of a P(VDF-TrFE) 56/44 thin film (Fig. 4.8), one can clearly see that although ε_1 exhibits a thermal hysteresis, suggesting a change of the transition order from second, known for bulk material, to first, ε_3 stays negative in the paraelectric phase. This indicates, that also the sign of the Landau parameter γ does not change. This could furthermore lead to the conclusion, that the origin of the thermal hysteresis observed for the temperature plot of ε_1 is a non-vanishing polarisation in some parts of the film, e.g. close to the surface, rather than a change in the phase transition order.

The situation becomes different, if the film thickness is further reduced. As displayed in Fig. 4.9, the thermal hysteresis can be observed for both, a 130 nm (left) and a 30 nm (right) unpoled thin film of 56/44 mol% P(VDF-TrFE). In the lower line of the figure, the comparison of ε_3 for both thicknesses shows that for the thinner

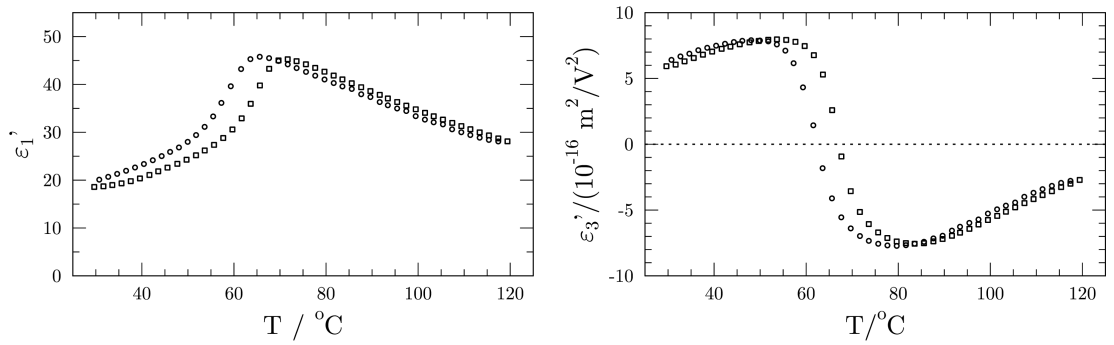

Figure 4.8: Real parts of ε_1 and ε_3 of a 200 nm thick 56/44 mol% P(VDF-TrFE) thin film in a heating (□) and cooling (○) cycle (similarly published in [90]).

30 nm film the behaviour of ε_3 changes. While alternating its sign in the paraelectric phase for the 130 nm film, the 30 nm film displays a positive ε_3 throughout the measured temperature range, including the paraelectric phase.

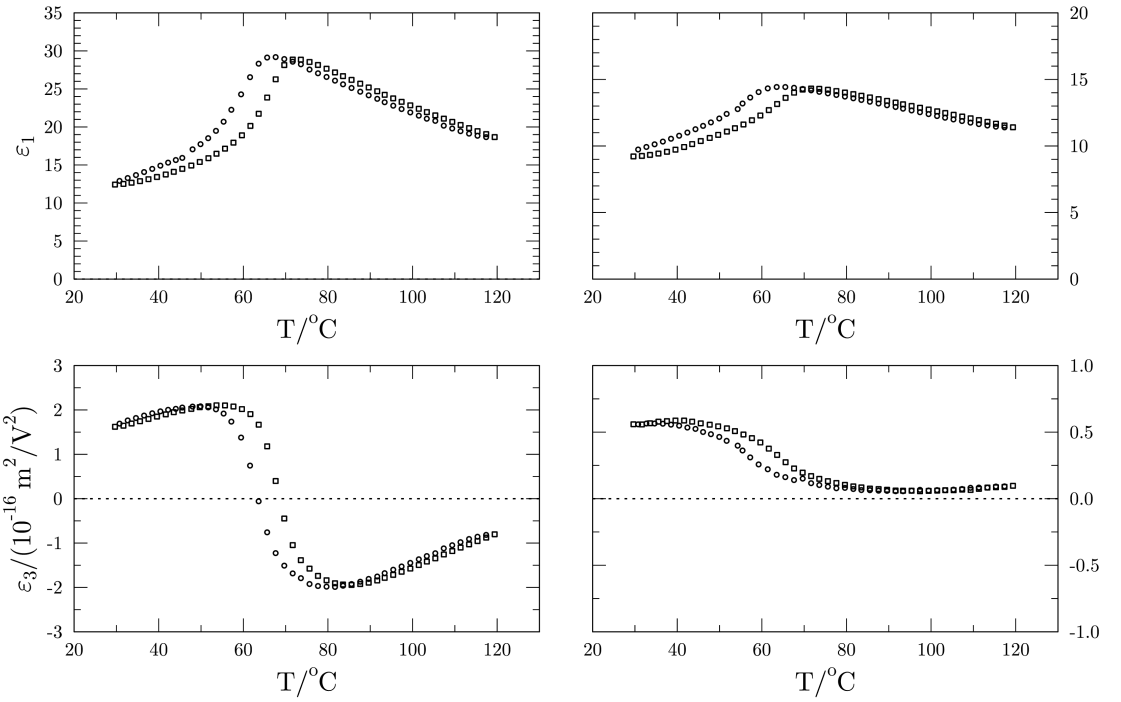

Figure 4.9: Real parts of ε_1 and ε_3 of a 130 nm (left) and a 30 nm (right) 56/44 mol% P(VDF-TrFE) thin film in a heating (□) and cooling (○) cycle. Both unpoled.

The origin of this behaviour could not been clarified yet. As will be shown in section 4.4.2, the energy difference J between the trans- and gauche phase is thought to have a significant impact in the transition behaviour. While theory predicts a first-order phase transition for negative values of J, positive values of J are assigned

to a second-order phase transition. Due to reasons emphasised in [55], e.g. the neglected dependence of Gibbs free energy on the lattice spacing, the phase transition of P(VDF-TrFE) 56/44 could be of first order instead, independent of the sign of J. This is the case, if the resulting electrostrictive coupling coefficient is sufficient in size. This conclusion would also explain the appearance of a thermal hysteresis in the discussed results. It does however, not explain the change in the behaviour of ε_3. Following Odajima's argumentation in [55], the latter should stay positive throughout the measurements, independent of the film thickness. It seems therefore advisable, to consider additional terms in further studies.

4.4 Interface-Related Effects in Ferroelectric Thin Films of P(VDF-TrFE)

The impact of surfaces and interfaces on the properties of the ferroelectric to paraelectric phase transition has been emphasised and discussed extensively (e.g. [37], [76]). In order to include the inevitable impact in the phenomenological approach, the change of polarisation close to the surfaces or interfaces has to be included. As motivated in [76], the common approach to the free energy F can be extended by a term considering the change of polarisation between bulk and surface as well as the surface polarisation itself

$$F/A = \int_{-t/2}^{t/2} dz \left\{ \frac{1}{2}\alpha P^2 + \frac{1}{4}\gamma P^4 + \frac{1}{2}\kappa \left(\frac{dP}{dz}\right)^2 \right\} + \frac{1}{2}\kappa\delta^{-1}\left(P_-^2 + P_+^2\right). \tag{4.3}$$

Without depolarisation fields and with strong interactions close to or within the surface layer, the extrapolation length is negative $\delta < 0$ and the transition temperature T_C of the surface layer is higher than the bulk transition temperature $T_{\mathrm{c}0}$ [37]. If non-negligible depolarisation fields being non-parallel to the surface occur, T_C will be found equal to $T_{\mathrm{c}0}$ [37]. In thin films of VDF-TrFE copolymers however, the finite size of the charge distribution in the metal electrodes sandwiching the film or bilayer will give rise to a depolarisation field partially compensated by the formation

of domains. Size, shape and switching dynamics of these domains however, strongly depend on the nature of the interface connected [25]. The appearance of an oxide layer at some electrodes and the mismatch associated with the substrate may lead to additional asymmetries.

Polarisation profiles of thin P(VDF-TrFE) films have been measured and described by Ploss and Smykalla in [71]. The material used for their samples has been taken from the same batches of P(VDF-TrFE) 56/44 and P(VDF-TrFE) 70/30 as the material used for the experiments in this work. In order to record a polarisation depth profile of a 40 μm thick bilayer, the pyroelectric current has been measured using the LIMM method. The first results displayed in Fig. 4.10 suggest, that the polarisation measured at the electrodes is significantly lower as the bulk polarisation. The very low pyroelectric current measured in this region could originate from dead dielectric layers as well as from layers having a high fraction of non-switchable polarisation. The polarisation in the vicinity of the electrodes on the other hand, experiences a sharp rise followed by a sharp drop, reaching a plateau representing the bulk polarisation value.

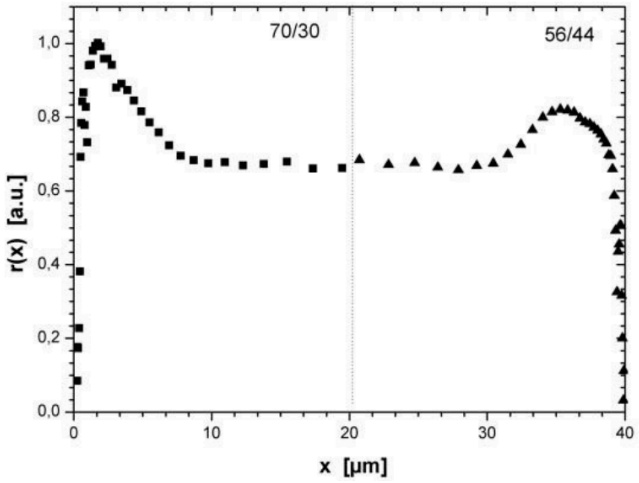

Figure 4.10: The spatial distribution of the pyroelectric coefficient $r(x)$ of a 40 μm thick VDF-TrFE bilayer of molar ratios 70/30 and 56/44 after electrode poling [71].

What can be derived from the results discussed so far is that depolarisation fields or static electric fields, which are always present in ferroelectric thin films, have a non-negligible impact on the thin film properties, i.e. on its polarisation. Therefore, the following sections will be attributed to the calculation of the existing field as

well as an evaluation of the impact of such a static electric field on the polarisation.

4.4.1 Shift of Transition Temperature

According to [8], a depolarisation field will cause a shift of the bulk transition temperature T_0 to $T^\star$, which is the films transition temperature. This change can be calculated using

$$T^\star = T_0 - \frac{\lambda}{\varepsilon_0 \varepsilon_\mathrm{e}\, d\, \beta} \tag{4.4}$$

where λ is the screening length, ε_e is the permittivity of the electrode material, d is thickness of the ferroelectric material and β is a positive, real number scaling the linear change of the first Landau parameter α under varying temperatures

$$\alpha = \beta\,(T - T_0)\,. \tag{4.5}$$

The permittivity of the metal $\varepsilon_0\varepsilon_\mathrm{e}$ can be assumed to be equal to ε_0, resulting from the following considerations. The Drude model, which can be used to describe the motion of electrons within a metal, can be written as

$$\dot{p} + \frac{p}{\tau} = -eE. \tag{4.6}$$

A possible solution for this linear equation of 1st order is

$$p(t) = p_0 e^{-i\omega t}. \tag{4.7}$$

Substituting solution 4.7 in equation (4.6) and assuming a harmonic excitation with $E = E_0 e^{-i\omega t}$ one gets

$$\frac{d(p_0 e^{-i\omega t})}{dt} = -\frac{p_0 e^{-i\omega t}}{\tau} - eE_0 e^{-i\omega t}, \tag{4.8}$$

which is

$$-i\omega p_0 = -\frac{p_0}{\tau} - eE_0. \tag{4.9}$$

Furthermore, it is known that the electronic current density j and the DC conductivity σ_0 are defined as

$$a) \quad j = -nev \quad \text{and} \quad b) \quad \sigma_0 = \frac{ne^2\tau}{m}, \tag{4.10}$$

respectively. Inserting equation (4.9) into equation (4.10) part a) and taking 4.10 part b) into account, the current density is given by

$$j = -\frac{\sigma_0}{1 - i\omega\tau} E_0 \tag{4.11}$$

where

$$\frac{\sigma}{1 - i\omega\tau} = \sigma(\omega). \tag{4.12}$$

Finally Ohm's law can be derived as

$$j = \sigma(\omega) E_0. \tag{4.13}$$

From equation (4.12) one can see that σ is a complex number, i.e.

$$\sigma = \sigma' + i\sigma''. \tag{4.14}$$

With Ohm's law, the relation between the dielectric displacement D and the applied electric field E

$$D = \varepsilon_0 \varepsilon(\omega) E \quad and \quad dD/dt = j \tag{4.15}$$

one can find the relation between the conductivity σ and the permittivity ε which is

$$\sigma = i\omega\varepsilon_0\varepsilon. \tag{4.16}$$

Knowing that aluminium has a relaxation time τ in the order of 10^{-14}s one can derive from equation (4.12) that $\sigma_e(\omega)$ is basically equal to the DC conductivity σ_0 and can

be considered as a real number. The permittivity is a pure imaginary number then and $\varepsilon_0\varepsilon_e$ is equal to ε_0. The screening length λ of the electrode is 45 pm according to [10]. Landau parameters have been calculated for a thin film of P(VDF-TrFE) with a molar fraction of 56/44 (Fig. 4.11 and Fig. 4.12) using the relation derived in section 2.4.3. The slope α_0 can be calculated using equation (4.5).

$$\beta = \frac{\mathrm{d}\alpha}{\mathrm{d}T} \quad \text{for} \quad T > T_0. \tag{4.17}$$

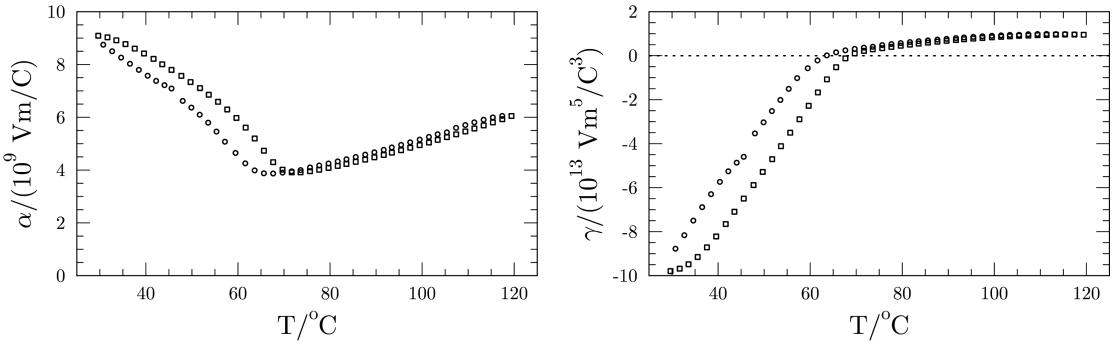

Figure 4.11: Landau parameters α and γ of a 200 nm thick 56/44 mol% P(VDF-TrFE) thin film in a heating (□) and cooling (○) cycle.

The first Landau parameter α has been modelled using previous calculations displayed in Fig. 4.12. Determining β, which is the slope of the line plotted in Fig. 4.12, leads to a similar result as observed in studies of thicker films of 56/44 VDF-TrFE copolymer [62]. Assuming a β of $3 \cdot 10^7$ Vm/(KC) and a thickness of 200 nm, the

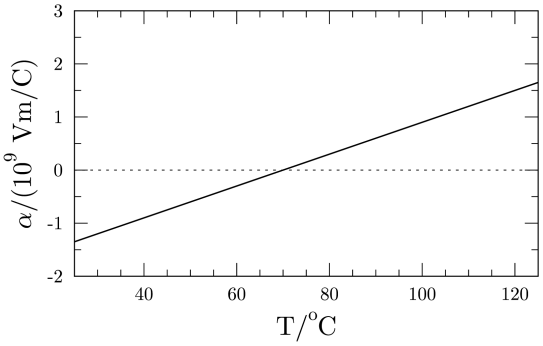

Figure 4.12: The first Landau parameter α modelled for a 200 nm thick 56/44 mol% P(VDF-TrFE) thin film.

transition temperature will be shifted by

$$T^{\star} = T_0 - \frac{45 \cdot 10^{-12}\,\mathrm{m}}{8.854 \cdot 10^{-12}\,\mathrm{Fm^{-1}} \cdot 200 \cdot 10^{-9}\,\mathrm{m} \cdot 3 \cdot 10^{7}\,\mathrm{Vm(KC)^{-1}}} = T_0 - 0.85\,\mathrm{K} \quad (4.18)$$

according to equation (4.4). As can be seen in Fig. 4.8, the shift is usually larger the the calculated $T_0 - 0.85\,\mathrm{K}$, exceeding 5 K, indicating that there are more mechanisms, other than screening, present in thin films of P(VDF-TrFE). One of them will be introduced in the following paragraphs.

Another approach is to start with the transition temperature shift observed in the results, in order to estimate the field present. By using equation

$$(T_{\mathrm{Peak}} - T_0) = \frac{3}{4}\left(\frac{4\gamma}{\beta^3}\right)^{1/3} E^{2/3} \quad (4.19)$$

derived in [45, pp. 171-172], the electric field can be directly calculated. After rearranging the equation with regard to the electric field E, one gets

$$E = \left(\frac{4 \cdot (T_{\mathrm{Peak}} - T_0)}{3\left(\frac{4\gamma}{\beta^3}\right)^{1/3}}\right)^{3/2} . \quad (4.20)$$

Substituting the physical quantities by the values determined for P(VDF-TrFE) thin films of a few μm in thickness in [62], one has to calculate

$$E = \left(\frac{4 \cdot 5\,\mathrm{K}}{3\left(\frac{4 \cdot 1 \cdot 10^{12}\,\mathrm{Vm^5C^{-3}}}{\left(3.3 \cdot 10^{7}\,\mathrm{Vm(KC)^{-1}}\right)^3}\right)^{1/3}}\right)^{3/2} . \quad (4.21)$$

Solving the equation, the field calculated is approximately $1.6 \cdot 10^6\,\mathrm{V/m}$. Considering the fact, that large fractions of the depolarisation field will be compensated by the formation of domains as well as by free charge carries available in the sample, the calculated value is of plausible size. Furthermore, the calculated field is lower than the coercive field measured in P(VDF-TrFE) thin films and lower than the electric field values used for in the non-destructive permittivity measurements.

Besides a shift of transition temperatures resulting in a thermal hysteresis and an impact on the shape of the thin film's polarisation profile, with the latter being a possible origin if the first, constant electric fields are known to have an impact on the remanent polarisation as a function of the temperature $P_{\mathrm{R}}(T)$. This possible impact will be discussed in the following section.

4.4.2 The Effect of a Constant Electric Field on P(T) for a Second-Order Phase Transition

It has been observed in the measurements, that the polarisation in multilayers, assembled of single layers with different compositions of P(VDF-TrFE), tends to change linearly with increasing temperature rather than showing the $\sqrt{(T_{\mathrm{C}} - T)}$ -behaviour predicted by theory. This might be attributed to an additional field, present in multilayers of different compositions.

As stated in [12] and [45], an external electric field of whatever nature has a considerable impact on the polarisation behaviour, i.e. close to the transition temperature. As discussed in the preceding sections, such a field can lead to a shift in the transition temperature and to the presence of a thermal hysteresis. Another effect is the blurring of the phase transition, making it rather continuous than discontinuous. In order to derive the polarisation as a function of the temperature for different electric fields, one can start with the common approach of a thermodynamic potential as used in equation (2.9)

$$F(D,T) = \frac{1}{2}\alpha D^2 + \frac{1}{4}\gamma D^4 - ED\,. \tag{4.22}$$

In order to simplify the calculation, only the linear and the non-linear terms up to D^4 will be considered. From the equation above one can derive

$$\frac{\partial F(D,T)}{\partial D} = \alpha\, D + \gamma\, D^3 - E\,. \tag{4.23}$$

At $\partial F/\partial D = 0$ the dielectric displacement D is equal to the spontaneous polarisation

P_S, so that

$$0 = \alpha\, P_S + \gamma\, P_S^3 - E \tag{4.24}$$

with $\alpha = \beta(T - T_C)$ and β as well as γ being positive constants for a second-order phase transition. Assuming zero electric field, the polarisation can be calculated by rearranging equation (4.23) and excluding the trivial solution $P_S = 0$

$$P_S{}^2 = -\frac{\alpha}{\gamma} \quad and \quad P_S{}^2 = -\frac{\beta(T - T_C)}{\gamma}\,. \tag{4.25}$$

If the electric field is non-zero however, the calculation becomes more complex. In order to simulate the impact of a static electric field on the thermal behaviour of the polarisation, the equation has to be set up as polarisation P as a function of temperature T under different constant electric fields E. Using *Maxima* to analytically resolve the equation one gets

$$P = \left(\frac{\sqrt{\frac{27E^2\gamma+4\alpha^3}{\gamma}}}{23^{\frac{3}{2}}\gamma} + \frac{E}{2\gamma}\right)^{\frac{1}{3}} - \frac{\alpha}{3\gamma\left(\frac{\sqrt{\frac{27E^2\gamma+4\alpha^3}{\gamma}}}{23^{\frac{3}{2}}\gamma} + \frac{E}{2\gamma}\right)^{\frac{1}{3}}}\,. \tag{4.26}$$

In order to simplify equation (4.26), the coefficients β and γ have been treated as constants with values taken from [62] (films of a few μm in thickness). Coefficients determined for films with a higher thickness were thought to be more appropriate for general calculations, avoiding an overlap with phenomena apparent in thinner films. Equation (4.24) then reappears as

$$0 = 3.3 \cdot 10^7\,\mathrm{Vm(KC)^{-1}}(T - T_C)\, P_S + 1 \cdot 10^{12}\,\mathrm{Vm^5C^{-3}}\, P_S^3 - E\,. \tag{4.27}$$

and equation (4.26) then simplifies to

$$P = \left(\frac{\sqrt{5.324 \cdot 10^9\,\mathrm{V^2m^{-2}K^{-3}}(T-T_\mathrm{C})^3 + E^2}}{2 \cdot 10^{12}\,\mathrm{Vm^5C^{-3}}} + \frac{E}{2 \cdot 10^{12}\,\mathrm{Vm^5C^{-3}}} \right)^{\frac{1}{3}} - \frac{11\,\mathrm{C^2K^{-1}m^{-4}}(T-T_\mathrm{C})}{1 \cdot 10^6 \left(\frac{\sqrt{5.324 \cdot 10^9\,\mathrm{V^2m^{-2}K^{-3}}(T-T_\mathrm{C})^3 + E^2}}{2 \cdot 10^{12}\,\mathrm{Vm^5C^{-3}}} + \frac{E}{2 \cdot 10^{12}\,\mathrm{Vm^5C^{-3}}} \right)^{\frac{1}{3}}} . \tag{4.28}$$

An equivalent approach might has been used in [46]. Although the equation was not mentioned in the publication, printing equation (4.28) in (Fig. 4.14) leads to a similar result as shown in the graphs in Fig. 4.13. Analysing the latter, one can clearly see irregularities for lower fields and lower temperatures. The origin of these can be derived form equation (4.28). For lower fields, the term $5.324 \cdot 10^9\,\mathrm{V^2m^{-2}K^{-3}}(T-T_\mathrm{C})^3 + E^2$ within the square root becomes negative and therefore, its solution is complex. In order to avoid missing results, Mr. Lu and co-workers might have chosen to use the absolute which leads to a gap-free graph as depicted in Fig. 4.13 (Lu) and Fig. 4.14 (right, own calculations).

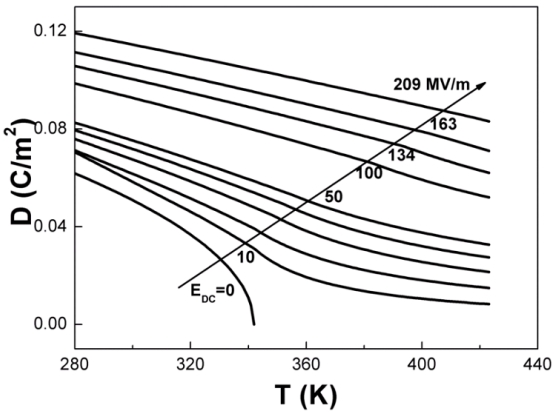

Figure 4.13: Polarisation versus temperature relationships with various DC biases for 55/45 copolymer [46].

In order to analyse the problem and find a gap-free solution, one can start with the more general explanation used in equation (4.26). The term $(27E^2\gamma + 4\alpha^3)/\gamma$ generally assembles the term $5.324 \cdot 10^9\mathrm{V^2m^{-2}K^{-3}}(T-T_\mathrm{C})^3 + E^2$ analysed in the paragraph above. Since α contains a linear dependence on the temperature T with

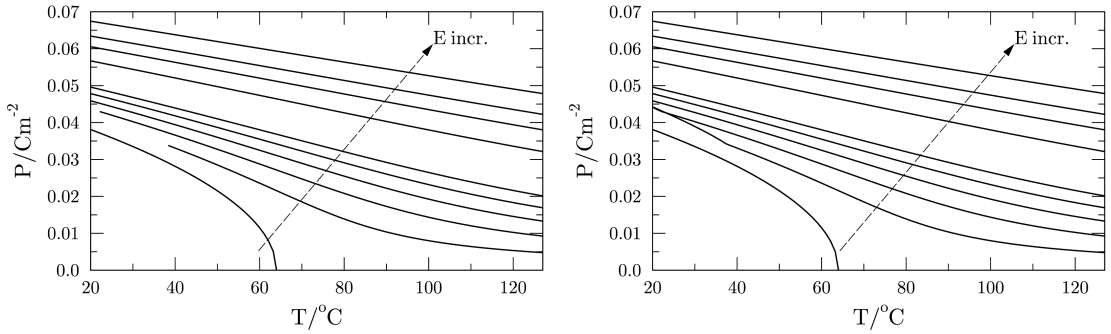

Figure 4.14: Polarisation versus temperature calculated for increasing DC biases (increase indicated by arrow, values equal to [46]) for 55/45 mol% P(VDF-TrFE). Left graph without using the absolute values within the square route.

$\alpha = \beta(T - T_C)$, the function containing α^3 can be considered hyperbolic, while the applied field E is shifting the intersection with the ordinate. If E is chosen sufficiently high, all values for positive (above T_C) or negative (below T_C) factors $(T - T_C)$ and therefore the whole term will be positive, even for temperatures far below T_C, e.g. at room temperature for E equal to 80 MV/m (Fig. 4.15).

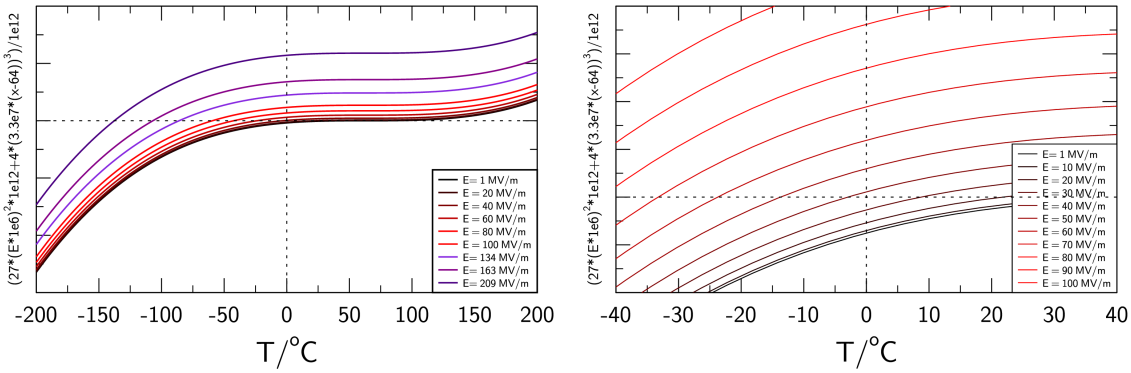

Figure 4.15: The term $(27E^2\gamma + 4\alpha^3)/\gamma$ for different electric fields and a positive γ. Right: magnified in the vicinity of the origin.

At this point it seems advisable to note that the value of 80 MV/m is approximately the size of the coercive field present in ferroelectric thin films of P(VDF-TrFE). Therefore, a calculation leading to a constant electric field of this size, penetrating through the whole thin film needs further consideration. A potential ansatz is to question the temperature-independent γ.

Considering $(27E^2\gamma + 4\alpha^3)/\gamma$ in equation (4.26), one can easily determine when $27E^2\gamma$ outruns $4\alpha^3$. Close to the transition temperature β is equal or bigger than

α. If β is in the order of $3.3 \cdot 10^7\,\mathrm{Vm(KC)^{-1}}$, as emphasised earlier, then $4\alpha^3$ is about $3.5 \cdot 10^{23}\,\mathrm{V^3m^3C^{-3}}$. If γ is $1 \cdot 10^{12}\,\mathrm{Vm^5C^{-3}}$, $27\,E^2$ has to be in the order of $1 \cdot 10^{11}\,\mathrm{V^2m^{-2}}$ in order to gain an approximately equal result for both therms. Considering a static electric field in the order of $1.6 \cdot 10^6\,\mathrm{V/m}$ as calculated earlier, the term $27E^2\gamma$ would be already approximately $500 \cdot 4\alpha^3$. Assuming a temperature-independent γ, the temperature dependence of $(27E^2\gamma + 4\alpha^3)/\gamma$ can therefore be neglected for fields exceeding a certain value, e.g. some MV/m. The polarisation P in equation (4.26) will solely depend on $-\alpha$ or $\beta(T - T_\mathrm{C})$, respectively. Further decreasing the temperature at a constant, small field will cause a domination off $4\alpha^3$ and therefore lead to complex results and the aforementioned incomplete graphs displayed in Fig. 4.14 (left). Further increasing the applied electric field will straighten the graph resulting in a line with a negative slope (Fig. 4.14), because the shape of the graph will again solely depend on $-\alpha$.

In order to achieve a stable and non-complex solution, gamma can be chosen to be negative in the ferroelectric phase, as emphasised in [62]. Therefore, the sign of the hyperbolic function will be switched for negative values of $T < T_\mathrm{C}$ as depicted in Fig. 4.16. If considering the unbiased case with E equal to zero and $P_\mathrm{S}^2 = -\alpha/\gamma$, a negative γ would lead to a complex solution, since $P^2 < 0$ is only true for complex numbers.

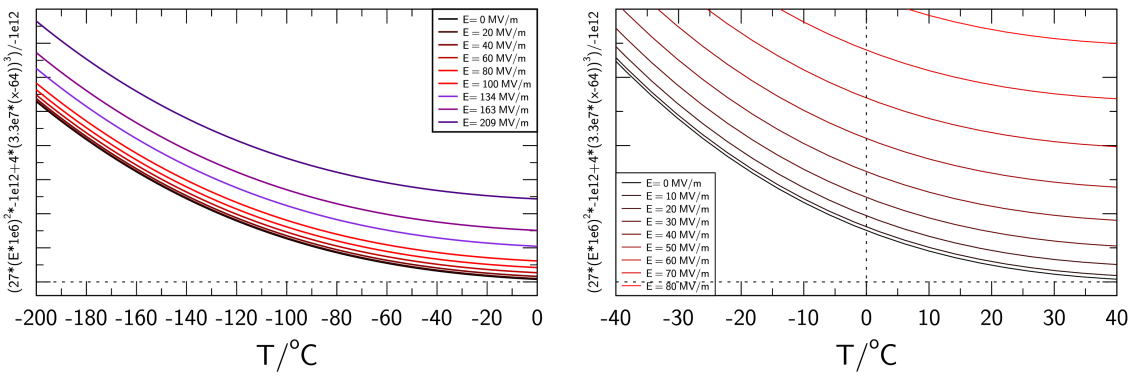

Figure 4.16: The term $(27E^2\gamma + 4\alpha^3)/\gamma$ for different electric fields and a negative γ. Right: magnified in the vicinity of the origin.

Lu and co-workers [46] additionally considered the field dependence of T_C. Since a consideration of the same would only change the slope of the graph, but would have no influence on its shape, it was neglected in the calculations presented here.

Another way to get information on the Landau parameters can be derived from an approach published by Odajima and co-workers [55]. As shown in chapter 2, the ansatz is based on statistical mechanics. Following this approach, all parameters depend on the temperature in a non-linear fashion with

$$\begin{aligned}
\alpha &= \left(\frac{kT}{\mu}e^{-J/kT} - \frac{zA}{2\mu}\right)/N\mu\,, \\
\gamma &= \frac{kT}{\mu}e^{-J/kT}\frac{1}{2}\left(1 - \frac{1}{3}e^{-2J/kT}\right)/(N\mu)^3 \quad \textit{and} \\
\delta &= \frac{kT}{\mu}e^{-J/kT}\frac{3}{4}\left(\frac{1}{2} - \frac{1}{3}e^{-2J/kT} + \frac{1}{10}e^{-4J/kT}\right)/(N\mu)^5\,.
\end{aligned} \tag{4.29}$$

This approach will be used to re-plot Fig. 4.14. Therefore, the parameters in equation (4.26) can be substituted by the parameters derived from Odajima's approach. For the sake of simplicity the Landau parameters in equation (4.24) will be substituted before transposing it, in order to find an expression for the spontaneous polarisation P_S as a function of temperature T for different electric fields E

$$0 = \frac{1}{N\mu}\left(\frac{kT}{\mu}e^{-J/kT} - \frac{zA}{2\mu}\right)P_\mathrm{S} + \frac{1}{(N\mu)^3}\frac{kT}{\mu}e^{-J/kT}\frac{1}{2}\left(1 - \frac{1}{3}e^{-2J/kT}\right)P_\mathrm{S}^3 - E \tag{4.30}$$

For plotting equation (4.30), it is necessary to determine the quantities contained. The dipole moment of P(VDF-TrFE) can be calculated considering the different molar fractions of VDF and TrFE

$$\mu_{\mathrm{P(VDF-TrFE)}} = x_\mathrm{VDF}\cdot\mu_\mathrm{VDF} + (1 - x_\mathrm{VDF})\cdot\mu_\mathrm{TrFE}\,. \tag{4.31}$$

With monomers having a dipole moment of $\mu_{\mathrm{m,VDF}} = 7\cdot10^{-30}\,\mathrm{Cm}$ and $\mu_{\mathrm{m,TrFE}} = 3.5\cdot10^{-30}\,\mathrm{Cm}$, the dipole moment of the copolymer is $\mu_{56/44} \approx 5.5\cdot10^{-30}\,\mathrm{Cm}$ following equation (4.31). As pointed out in [18], the unit cell of PVDF consists of 5 dipolar units, one in the center and the other 4 cornering the cell. The resulting dipole moment is therefore $\mu_\mathrm{cell} = \mu_\mathrm{m} + 4\cdot\mu_\mathrm{m}/4 = 2\,\mu_\mathrm{m}$. The volume of the unit cell is $V_\mathrm{cell} = 0.256\,\mathrm{nm}\cdot0.858\,\mathrm{nm}\cdot0.491\,\mathrm{nm} = 0.108\,\mathrm{nm}^3$. The dipole density is therefore

$18/\mathrm{nm}^3$ for pure PVDF. Considering the unit cell measures published in [75], the number of monomers per volume N_m for P(VDF-TrFE) with a molar fraction of 56/44 is approximately $16/\mathrm{nm}^3$. According to Odajima's theory, a dipole moment is assigned to each lattice point represented by a carbon atom in a chain or in a crystal. The number N_m therefore doubles while the dipole moment is half of the value calculated earlier: $N = N_\mathrm{m} \cdot 2 = 32/\mathrm{nm}^3$ and $\mu = \mu m/2 = 2.75\,\mathrm{Cm}$. Assuming the intersection of the Landau parameter α with the temperature axis is equal to the transition temperature $\alpha(T_0) = 0$, the interchain interaction energy zA can be described by $zA = 2kT_0 e^{-J/kT_0}$. As emphasised in [64], Odajima's theory does not include the effects of domain wall motion. Therefore, T_0 has to be chosen to match the value of a poled sample, which is 72°C for P(VDF-TrFE) 56/44.

Discussing the energy difference J is a rather complex matter. The energy difference J between (all-)trans and (trans-)gauche bondings for P(VDF-TrFE) has been determined for different compositions using different methods. In their measurements and calculations B.Ploss and B.Ploss ([62], [64]) used measurements of the dielectric non-linearities to determine $J = u_\mathrm{G} - u_\mathrm{T}$ and compared them with the results published by Tashiro and co-workers, who used infrared absorbance measurements to calculate $\Delta u = u_\mathrm{TT} - u_\mathrm{TG}$ [75]. Since all energy values are positive, there should be just a difference in the sign using the two equations. Nevertheless, while the results for measurements of the 70/30 P(VDF-TrFE) thin films reproduced Tashiro's results well, the measurements of the 56/44 P(VDF-TrFE) thin films deviated significantly. Using the dielectric non-linearities measurement yields a value of $-1.52\,\mathrm{kJ/mol}$ for P(VDF-TrFE) with a molar fraction of 56/44, while the infrared absorbance yields a value of $6.4\,\mathrm{kJ/mol}$ (sign corrected). Following Odajima's theory, the first negative value indicates a first-order phase transition. The value measured by Tashiro and co-workers indicates a second-order phase transition instead, since J is clearly positive. Although Tashiro's results meet Odajima's predictions, the latter brought up the issue that experimental results have shown that P(VDF-TrFE) with a molar composition if 56/44 shows the behaviour of a first-order phase transition rather than second-order phase transition properties. Odajima argues, that the electrostrictive term has to be included in the calculation, since the material is

not confined in all the directions. The volume can therefore change, changing the lattice spacing as well, or vice versa. While the measurements suggest a change in sign of ε_3 for thicker films, the values stayed positive throughout the measured temperature range for thinner films, as shown in Fig 4.9. The latter would indicate a negative γ as expected for a first-order phase transition and as plotted using a trans-gauche energy difference smaller than zero ($J < 0$). Using $J = 6.4\,\mathrm{kJ/mol}$ to plot γ gives positive values only (Fig. 4.17), which indicates a second-order phase transition according to Odajima's theory. In order to decide in favour of one value for the calculations, one has to consider the measurement results gained from thicker films of 80 nm and more. Firstly, ultra-thin films pose a special case not covered by the theory used here. And secondly, using $J = -1.52\,\mathrm{kJ/mol}$ ([62], [64]) produces a γ changing the sign in the vicinity of the phase transition (Fig. 4.17) equal to what has been derived from the ε_3-measurements in Fig. 4.9 (bottom left). And finally, this particular result was gained using the same measurement technique used in [62] to measure the dielectric non-linearities.

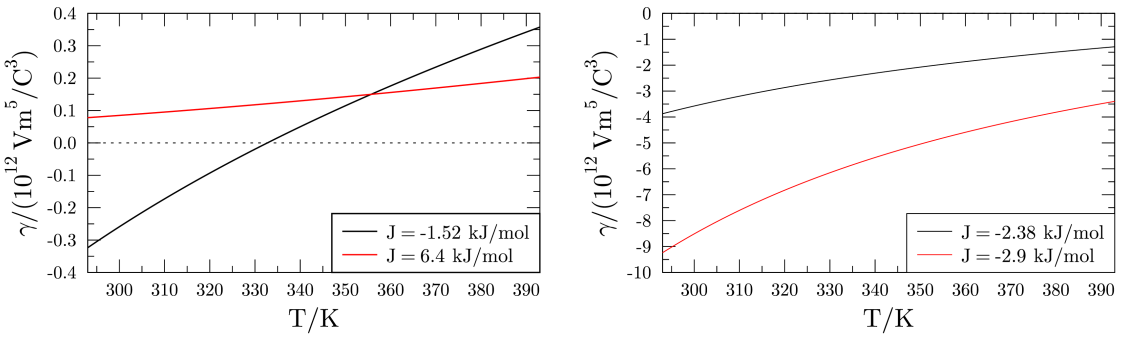

Figure 4.17: Landau's parameter γ for different compositions of P(VDF-TrFE) and different measurement techniques. Similar compositions plotted in one diagram. P(VDF-TrFE) 56/44 mol% (black line, [62], [64]) and 55/45 mol% (red line, [75]) left. P(VDF-TrFE) 70/30 mol% (black line, [62], [64]) and P(VDF-TrFE) 72/28 mol% (red line, [75]) right.

Resolving equation (4.30) with regard to P one gets

$$P = \left(\frac{\sqrt{-\frac{(8b^3-9E^2b)\,d^3-24b^2c\,d^2+(24b\,c^2+27E^2b)d-8c^3}{bd\,(d^2-3)}}}{a^3bd\;(d^2-3)} - \frac{3E}{a^3b\;(d^3-3d)} \right)^{\frac{1}{3}} + \frac{2bd-2c}{a^2b\;(d^3-3d)\left(\frac{\sqrt{-\frac{(8b^3-9E^2b)\,d^3-24b^2c\,d^2+(24b\,c^2+27E^2b)d-8c^3}{bd\,(d^2-3)}}}{a^3bd\,(d^2-3)} - \frac{3E}{a^3b\,(d^3-3d)} \right)^{\frac{1}{3}}} \tag{4.32}$$

with $a = 1/(N\,\mu)$, $b = k\,T/\mu$, $c = (z\,A)/(2n\mu)$ and $d = e^{(-J/(nkT))}$. Figure 4.18 shows the polarisation as a function of temperature for $J = -1.52\,\mathrm{kJ/mol}$ at different electric fields. As can be seen, the behaviour of the polarisation as a function of the temperature is completely different if Odajima's theory is used. Rather than displaying a decreasing polarisation with increasing temperature, the graph shows a polarisation continuously rising with a sharp increase close to the transition temperature of the unpoled samples, which is approximately 60°C. The point of discontinuity matches the null of γ displayed in Fig. 4.17.

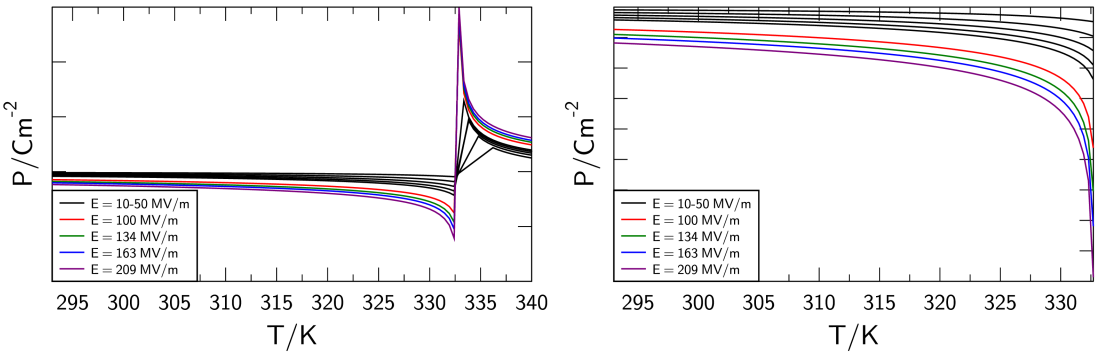

Figure 4.18: $P(T)$ for different electric fields ($J = -1.52\,\mathrm{kJ/mol}$, P(VDF-TrFE) 56/44 mol%).

The results discussed above, using the parameters gained through Odajima's theory should be the subject of further consideration. The result plotted in Fig. 4.18 does not match the expectations and more importantly does not give the expected result for a zero electric field. One possible reason is that the parameters gained though Odajima's theory have been used in an equation derived using the phenomenological approach. Therefore, it seems advisable to use Odajima's parameters with equation (2.22) rather than using them with equation (4.26).

4.5 Dielectric Non-Linearities and Ferroelectric Devices

4.5.1 Polarisation State from Non-Linearities

As derived in section 2.4.3, the polarisation state of the ferroelectric can be directly accessed by using the dielectric permittivities of first and second order, ε_1 and ε_2. Considering the given assumptions, e.g. that the Landau parameters γ and δ are temperature-independent, the calculated value is then directly proportional to the remanent polarisation. This method is non-destructive, highly sensitive and easy to implement, which makes it favourable for all kinds of measurements and applications. The polarisation can be plotted as a function of temperature as well as a function of time. A 3D-plot combining both variables would be of particular interest for the characterisation of materials for memory applications. As derived in section 4.2, the sign of the second-order permittivity ε_2 would be sufficient in order to determine the state of polarisation. The sign could then simply be assigned to ”0” or ”1” in order to define the states of a ferroelectric memory device.

Polarisation for Different Molar Compositions of P(VDF-TrFE)

Polarisation as a function of temperature has been determined for two types of copolymers having different molar ratios of VDF and TrFE, which are 70/30 and 56/44. It can be seen from Fig. 4.19, that the maximum value for the polarisation varies for different molar ratios. P(VDF-TrFE) with a molar ratio of 70/30 shows higher values of remanent polarisation than 56/44. The higher polarisation originates from a higher amount of dipoles present in PVDF. As suggested in [19], the remanent polarisation peaks at a molar fraction of PVDF approaching 80 %. Exceeding 80 % however, results in a loss of crystallinity and in a loss of the ferroelectric β-phase, barely present in unstrained PVDF. Increasing the amount of PVDF furthermore increases the transition temperature, as can be seen from Fig. 4.19. It has also been suggested to change the type of phase transition from second order for P(VDF-TrFE) 56/44 to first order for P(VDF-TrFE). The latter might be limited

to the deviations for thin films of P(VDF-TrFE) 56/44 discussed in section 4.3.

While the order of the phase transition is changed, the transition temperature for the cooling cycle stays constant. Polarisation starts to drop at approximately or even below 50°C for P(VDF-TrFE) with a molar fraction of 56/44. In P(VDF-TrFE) 70/30 the polarisation remains stable up to 80°C, far exceeding the working temperatures of commercially used memories, i.e. solid state drives. Furthermore, it can be seen that the polarisation is different for different directions of poling. The asymmetry partially originates from effects discussed in 4.4.

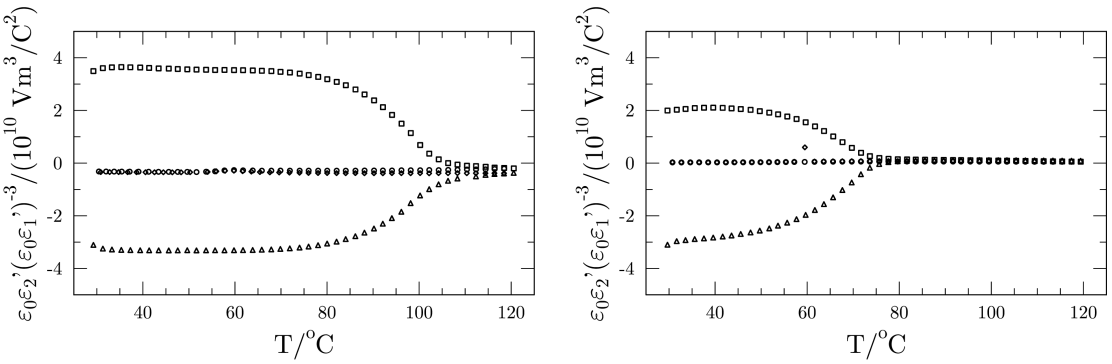

Figure 4.19: Comparison of two P(VDF-TrFE) thin films, left molar fraction of 70/30 and right molar fraction of 56/44, poled in both directions (□, △: heating, ○, ◇: cooling) (similarly published in [90]).

Non-Switchable Temperature-Independent Polarisation

As discussed before, phase transition temperatures were found to be higher in thin films, while the remanent polarisation was found to be smaller. If present, the thermal hysteresis is more pronounced. Additionally, a temperature-independent polarisation can be observed. As can be seen in Fig. 4.20 and its magnification Fig. 4.21, the term proportional to the remanent polarisation is non-zero after exceeding the transition temperature and throughout the cooling cycle. This non-switchable part of the polarisation is independent of the poling direction and appears to be approximately 10 % of the remanent polarisation measured in this films. In all measurements the non-vanishing polarisation vector points from the bottom to the top electrode. A non-switchable polarisation was also observed for thicker films of P(VDF-TrFE) with 56/44 mol% [62]. In the case of these thicker films the asymmetry has been

achieved by pre-poling the films before the annealing procedure. This however, has not been done intentionally in the measurements discussed here.

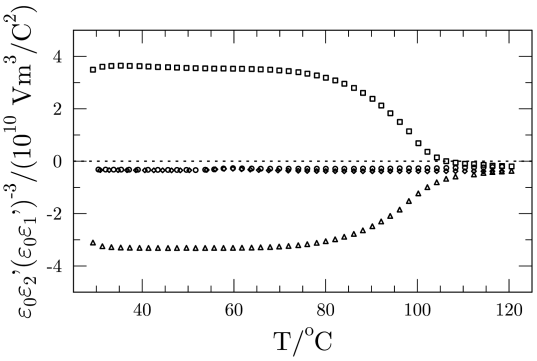

Figure 4.20: Remanent polarisation as a function of temperature for a 175 nm thin 70/30 mol% P(VDF-TrFE) film. The film was poled in both directions indicated by different symbols (□, △: heating, ○, ◇: cooling) [87] ©2012 IEEE.

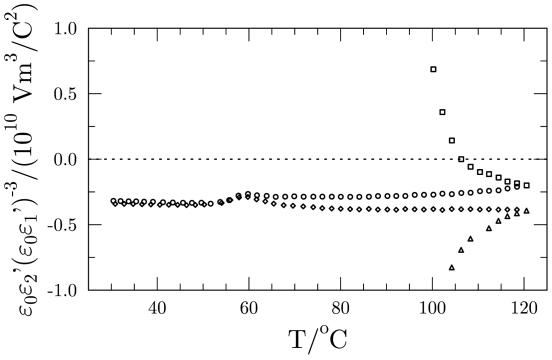

Figure 4.21: $\varepsilon_0\varepsilon_2'/(\varepsilon_0\varepsilon_1')$ as a function of temperature for a 175 nm thin 70/30 mol% P(VDF-TrFE) film (magnification Fig. 4.20) [87] ©2012 IEEE.

As published in [87], the non-vanishing, temperature-independent polarisation is proposed to originate from charges trapped at the surface and at the interface. These charges are commonly observed in lossy ferroelectrics. Considering that the polarisation vector has its origin on the bottom electrode and is pointing from negative charge to positive charge, this hypothesis can be approved or at least supported. The negative charges appear to be trapped at the bottom electrode. In order to estimate the field present, one can use Fig. 4.20 and Fig. 4.21 and hysteresis measurements published in [87] (Fig. 4.22). The dielectric displacement D for the film measured was approximately 60 mC/m^2. For $E = 0$ the dielectric displacement D is equal to P_R.

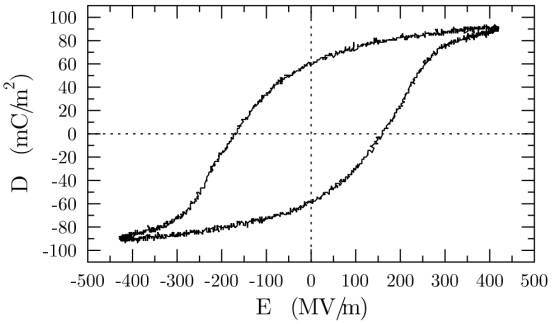

Figure 4.22: Hysteresis loop of dielectric displacement D as a function of the electric field E of a 175 nm thick 70/30 mol% thick VDF-TrFE copolymer film at 25°C [87] ©2012 IEEE.

In order to calculate the field for the remaining 10 % non-switchable polarisation, one can take the properties of the film measured in [87] and the linear equation

$$D = \varepsilon_0 \, \varepsilon_\mathrm{r} \, E \quad \text{and} \quad E = \frac{D}{\varepsilon_0 \, \varepsilon_\mathrm{r}} \, . \tag{4.33}$$

Filling equation (4.33) with numbers one gains

$$\frac{60 \cdot 10^{-3}}{10.25 \cdot 8.854 \cdot 10^{-12}} \quad \frac{\mathrm{CVm}}{\mathrm{m^2C}} \quad \approx \quad 661 \, \frac{\mathrm{MV}}{\mathrm{m}} \, . \tag{4.34}$$

The calculated field is rather high and therefore contradicts the requirements for the linear approximation used above. It seems advisable to use another approach to estimate the field present inside the film. Therefore, the hysteresis loop displayed in Fig. 4.22 can be linearised between the intersection with the D-axis and the E-axis. That does not exactly fit the graph in this part of the hysteresis, but sufficiently approximates the wanted field. In order to estimate this field one can, in the case of the linear approximation, take 10% of the coercive field, which is approx 15 MV/m. The same value will be achieved, if the hysteresis curve in the vicinity of E_C only is linearised and $\Delta E / \Delta P$ for 10% of the remanent polarisation (6 mC/m^2) has been calculated.

As mentioned before, the same non-switchable polarisation was observed in [62]. The thin films measured in this work had a thickness of 1.5 μm to 2.4 μm and a molar composition of 56/44. They have been poled prior annealing. The non-switchable polarisation was pointing in the direction used for the pre-poling procedure and was

in the order of some hundred μC, i.e. 190 μC and 240 μC. This behaviour was interpreted to originate from amorphous regions oriented during the poling phase and fixed or clamped during the crystallisation process fostered by the annealing. There has been no intended pre-poling in the experiments conducted for this work. Furthermore, the non-switchable polarisation could not be observed in all samples, i.e. it was absent in samples with a molar composition of 56/44. Provided the case that a permanent and temperature-independent polarisation originates from amorphous regions clamped or fixed by crystalline regions during the annealing process, the origin of the orientation has to be clarified. In the absence of a pre-poling process, strain generated during the deposition process could be the origin of a preferred orientation. On the other hand, charges induced during the pre-measurement poling are a possible origin of the temperature-independent electric field.

4.5.2 Retention Behaviour from Dielectric Non-Linearities

As discussed in section 4.4, depolarisation fields and therefore the loss of polarisation play a major role in ferroelectric thin films. A potential use of thin film devices in ferroelectric memories and other applications in which the remanent polarisation is the main quantity, has to consider or use depolarising fields. What might be problem in information storage, could be a chance in energy storage.

In order to determine the temporal development of the polarisation, the factor calculated in equation (2.44) has been used. Therefore, the permittivities ε_1 and ε_2 have been measured over time at constant temperature. Initial poling has been generated by applying a series of triangular shaped pulses. The amplitude of the pulses has been changed in order to study the impact of non-saturated polarisation on the retention behaviour. Retention has been measured for both possible states of polarisation, up and down, to determine asymmetries.

As emphasised in [93] ©2013 IEEE, "at 30°C we observed an initial decrease of the polarisation with a time constant of about 1 hour which finally settled at about

85 per cent of the initial value (Fig. 4.23). This reduction after poling might be essentially attributed to the rearrangement of charges injected into the ferroelectric film by the poling pulses."

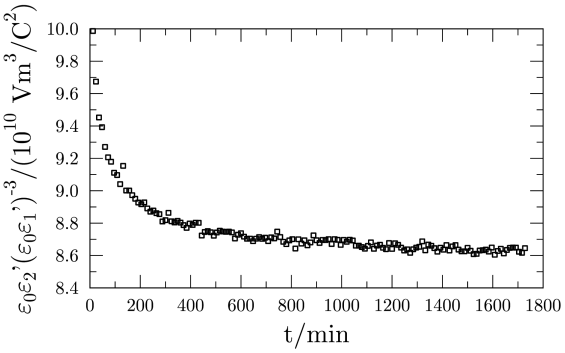

Figure 4.23: Temporal development of the polarisation [93] ©2013 IEEE.

The polarisation-proportional factor $\varepsilon_0\varepsilon_2/(\varepsilon_0\varepsilon_1)^3$ has also been recorded for approximately 5200 min, which is equal to more than three days. As shown in Fig. 4.24, no further significant loss of polarisation occurs after the initial decay already seen in Fig. 4.23. "A similar behavior has been observed for the two states of polarisation up and down (Figure 4.25). There is no remarkable change after the initial loss of less than 20 per cent. Both polarisation states remain well defined.

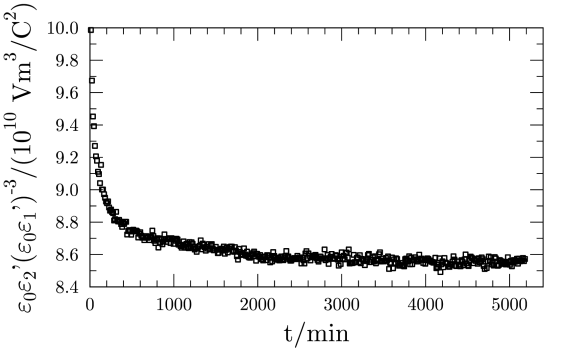

Figure 4.24: Temporal development of the polarisation over several days [93] ©2013 IEEE.

Reducing the polarising pulse amplitude to 80 per cent of the value which was used in the measurements in Fig. 4.23, Fig. 4.24 and Fig. 4.25 led to a significantly lower stable polarization (less than 10 per cent), a lower time constant for the polarization loss, and a loss of about 70 per cent of the initial polarisation (Fig. 4.26). The absolute amount of the decrease in polarization, however, is comparable to the result

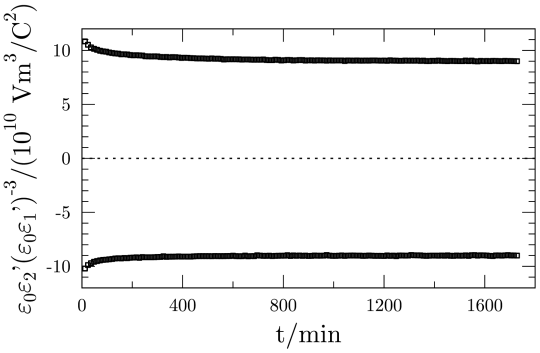

Figure 4.25: Temporal development for different polarisation states [93] ©2013 IEEE.

when the sample had been polarised with higher pulse amplitude. I.e., when the poling pulse amplitude is reduced to value at which the degree of polarisation is less than 10 per cent, the injection of charge and their subsequent rearrangement remains essentially unchanged." [93] ©2013 IEEE

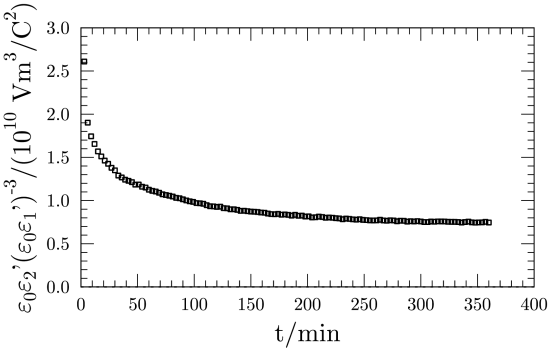

Figure 4.26: Temporal development of the polarisation of a sample polarised with lower pulse amplitude [93] ©2013 IEEE.

As can be seen from the results above, the method used to determine the retention time of VDF-TrFE copolymer thin films is a very sensitive, non-destructive method and therefore advantageous if used for ferroelectric memory devises. It has been shown, that the polarisation in P(VDF-TrFE) thin films remains stable throughout the time measured. The amount of stable polarisation is heavily dependent on the initial polarisation. Both states of polarisation, up and down, show a similar stability if poled with equal amplitudes.

4.6 Phase Transition and Polarisation in Ferroelectric Multilayer Structures

As defined earlier, a ferroelectric multilayer is a structure containing at least one layer made of a ferroelectric material. Adapting this definition, even a simple transistor can be considered being of multilayered nature. This is due to inhomogeneities as well as surface and oxide layers unavoidable in a real structure. This section however, focuses on multilayers, which have been intentionally designed and deposited.

Two main structures have been designed and characterised. The first type of device under investigation is a two-terminal device, a multilayered capacitor. Basically, a single layered capacitor has been extended by depositing several layers of the same or different copolymer compositions (e.g. Fig. 3.4). The second structure is a three-terminal device, a ferroelectric field-effect transistor, e.g. as depicted in Fig. 4.40.

4.6.1 Dielectric Non-Linearities in Bilayer Structures

Findings discussed in this section have been published in a similar form in [95] ©2016 IEEE. Deviations from the original text have been marked using square brackets. Deletions have been marked using [...]. Labelling of figures, equations and citations has been changed without marking in order to increase readability.

As emphasised in [95] ©2016 IEEE, "it has been shown, that bilayers and also multilayers of copolymer [thin films] can be fabricated by spin coating. It is crucial for the process to use a solvent like DEC in which the copolymer is dissolved very slowly (the copolymer solution is prepared at elevated temperatures of about 80°C where still some hours of time are needed). Furthermore, it is essential that the first layer has been annealed before the second layer will be deposited as the annealed material is substantially more stable against dissolution [than its pristine equivalent][...]. By using the electrode design shown in Fig. 3.4 the dielectric properties of the individual layers as well as of the bilayer can be characterised. It has been found that the properties of the individual layers match the results for single layers published earlier [87].

Chew and co-workers recently suggested a new model considering the existence of an interface layer natively present in all multilayer systems. They assumed, that if the whole spatial variation of the polarisation takes place along the z-direction, the Helmholtz free energy per unit area for one period of the superlattice can be explained by [44]:

$$F = F_{\mathrm{FE}} + F_{\mathrm{PE}} + F_{\mathrm{I}}, \tag{4.35}$$

with F_{FE} and F_{PE} representing the Helmholtz free energy of the two layers (in [44] one ferroelectric and one paraelectric) and F_{I} that of an interface layer. Since we use a system of two ferroelectric layers,

$$\begin{aligned}[\quad F = \sum_{i=1}^{n} \left(\frac{\alpha_i}{2} D_i^2 + \frac{\gamma_i}{4} D_i^4 + \frac{\delta_i}{6} D_i^6 + f_{PT,i} - E_i D_i \right) V_i + \ldots \\ + \sum_{j=1}^{m} \left(f_{\mathrm{I},j} - E_{\mathrm{I},j} D_{\mathrm{I},j} \right) V_{\mathrm{I},j}. \quad]\end{aligned} \tag{4.36}$$

equation (4.36) has to be modified to:

$$F = F_{\mathrm{FE},1} + F_{\mathrm{FE},2} + F_{\mathrm{I}}. \tag{4.37}$$

[Describing the impact of the interface layer(s) with the deviation from the results observed for thicker films of P(VDF-TrFE), the term F_{I} has to be excluded in the following considerations.] Assuming a serial connection of two layers of equal thickness one can calculate the real part of the linear effective permittivity of the system using the simple formula:

$$\varepsilon = 2\,\varepsilon_{\mathrm{FE},1}\,\varepsilon_{\mathrm{FE},2} / \left(\varepsilon_{\mathrm{FE},1} + \varepsilon_{\mathrm{FE},2} \right). \tag{4.38}$$

Figure 4.27 shows the linear dielectric permittivities of the individual layers and the bilayer over temperature measured in a heating and a cooling run. Also included is the permittivity calculated using equation (4.38) and the measured permittivities of the individual layers. It is obvious that the [behaviour of individual layers is in

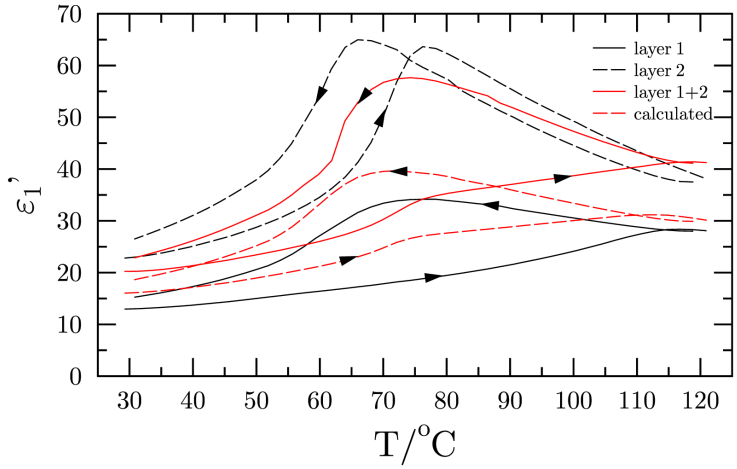

Figure 4.27: Real part of the linear permittivity of individual layers 1 (P(VDF-TrFE) 70/30 mol%, 200 nm), 2 (P(VDF-TrFE) 56/44 mol%, 200 nm) and the bilayer 1+2. Heating and cooling cycles are indicated by arrows [95] ©2016 IEEE.

accordance with the graphs discussed earlier, i.e. in section 4.4. The] calculated curve shows the same temperature dependence as the measured one. Especially the additional slope between 70°C and 80°C caused by the phase transition in layer 2 is reproduced excellently. However, the absolute values of the measured and the calculated data of the bilayer do not match well. This may be partially caused by a discrepancy of the layer thicknesses. I.e. there may be a difference in the top layers' thickness depending if deposited on the intermediate electrode or directly on the bottom copolymer layer. Furthermore, the formation of a very thin blend layer at the interface between the copolymer films may contribute to this deviation.

The strongest contribution to the discrepancy may be caused by electric fields. It is known that the permittivity of VDF-TrFE copolymer is strongly influenced by a DC bias field. At the Curie transition temperature and beyond the permittivity of 55/45 copolymer is reduced by more than 30% under the influence of a DC bias field of 10 V/µm [46].

In the absence of free charge the electric displacement within the layers of a bilayer or multilayer stack is the same according to Gauss's law. The electric field and polarisation, however, will vary from layer to layer. If the temperature of the bilayer is changed, the electric fields will change accordingly if no or not sufficient charge can flow to the interface of the bilayer. Particularly strong changes in the electric fields

will arise in the vicinity of the Curie transition temperatures of the single layers. Electric fields within the bilayer appear to be the most reasonable explanation why equation (4.38) does not fully describe the permittivity of the bilayer.[...]

A property crucial for memory applications is the remanent polarisation, in particular its value and its temperature stability. Therefore we have a look at it from these two viewpoints. Figure 4.28 shows hysteresis loops recorded for a bilayer and its individual components at room temperature. Layer 1 and layer 2 are [thin films of] P(VDF-TrFE) in molar ratios 56/44 and 70/30, respectively. [As can be seen, measuring the stack of both layers leads to a higher remanent polarisation and a coercive field similar to the single layer values. The results therefore partially (P_R) contradict the result predicted in section 2.5.1.] The higher remanent polarisation of the layer system might be subjected to a higher crystallinity or to a less impacting electrode-polymer boundary layer. A very similar result is observed for a bilayer of inversed structure as displayed in Fig. 4.29. The result is therefore independent of the deposition sequence.

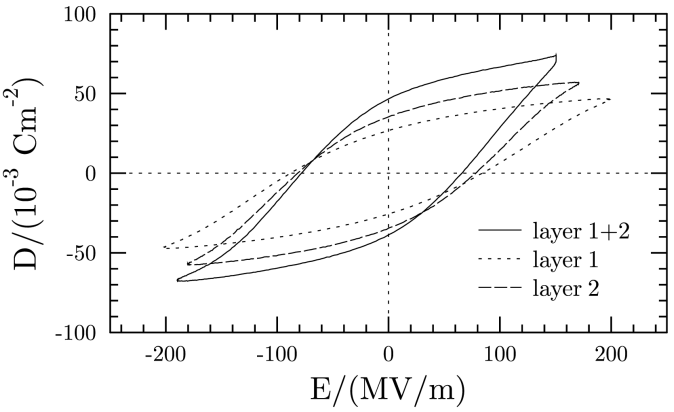

Figure 4.28: Hysteresis loops recorded for a bilayer (layer 1+2) and its individual components at 1 kHz. Layer 1: P(VDF-TrFE) 56/44 mol%, layer 2: P(VDF-TrFE) 70/30 mol %. Each layer has a thickness of 200 nm [95] ©2016 IEEE.

As derived in section 2.4.3 the factor $\varepsilon_0\varepsilon_2/(\varepsilon_0\varepsilon_1)^3$ is proportional to the remanent Polarisation P_r. Plotting the results measured at the individual layers we obtain graphs similar to those in an earlier publication [88]. The bilayer, in contrast, shows essentially a linear dependence of the remanent polarisation on temperature as depicted in Fig. 4.30. Furthermore, there is still a significant polarisation detected

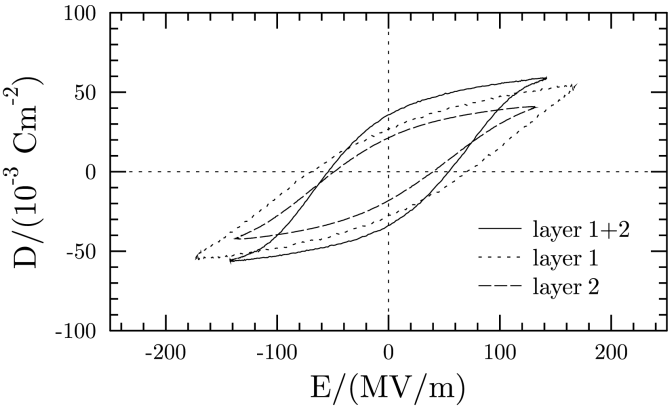

Figure 4.29: Hysteresis loops recorded for a bilayer (layer 1+2) and its individual components at 1 kHz. Layer 1: P(VDF-TrFE) 70/30 mol%, layer 2: P(VDF-TrFE) 56/44 mol %. Each layer has a thickness of 200 nm [95] ©2016 IEEE.

at temperatures above 110°C where the individual layers are paraelectric.

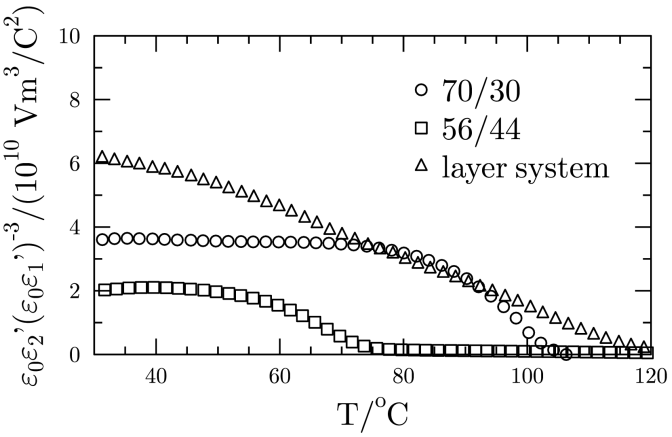

Figure 4.30: Polarisation behaviour calculated from measured non-linearities (upon heating) for individual layers (200 nm each) and bilayer [95] ©2016 IEEE.

The same behaviour can be observed for the temperature dependent shape of the hysteresis loops recorded for a bilayer as shown in Fig. 4.31 [and Fig. 4.32]. The remanent polarisation declines with rising temperature and vanishes above the transition temperature of layer 1. If plotted over the whole temperature range, the hysteresis measurements [qualitatively] match the results obtained by the nonlinearities (Fig. 4.32). [This proves that both methods, hysteresis loop recording and non-linearity measurement are similar in results. Therefore, the latter can be considered being an equally suitable method to determine the polarisation of the sample. The additional advantage of being non-destructive, makes it even more suitable for

ferroelectric memory applications.]

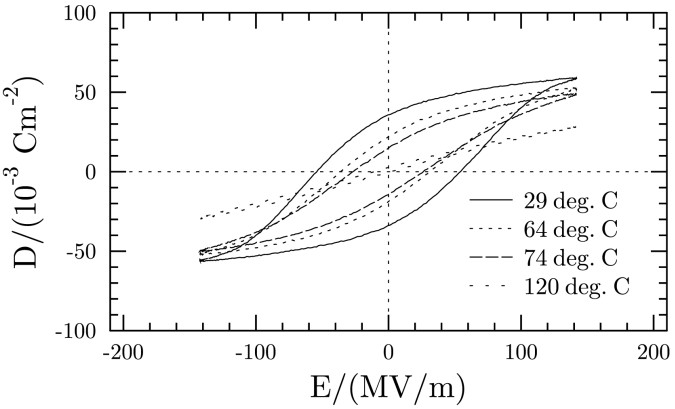

Figure 4.31: Hysteresis loops as a function of temperature recorded for a bilayer (layer 1+2) at 1 kHz. Layer 1: P(VDF-TrFE) 70/30 mol%, layer 2: P(VDF-TrFE) 56/44 mol%. Each layer has a thickness of 200 nm [95] ©2016 IEEE.

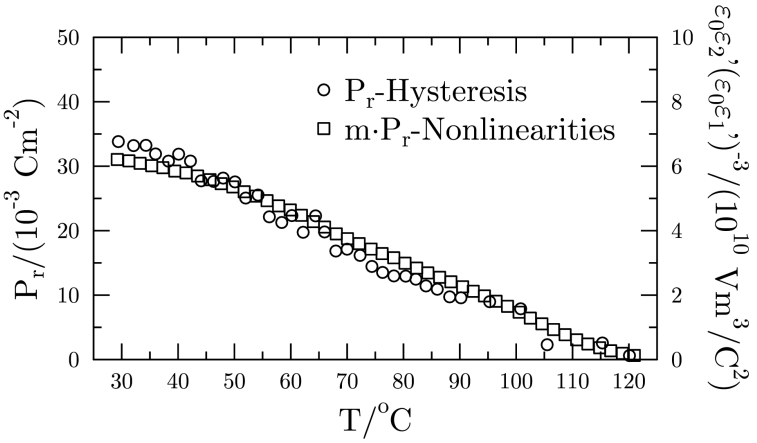

Figure 4.32: Remanent polarisation of a bilayer (Layer 1: P(VDF-TrFE) 70/30 mol%, 200 nm; layer 2: P(VDF-TrFE) 56/44 mol%, 200 nm) calculated from hysteresis and non-linearity measurements [95] ©2016 IEEE.

Dawber et al have given a qualitative interpretation for a phenomenologically similar effect in superlattices [11]. They stated that the phenomenon originates in an improper ferroelectric behaviour at the surface between adjacent layers. They further assume that the impact is increased, if the two layers are of equal thickness. In a superlattice the zone boundary distortion is the reason for an interface coupling which gives rise to improper ferroelectricity.

In a bilayer of organic ferroelectrics, the electric fields which have already been discussed above can cause coupling between the layers. It [has been shown in section

4.4] [...] that the ferroelectric to paraelectric transition of a ferroelectric material is shifted to higher temperatures or even completely hindered under the influence of a DC bias field. Moderate fields of 10 MV/m keep a 55/45 VDF-TrFE copolymer polar up to temperatures of more than 140°C [46]. The electric fields in a copolymer bilayer caused by the absence of sufficient free charge at the dielectric-dielectric interface influencing the permittivity will also modify the polarisation versus temperature relation. I.e. they can still keep the bilayer polar above the Curie temperatures of the single layers.

It has been shown that the dielectric and hysteresis properties of ferroelectric copolymers can be tuned by the formation of bilayers. The small and large signal nonlinearities of bilayers cannot be fully explained by a simple series connection of the capacities of the individual layers. Furthermore, the remanent polarisation of the bilayers shows essentially a linear decrease with temperature[, differing from the behaviour observed for the single layers (Fig. 4.30)]. It reaches zero at temperature 120°C which is significantly higher than the Curie temperature of the two ferroelectric materials involved. Phenomenologically this behaviour reminds on the polarisation over temperature observed in superlattices.

In bilayers of VDF-TrFE copolymers with different molar ratios the constituent layers show a different temperature [and spatial] dependence of the remanent polarisation. [While parts of the multilayer might still be fully polarised, others might be depolarised due to a ferroelectric-paraelectric phase transition.] This will give rise to an electric field within the layers if the temperature is changed and there is not sufficient free charge available migrating to the interface to compensate these differences.

[It has been shown in section 4.4.2 that an electric bias field causes a substantial change in the polarisation behaviour with regard to the temperature.] It is [also] known that an electric bias field causes a substantial reduction of the permittivity in VDF-TrFE copolymer. That is electric fields in the bilayer will cause a reduction in the permittivity of the bilayer in comparison to a serial connection model as observed. Furthermore, these fields will also induce a polarisation at temperatures above the Curie temperatures of the two materials involved. In effect, the electric

fields form a coupling term between the two layers which causes phenomenological similarities to the interface coupling known in superlattices.

[As has been discussed elsewhere (e.g. [46], [45]) and before (section 4.4), electric fields in general have a considerable influence on the behaviour of the ferroelectric polarisation or the dielectric displacement, respectively. Despite fields originating from finite size effects (electrodes) or interface layers, a field can be generated by combining a double or multilayer of different materials or properties as done in the above experiments.] Further investigations of the field dependence of the permittivity and the induced polarisation within the single layers are required in order to provide an experimental base for a quantitative modelling." [95]

4.6.2 Organic Ferroelectric Field-Effect Transistor (FerrOFET)

Most of the work done in the FerrOFET research has been conducted during research projects with the *Hong Kong Polytechnic University*. FerrOFETs are thin film devices far exceeding the complexity of ferroelectric thin films sandwiched between electrodes. Therefore, the success is limited by the time available for experiments. Nevertheless, the results gained during the projects are important for further efforts and should not go unmentioned.

In the studies, two different organic semiconductors have been used to realise ferroelectric organic field-effect transistors in combination with P(VDF-TrFE) as a gate dielectric. The first material used was pentacene. Experiments using pentacene for transistor setups never resulted in working devices. After becoming available, the focus was therefore shifted to powder-shaped DNTT. Due to the relatively high price, solution based DNTT has not been used. DNTT has been chosen due to its advantage of a higher air stability. Another advantage over pentacene became apparent after combining it with a relatively rough gate dielectric. Its performance is less sensitive to rough surfaces.

An increasing surface roughness on P(VDF-TrFE) thin films is often ascribed to an increasing crystallinity during the annealing process ([16, 33]). The rod-shaped lamellae, being the appearance of a folded P(VDF-TrFE) polymer chain, can be observed using an AFM. These lamellae agglomerate and build up wood-pile shaped

stacks of random orientation if the copolymer layer has been annealed, as depicted in Fig. 4.33. A maximum crystallinity is, however, needed in order to achieve a substantial remanent polarisation, since the latter originates from the crystalline parts of the thin film. Although a higher crystallinity comes with a higher roughness, it was not possible to prove that this increase is substantial. Whereas, a significant change in the surface properties can be observed if a thin film is annealed above its melting temperature, as shown in [16] and [33]. Long strands, far exceeding the length of lamellae, bent or straight, have been shown to be a strong indicator for molten films [43]. Melting however is undesirable, since it promotes an irreversible loss of ferroelectric properties [60].

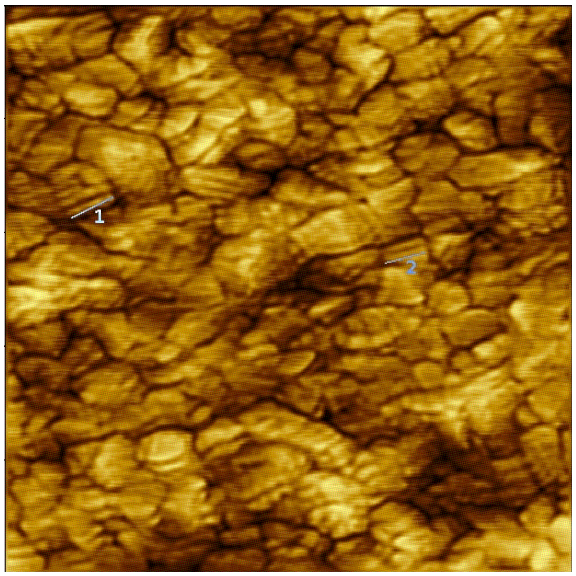

Figure 4.33: Structure of a P(VDF-TrFE) 75/25 thin film annealed for 2 hours at 122°C. Film thickness about 200 nm. Scan size 500 nm edge length with a single lamellae of approximately 40 nm indicated by 1 and 2.

The devices used for the studies in this work follow the Metal Insulator Semiconductor Field-Effect Transistor (MISFET) design. The performance of a (p-type) MISFET strongly depends on the properties of the ferroelectric layer, such as ferroelectric performance and surface morphology. Improving the former can lead to a degradation of the latter and the other way around. While the ferroelectric properties can be improved by a heat treatment, the surface morphology tends to change (AFM image Fig. 4.34) towards a higher roughness. If organic semiconductors, i.e. pentacene or DNTT are now placed on the dielectric's surface, the conductive chan-

nel will build up in a thin layer of the semiconductor in contact with the adjacent dielectric. While operating the device, the roughness of the latter will have a significant impact on the mobility of the charge carriers within the channel layer. Therefore a higher roughness has to be avoided. Several ways have been tried to overcome this issue, as emphasised in 3.1.3.

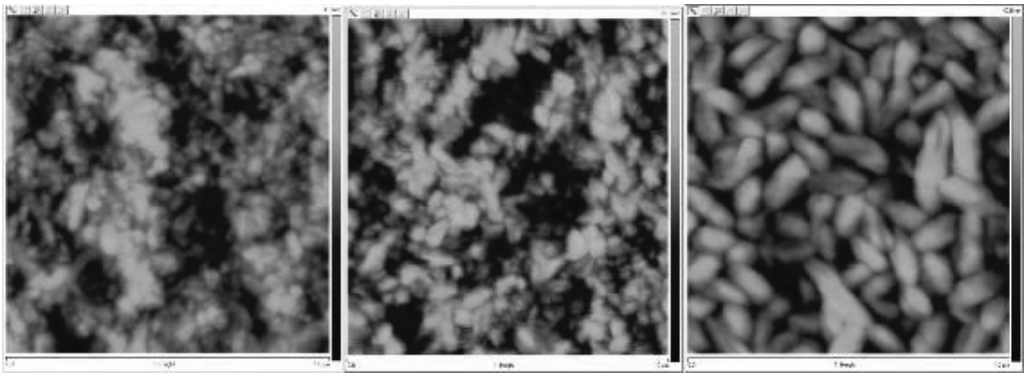

Figure 4.34: P(VDF-TrFE) 70/30 mol% samples 60 nm thick annealed at 90°C, 100°C and 110°C, respectively, 1 μm^2 each.

The first attempt has been to flatten the rough surface by imprinting a flat surface at elevated temperatures. For this process, which is similar to hot pressing, PDMS films were deposited on silicon wafers. After removal, they where pressed on the heated polymer surface applying a 1.5 kg weight (approximately 24 kN/m^2) on top of the sample. The pressing was conducted at 180°C. The heated structure was then carefully cooled at a rate of 10°C/min. As shown in Fig. 4.35, a needle-like structure was obtained after completing the cooling cycle. Although samples where considerably smoother than as-deposited and annealed films, the ferroelectric properties were rather poorly developed. The reason for the reduced performance can be found in the needle-like structure observed, which typically indicates a molten polymer. It is known that annealing above the melting temperature may lead to a complete and irreversible extinction of the polarisation in P(VDF-TrFE) [60]. Hot pressing close to or below the melting temperature however, did not result in a significant change of the surface roughness.

Approach number two and three, decreasing the annealing temperature below 140°C or even skip the annealing step led to a more general question. As discussed in one of the first paragraphs of this section, annealing significantly improves

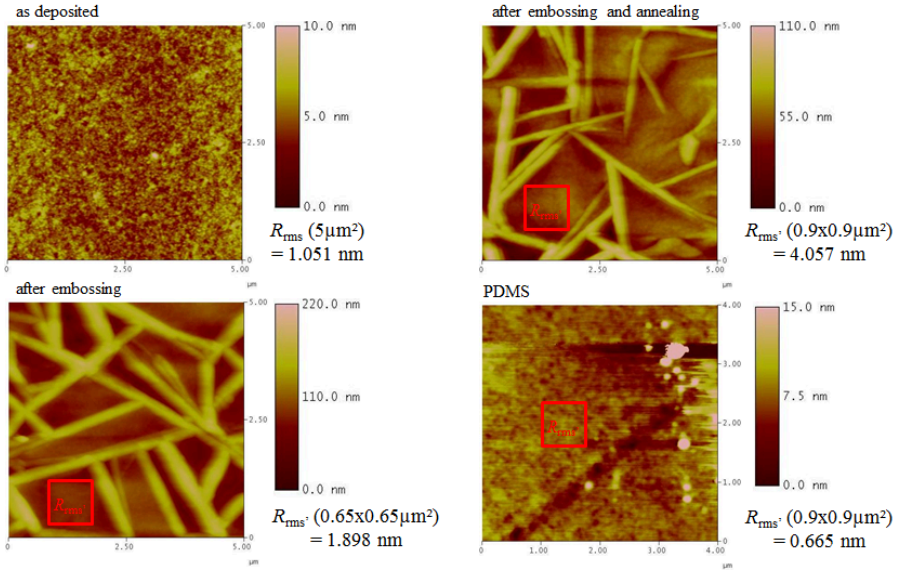

Figure 4.35: P(VDF-TrFE) thin films as-deposited and after embossing (left), after embossing and annealing plus the PDMS surface (right).

the crystallinity of the material and therefore the ferroelectric properties, i.e. the remanent polarisation. Nevertheless, it has been proven in [48] that ferroelectric properties can be activated without annealing, e.g. by applying an electric field of sufficient strength for a sufficient number of cycles. The remanent polarisation however, might not be similar to the one achieved by annealing and therefore not capable of providing enough strength to built up a channel in the semiconductor material. Furthermore, the retention time might be effected as discussed in section 4.5.2, leading to a faster degrading polarisation. As a consequence, decreasing the annealing temperature to values of 120°C and below has been the improvement of choice.

The value of 120°C has been chosen due to results from measurements conducted during an internship at the *Tokyo University of Science*. The P(VDF-TrFE) samples with a molar composition of 75/25, annealed at different temperatures from 100°C to 140°C in steps of 1°C have shown no significant change in structure at annealing temperature above 122°C. The main change in the surface structure has been observed for temperatures up to 110°C as shown in Fig. 4.36.

A further reason to lower the annealing temperature was the use of a decreased film thickness of P(VDF-TrFE). In order to use a switching voltage not exceeding

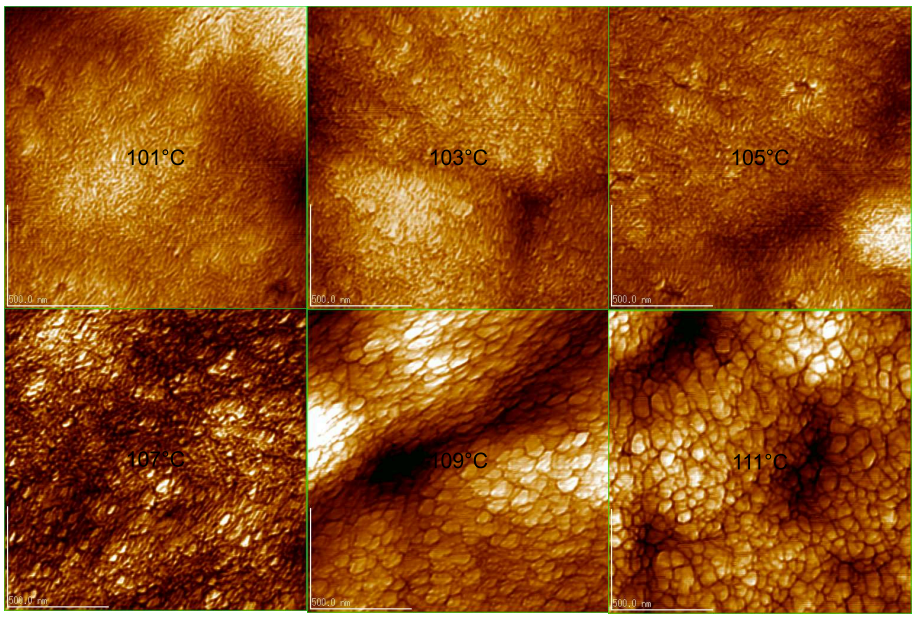

Figure 4.36: P(VDF-TrFE) 75/25 mol% copolymer thin films (200 nm) annealed for two hours. Annealing temperatures have been varied starting at 101°C (upper left) to 111°C (lower right) in steps by 2°C. Each scan has a size of 1.5 μm times 1.5 μm.

5 V, the thickness has to be kept lower than 100 nm, especially with regard to the use of extra layers, i.e. parylene C. For thin films with thicknesses below 100 nm a loss of ferroelectric properties, namely a vanishing hysteresis curve, was observed for annealing temperatures of 140°C. Both films used for the hysteresis measurements displayed in Fig. 4.37 have been deposited from the same solution of P(VDF-TrFE), with a molar fraction of 70/30 mol%, solved in DEC with a fraction of 2.5 wgt%. While the left graph lacks most of the typical properties of a hysteresis curve, the right graph clearly shows the known features. The loss of ferroelectric properties might be attributed to a thickness dependent melting temperature, as reported elsewhere for other polymers [35, 31]. It is therefore necessary to adjust the annealing temperature accordingly. Doing so, switching occurs in ultra-thin films of ferroelectric P(VDF-TrFE) as well (Fig. 4.38). This shift in the melting temperature has to be considered during further steps, e.g. the thermal evaporation of the semiconductor material and the top electrodes.

The change of the annealing temperature has led to an acceptable ferroelectric performance of the P(VDF-TrFE) ferroelectric thin films and even increased the performance of ultra-thin films. But it did not sufficiently decrease the surface

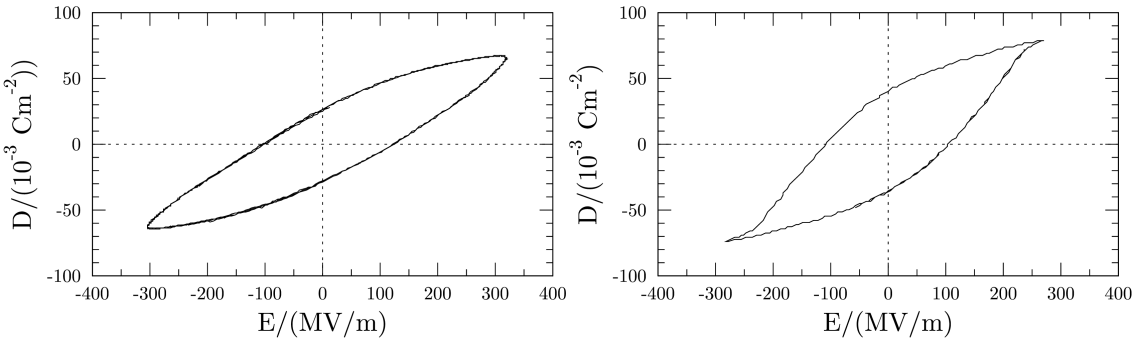

Figure 4.37: P(VDF-TrFE) thin films deposited under similar conditions, annealed at 140°C (left, [87] ©2012 IEEE) and 120°C (right).

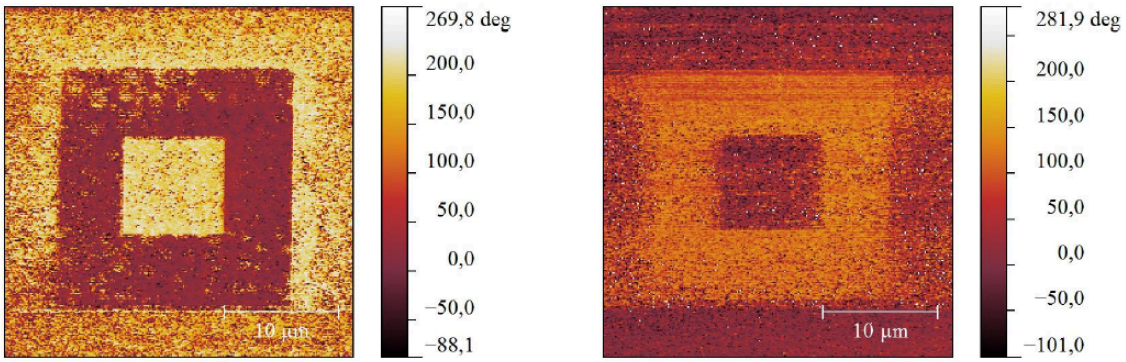

Figure 4.38: PFM of P(VDF-TrFE) thin films 230 nm (left) and 20 nm (right).

roughness.

The fourth approach has been to flip over the design and use a top gate structure, adding the advantage of depositing the organic semiconductor first (Fig. 4.39). This step has been tried for pentacene devices only. As mentioned in subsection 3.1.3, mobility and therefore performance of a surface-channel-MISFET (sometimes called IGFET) largely depend on the dielectric-semiconductor interface morphology. Hence, if using a bottom gate design, the main effort has to be put into a low surface roughness of the dielectric layer as discussed in [33] and [69]. In the top gate design however, the semiconducting layer defines the surface roughness, guaranteeing the desired flatness. But using the top-gate design creates two major issues, which have to be taken into consideration. First of all, the glass transition temperature of pentacene is approximately 120°C, which is the minimum annealing temperature in order to improve the crystallinity of thin P(VDF-TrFE) films. Secondly, although it has been shown that using DEC as a solvent for P(VDF-TrFE) solution does no

harm to the deposited pentacene, transistor devices deposited in this design have shown a poor performance. For this reasons, the idea of a top-gate design has not been implemented and used in later experiments.

Figure 4.39: Bottom-gate and top-gate design for pentacene-based ferroelectric field-effect transistors.

The multilayer approaches 5 and 6, a combination of an annealed and a pristine P(VDF-TrFE) as well as a combination of a thin P(VDF-TrFE) layer covered with a parylene C layer, have been included in the experiments. While the first set-up was of limited success because the surface roughness could not be decreased, the second led to the fabrication of a functioning device, as will be shown in the last part of this section (Fig. 4.44).

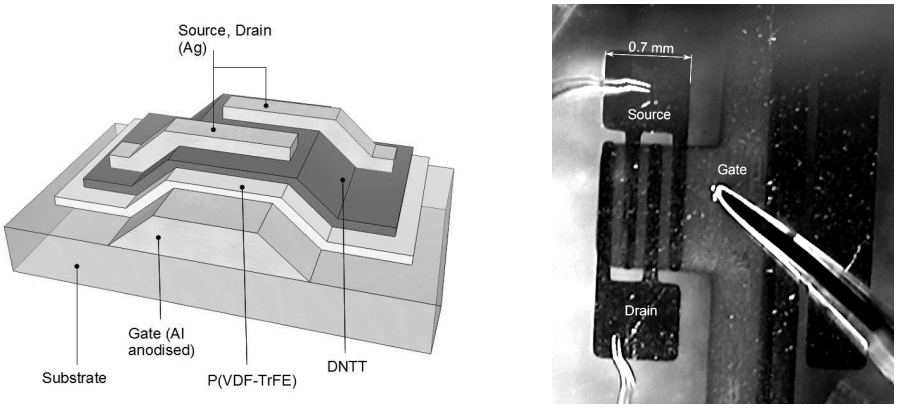

(a) Schematic (b) Sample

Figure 4.40: (a) Organic field-effect transistor with ferroelectric gate dielectric [98]. (b) Transistor sample.

The electrical characterisation of the fabricated devices has been conducted in a nitrogen glove box with humidity and temperature control. Doing so, further degradation of the samples could be avoided. Transfer and output characteristics have been measured using two LabVIEW-controlled Keithley 2400 source meters available in the lab of the *Hong Kong University*.

The first samples deposited revealed a high leakage current. In order to suppress the latter, the bottom aluminium electrodes have been anodised. Depending on the growth regime of the oxide a higher surface roughness or a lower density can be the consequence. Therefore, the surface roughness of different aluminium layers has been measured using an AFM. It has been found, that the anodisation and a subsequent annealing have no considerable impact on the roughness of the aluminium oxide layer as shown in Fig. 4.41.

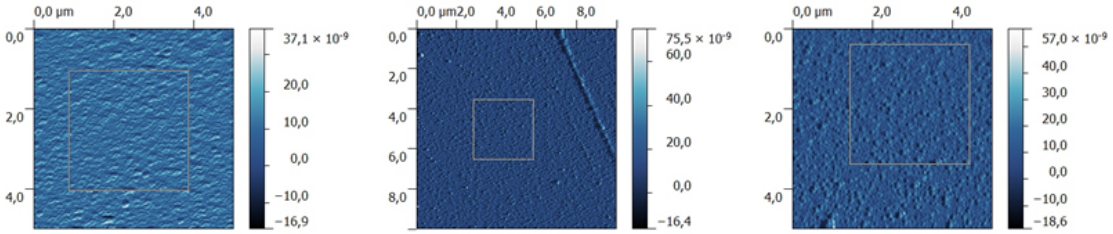

Figure 4.41: Left: native grown oxide, no heat treatment, $R_a = 5.03\,\text{nm}$; center: anodised oxide, no heat treatment, $R_a = 5.03\,\text{nm}$; right: anodised oxide, annealed for 2 hours at 120°C, $R_a = 5.80\,\text{nm}$.

Another approach to control an unwanted leakage current and the surface morphology at the same time is to deposit a thin layer of parylene C (Fig. 4.42) on top of the polymer gate dielectric. This material is an excellent insulator and provides a low surface roughness. There are two main drawbacks while working with this material. Firstly, it is difficult to control the thickness of the deposited layer, since the material is polymerised directly on the samples surface. Producing defined ultra thin layers in a reproducible quality therefore requires a lot of experience and ideal conditions. Secondly, adding a layer of insulating material increases the voltage needed to switch the ferroelectric layer.

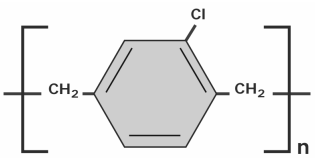

Figure 4.42: Parylene C monomer (source: scscoatings.com).

In order to prove ferroelectricity, hysteresis loops were recorded for each layer system. Figure 4.43 shows the dielectric displacement as a function of the ap-

plied electric field for a layer system of AlO_x (approximately 20 nm), P(VDF-TrFE) 70/30 mol% (approximately 220 nm) and DNTT (approximately 40 nm) measured at 1 kHz. Ferroelectric properties, although clearly apparent, deteriorate if compared to results for single layers published in [87, 89]. Exceedingly noticeable is the asymmetry for positive and negative polarisations as shown in Fig. 4.43. The same phenomena was observed in [3] if measurements were conducted without illumination. In [3] a TGS sample has been sandwiched in-between a single-crystal silicon wafer and a gold electrode. The asymmetry or the partial suppression of the hysteresis curve assigned to the positive polarisation, was assigned to a lack of minority carriers. If the minority carriers were generated by illumination, the asymmetry became weaker and finally vanished.

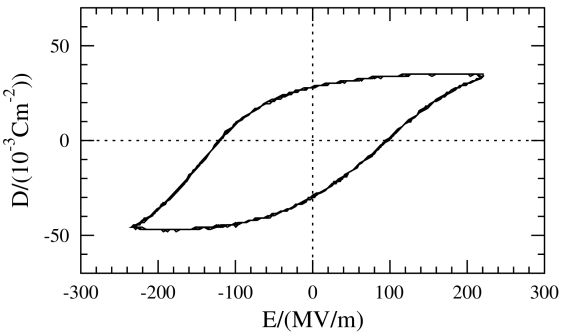

Figure 4.43: Hysteresis curve of a layer system AlOx, P(VDF-TrFE) 70/30 mol% and DNTT, thickness approximately 280 nm.

Two typical transfer curves displaying a clockwise hysteresis loop are shown in Fig. 4.44. The left graph has been recorded for a transistor design not using an additional parylene C layer. The transistor design used for the measurements in the right graph had an additional layer of the insulating, smoothing material parylene C. It can be clearly seen that the ferroelectric effect is barely visible. The drain-source current I_{DS} differs only slightly at zero volts for both cycles. Although the mobility has been improved by a factor of 10 by adding a thin layer of parylene C, it remains poor, not exceeding $6 \cdot 10^{-2}\,cm^2/(Vs)$. This was attributed to the copolymer's rough surface originating from the annealing process. Although the additional parylene C smoothing layer led to a significant increase in mobility, the surface roughness of the gate dielectric might not has been completely compensated. Furthermore, the

additional layer lead to a significant increase in the programming voltage, due to a higher coercive field E_C.

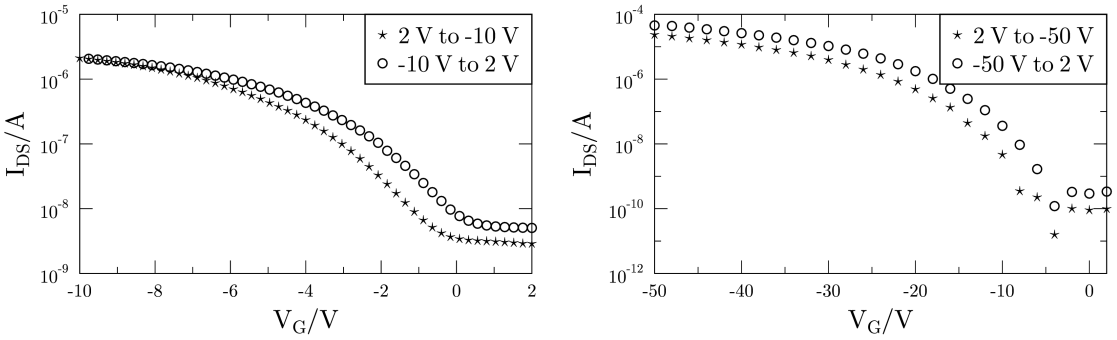

Figure 4.44: Drain-source currents of DNTT organic field-effect transistors with ferroelectric VDF-TrFE copolymer gate dielectric (left) and with additional parylene C layer (right) recorded at rising (⋆) and falling (∘) gate-source voltage.

The experiments have been shown, that it is generally possible to fabricate an organic field-effect transistors with the ferroelectric VDF-TrFE copolymer as a gate dielectric. In order to avoid an unwanted leakage current, it is advisable to either anodise the bottom electrode or add an additional layer of parylene C on top of the gate dielectric. A thin layer of parylene C additionally provides a less rough surface for the conductive channel. This has led to a significantly improved mobility. On the other hand, additional layers have caused a higher programming voltage, a lower remanent polarisation and a smaller programming window.

5 Conclusion and Outlook

5.1 Conclusion

It has been shown that dielectric non-linearities are a powerful tool to study ferroelectric thin and ultra-thin films of P(VDF-TrFE). The measurement technique used to determine the permittivities is non-destructive and highly sensitive. Several topics related to P(VDF-TrFE) ferroelectric thin films for memory applications have been successfully covered.

The results gained and discussed emphasise the deviating properties of thin films of ferroelectric P(VDF-TrFE) if compared to thicker films of the same material. Considering the discussion in sections 4.3 and 4.4, the type of phase transition in P(VDF-TrFE) with a molar fraction of 56/44 is still not clear. Especially for thin films, the theory has to be extended in order to describe the behaviour observed for ε_3. Furthermore, the origin of the thermal hysteresis observed in thin films of P(VDF-TrFE) 56/44 has to be clarified.

As discussed in (4.4), the impact of a DC electric field on thin films of P(VDF-TrFE) has been shown to be non-negligible. Besides a shift of the transition temperature to higher values, static electric fields can change the polarisation versus temperature behaviour significantly. Although it could not finally be proven, extending the temperature dependence to Landau parameters other than α, i.e. γ, and using Odajima's approach might help to successfully predict $P(T)$ for P(VDF-TrFE) thin films and multilayers.

In section 4.5.1 possible applications of dielectric non-linearities have been emphasised. Besides the characterisation of the temperature-dependent development of the polarisation for different compositions of P(VDF-TrFE), the state of polar-

isation and a non-switchable polarisation have been identified. Furthermore, the memory-application related retention behaviour has been measured. The retention measurements of thin ferroelectric VDF-TrFE copolymer films discussed in section 4.5.2 have shown that a decrease in polarisation over time can be measured by the use of dielectric non-linearities. For this purpose, the state of polarisation has been recorded continuously and non-destructive over several decades of time. The same non-destructive method can also be used to read out the polarisation state of a ferroelectric memory cell making a rewrite of the initial polarisation dispensable. Thus, the readout speed and the lifetime of the cell can be improved significantly.

In the concluding section 4.6.2 it has been shown that working ferroelectric field-effect transistors using P(VDF-TrFE) as a gate dielectric can be fabricated. Leakage currents have been suppressed using anodised bottom electrodes as well as additional layers of parylene C. Besides its effect on electric insulation, the latter additionally reduces the surface roughness of the gate dielectric and therefore enhance the charge-carrier mobility within the conducting channel.

5.2 Outlook

Although often intended, studies might rarely give final answers on the topic under research. Thus, it seems advisable to mention starting points for further studies. That has been done mostly at the end of the appropriate section, where problems have been left unsolved. In order to give ideas on future topics, the following sections will motivate additional issues.

5.2.1 Measurements using a Non-Linear Excitation Signal

A common technique to measure dielectric non-linearities is to use a single-frequency sinusoidal excitation signal. The response will then be measured at multiples (higher harmonics) of the excitation frequency. Using this technique, each harmonic has to be measured separately. In order to access a variety of dielectric non-linearities more easy, it is favourable to use an excitation signal composed of different frequencies. Although this technology was not used during the measurements for this work, the

idea seems worth to mention and worth to be considered for future works.

5.2.2 Energy Storage in Ferroelectric Polymer Multilayers

Due to economical and ecological reasons, cost effective energy storage with a high efficiency and a reasonably small volume is one of the most important branches of application-related research nowadays. According to the relationship shown in equation (5.1), a high permittivity and a high breakdown field are the key quantities to maximise the energy-storage density J. The first prerequisite can be met by high permittivity materials, e.g. ferroelectrics. In order to keep the energy dissipated by the system low, the remanent polarisation has to be small. This can be achieved by using a relaxor-ferroelectric material, an anti-ferroelectric material or by poling a classic ferroelectric near the f-p transition temperature. All three, however, will have a considerable influence on the break down voltage E_b, which is lowering it.

$$J = \int_0^{E_\mathrm{b}} D dE = \varepsilon_0 \int_0^{E_\mathrm{b}} \varepsilon(E) E dE \tag{5.1}$$

Ferroelectric Polymers, e.g. PVDF and its copolymers, are known to have very high breakdown field of some hundred MV/m. Unfortunately, their relative permittivity is comparably low, around 20 at the utmost for P(VDF-TrFE) with a molar fraction of 56/44. Combining high permittivity ferroelectric ceramics and high E_b ferroelectric polymers in composite materials is therefore believed to provide a solution, using the strength of each material [26]. At the same time, this solution creates new challenges, of course. Homogeneity and size-dependent particle properties are just two key words in this context. In order to meet homogeneity requirements, multilayers, or in the case of ceramics superlattices, might be a possible configuration.

Appendix

A.1 Non-Linearities

Considering a solely real excitation voltage not containing higher harmonics, which is

$$E_E(t) = \frac{U_E(t)}{d} = \frac{\widehat{U}_E}{d}\cos(\omega_0 t) \tag{A.1}$$

with $\widehat{U}_E$ being the amplitude. The dielectric displacement is

$$D(t) = \varepsilon_0\varepsilon_1 E + \varepsilon_0\varepsilon_2 E^2 + \varepsilon_0\varepsilon_3 E^3. \tag{A.2}$$

Substituting $E = E_E$ one gets

$$\begin{aligned} D(t) &= \varepsilon_0\varepsilon_1\frac{\widehat{U}_E}{d}\cos(\omega_0 t) + \varepsilon_0\varepsilon_2\left(\frac{\widehat{U}_E}{d}\cos(\omega_0 t)\right)^2 + \varepsilon_0\varepsilon_3\left(\frac{\widehat{U}_E}{d}\cos(\omega_0 t)\right)^3 \\ &= \sum_{m=1}^{n}\varepsilon_0\varepsilon_m\left[\frac{\widehat{U}_E}{d}\cos(\omega_0 t)\right]^m \qquad m,n\in\mathbb{N}^* \end{aligned} \tag{A.3}$$

Having a look at equation (A.3), one can see that D contains cosines to the power of m. Following the addition theorems

$$\cos^2(\omega_0 t) = \frac{1}{2} + \frac{1}{2}\cos(2\,\omega_0 t) \quad \text{and} \quad \cos^3(\omega_0 t) = \frac{3}{4}\cos(\omega_0 t) + \frac{1}{4}\cos(3\,\omega_0 t) \tag{A.4}$$

the equation can be re-written as

$$\begin{aligned} D(t) =& \varepsilon_0\varepsilon_1\frac{\widehat{U}_E}{d} + \varepsilon_0\varepsilon_2\frac{\widehat{U}_E^2}{d^2}\left(\frac{1}{2} + \frac{1}{2}\cos\left(2\omega_0 t\right)\right) \\ &+ \varepsilon_0\varepsilon_3\frac{\widehat{U}_E^3}{d^3}\left(\frac{3}{4}\cos\left(\omega_0 t\right) + \frac{1}{4}\cos\left(3\omega_0 t\right)\right) . \end{aligned} \tag{A.5}$$

It becomes apparent, that while measuring at excitation frequency, parts related to ε_1 and parts related to ε_3 will be captured. Hence, it is necessary to choose the amplitude $\widehat{U}_E$ small enough to limit the impact of the higher order non-linearities, while at the same time preventing them from vanishing.

Since the material is likely to exhibit loss, the permittivities can be expected to be complex (denoted by an underline) with $\underline{\varepsilon}_n = \varepsilon_n' - i\varepsilon_n''$. The dielectric displacement is then a complex quantity as well: $\underline{D}_n = D_n' - iD_n''$. The real amplitude $\widehat{U}_E$ on the right-hand side is multiplied by the complex permittivity $\underline{\varepsilon}_n$. The cosine, representing only the real part of a complex signal, can therefore be replaced by the exponential expression $\mathrm{e}^{i\omega_0 t}$. At the same time it seems advisable to separate amplitudes assigned to the excitation frequency an its integer multiples

$$\begin{aligned} \underline{D} =& \left(\varepsilon_0\underline{\varepsilon}_1\frac{\widehat{U}_E}{d} + \varepsilon_0\underline{\varepsilon}_3\frac{3}{4}\frac{\widehat{U}_E^3}{d^3}\right)\mathrm{e}^{i\omega_0 t} + \left(\varepsilon_0\underline{\varepsilon}_2\frac{1}{2}\frac{\widehat{U}_E^2}{d^2}\right)\mathrm{e}^{i2\omega_0 t} + \left(\varepsilon_0\underline{\varepsilon}_3\frac{1}{4}\frac{\widehat{U}_E^3}{d^3}\right)\mathrm{e}^{i3\omega_0 t} \\ &+ \varepsilon_0\underline{\varepsilon}_2\frac{1}{2}\frac{\widehat{U}_E^2}{d^2} . \end{aligned} \tag{A.6}$$

An alternating voltage will change the dielectric displacement and therefore create a displacement current density $J(t) = dD/dt$. The voltage $U_M = J_M \cdot A \cdot R_M$ measured at the resistor R_M can be described as

$$\begin{aligned} \underline{U}_M =& i\omega_0 A R_M\left(\varepsilon_0\underline{\varepsilon}_1\frac{\widehat{U}_E}{d} + \varepsilon_0\underline{\varepsilon}_3\frac{3}{4}\frac{\widehat{U}_E^3}{d^3}\right)\mathrm{e}^{i\omega_0 t} + i2\omega_0 A R_M\left(\varepsilon_0\underline{\varepsilon}_2\frac{1}{2}\frac{\widehat{U}_E^2}{d^2}\right)\mathrm{e}^{i2\omega_0 t} \\ &+ i3\omega_0 A R_M\left(\varepsilon_0\underline{\varepsilon}_3\frac{1}{4}\frac{\widehat{U}_E^3}{d^3}\right)\mathrm{e}^{i3\omega_0 t} . \end{aligned} \tag{A.7}$$

The signal measured from the sample can generally be expected to be of complex

nature with

$$\underline{U}_M(t) = \widehat{\underline{U}}_M \mathrm{e}^{i\omega_0 t} = U'_M + iU''_M \tag{A.8}$$

with U'_M and U''_M referring to the real and the complex part of the amplitude, respectively. Considering the higher harmonics of the excitation frequency contained in the measured signal $U_M(t)$ can be written as the sum

$$\underline{U}_M(t) = \sum_{m=1}^{n} \widehat{\underline{U}}_{M,n} \mathrm{e}^{in\omega_0 t} \,. \tag{A.9}$$

Using a lock-in amplifier for the measurements, only signal components at the excitation frequency will be amplified. Furthermore, components at higher harmonics and of different phase will be attenuated. Bearing the aforementioned in mind and considering the excitation signal being solely real, the first-order permittivity can be calculated by

$$\varepsilon_0 \underline{\varepsilon}_1 = \left(\frac{\widehat{\underline{U}}_{\mathrm{M},1} \mathrm{e}^{i\omega_0 t}}{\mathrm{e}^{i\omega_0 t} i\omega_0 A R_{\mathrm{M}}} - \varepsilon_0 \underline{\varepsilon}_3 \frac{3}{4} \frac{\widehat{U}_{\mathrm{E}}^3}{d^3} \right) \frac{d}{\widehat{U}_{\mathrm{E}}} \,. \tag{A.10}$$

If the excitation amplitude has been chosen small enough, so that non-linear permittivities of increasing order are decreasing in amplitude proportional the applied electric field, the higher order impact can be generally neglected because

$$\varepsilon_0 \underline{\varepsilon}_1 \frac{\widehat{U}_{\mathrm{E}}}{d} \gg \varepsilon_0 \underline{\varepsilon}_3 \frac{3}{4} \frac{\widehat{U}_{\mathrm{E}}^3}{d^3} \,. \tag{A.11}$$

The permittivity $\varepsilon_0 \underline{\varepsilon}_1$ then simplifies to

$$\varepsilon_0 \underline{\varepsilon}_1 = \frac{d}{\mathrm{e}^{i\omega_0 t} i\omega_0 A R_{\mathrm{M}} \widehat{U}_{\mathrm{E}}} \widehat{\underline{U}}_{\mathrm{M},1} \mathrm{e}^{i\omega_0 t} = \frac{d}{i\omega_0 A R_{\mathrm{M}} \widehat{U}_{\mathrm{E}}} \widehat{\underline{U}}_{\mathrm{M},1} \,. \tag{A.12}$$

In order to prove the previous derivation, one can substitute $\widehat{U}_{\mathrm{E}}/d = E_{\mathrm{E}}$, $\widehat{\underline{U}}_{\mathrm{M},1}/(R_{\mathrm{M}} \cdot A) = J_{\mathrm{M},1}$ and $i\omega_0 \varepsilon_0 \varepsilon = \sigma$ to finally return to Ohm's law $J_{\mathrm{M}} = \sigma E_{\mathrm{E}}$, with J_{M} and σ

being complex quantities. Similarly the ε_2 and ε_3 can be derived as

$$\varepsilon_0 \underline{\varepsilon}_2 = \frac{d^2}{i\omega_0 A R_\mathrm{M} \widehat{U}_\mathrm{E}^2} \, \underline{\widehat{U}}_{\mathrm{M},2} \tag{A.13}$$

and

$$\varepsilon_0 \underline{\varepsilon}_3 = \frac{4d^3}{i\omega_0 3 A R_\mathrm{M} \widehat{U}_\mathrm{E}^3} \, \underline{\widehat{U}}_{\mathrm{M},3} \, . \tag{A.14}$$

Multiplying nominator and denominator by the imaginary unit i and using the algebraic expression of a complex amplitude, it can be shown that the real parts of the permittivities are interrelated with the imaginary parts of the measured voltages and vice versa

$$\begin{aligned}
\varepsilon_1' - i\varepsilon_1'' &= \frac{d}{i\omega_0 \varepsilon_0 A R_\mathrm{M} \widehat{U}_\mathrm{E}} \left(U_{\mathrm{M},1}'' - i U_{\mathrm{M},1}' \right) \\
\varepsilon_2' - i\varepsilon_2'' &= \frac{d^2}{i\omega_0 \varepsilon_0 A R_\mathrm{M} \widehat{U}_\mathrm{E}^2} \left(U_{\mathrm{M},2}'' - i U_{\mathrm{M},2}' \right) \\
\varepsilon_3' - i\varepsilon_3'' &= \frac{4d}{i\omega_0 \varepsilon_0 3 A R_\mathrm{M} \widehat{U}_\mathrm{E}^3} \left(U_{\mathrm{M},3}'' - i U_{\mathrm{M},3}' \right) \, .
\end{aligned} \tag{A.15}$$

References

[1] Anonymous. Minutes of the Washington Meeting, April 23 and 24, 1920. *Phys. Rev.*, 15:505–564, Jun 1920.

[2] Kang-Jun Baeg, Soon-Won Jung, Dongyoon Khim, Juhwan Kim, Dong-Yu Kim, Jae Bon Koo, Jordan R. Quinn, Antonio Facchetti, In-Kyu You, and Yong-Young Noh. Low-voltage, high speed inkjet-printed flexible complementary polymer electronic circuits. *Organic Electronics*, 14(5):1407 – 1418, 2013.

[3] I. P. Batra, P. Wurfel, and B. D. Silverman. Depolarization-Field-Induced Instability in Thin Ferroelectric Films-Experiment and Theory. *Phys. Rev. Lett.*, 30:384–387, 1973.

[4] J.G. Bergman, J.H. McFee, and G.R. Crane. Pyroelectricity and optical second harmonic generation in polyvinylidene fluoride films. *Applied Physics Letters*, 18(5):203–205, Mar 1971.

[5] Kurt Binder. Surface effects on phase transitions in ferroelectrics and antiferroelectrics. *Ferroelectrics*, 35(1):99–104, 1981.

[6] AM Bratkovsky and AP Levanyuk. Smearing of phase transition due to a surface effect or a bulk inhomogeneity in ferroelectric nanostructures. *Physical review letters*, 94(10):107601, 2005.

[7] Jack C. Burfoot. *Ferroelectrics*. D. van Norstrand Company Ltd., 1967.

[8] Premi Chandra and Peter B Littlewood. A Landau primer for ferroelectrics. In *Physics of ferroelectrics*, pages 69–116. Springer, 2007.

[9] M. G. Cottam, D.R. Tilley, and B. Zeks. Theory of Surface Modes in Ferroelectrics. *J. Phys. Phys. C: Solid State Phys.*, 17:1793–1823, 1984.

[10] M Dawber, P Chandra, PB Littlewood, and JF Scott. Depolarization corrections to the coercive field in thin-film ferroelectrics. *Journal of Physics: Condensed Matter*, 15(24):L393, 2003.

[11] Matthew Dawber, Nicolas Stucki, Céline Lichtensteiger, Stefano Gariglio, and Jean-Marc Triscone. New phenomena at the interfaces of very thin ferroelectric oxides. *Journal of Physics: Condensed Matter*, 20(26):264015, 2008.

[12] AF Devonshire. Theory of ferroelectrics. *Advances in physics*, 3(10):85–130, 1954.

[13] J. W. Diggle, Thomas C. Downie, and C. W. Goulding. Anodic oxide films on aluminum. *Chemical Reviews*, 69(3):365–405, 1969.

[14] K El-Hami and K Matsushige. Lamellae orientation effect on local polarized domain in P(VDF/TrFE) copolymer: Application in data storage. *Journal of applied polymer science*, 96(4):1410–1413, 2005.

[15] J.F. Legrand et al. Ferroelectricity in VF_2 based copolymers. *Ferroelectrics*, 78(1):151–158, 1988.

[16] Tingting Feng, Dan Xie, Yongyuan Zang, Xiao Wu, Tianling Ren, and Wei Pan. Temperature Control of P(VDF-TrFE) Copolymer Thin Films. *Integrated Ferroelectrics*, 141(1):187–194, 2013.

[17] Takeo Furukawa. Phenomenological Aspect of a Ferroelectric Vinylidene Fluoride/Trifluoroethylene Copolymer. *Ferroelectrics*, 57:63, 1984.

[18] Takeo Furukawa. Ferroelectric properties of vinylidene fluoride copolymers. *Phase Transitions*, 18(3-4):143–211, 1989.

[19] Takeo Furukawa. Recent advances in ferroelectric polymers. *Ferroelectrics*, 104(1):229–240, 1990.

[20] Takeo Furukawa, Kenji Nakajima, Tomoyoshi Koizumi, and Munehiro Date. Measurements of nonlinear dielectricity in ferroelectric polymers. *Japanese Journal of Applied Physics*, 26(7R):1039, 1987.

[21] Takeo Furukawa, Takashi Nakajima, and Yoshiyuki Takahashi. Factors Governing Ferroelectric Switching Characteristics of Thin VDF/TrFE Copolymer

Films. *IEEE Transactions on Dielectrics and Electrical Insulation*, 13:1120, 2006.

[22] A. R. Geivandov, S. G. Yudin, V. M. Fridkin, and S. Ducharme. Manifestation of a Ferroelectric Phase Transition in Ultrathin Films of Polyvinylidene Fluoride. *Physics of the Solid State*, 47:1590, 2005.

[23] M. D. Glinchuk, E. A. Eliseev, V. A. Stephanovich, and R. Farhi. Ferroelectric thin film properties - Depolarization field and renormalization of a "bulk" free energy coefficients. *Journal of Applied Physics*, 93(2):1150–1159, 2003.

[24] MD Glinchuk, BY Zaulychny, and VA Stephanovich. Depolarization field and properties of thin ferroelectric films with inclusion of the electrode effect. *Physics of the Solid State*, 47(7):1331–1339, 2005.

[25] M.-G. Han, M. S. J. Marshall, L. Wu, M. A. Schofield, T. Aoki, R. Twesten, J. Hoffman, F. J. Walker, C. H. Ahn, and Y. Zhu. Interface-induced nonswitchable domains in ferroelectric thin films. *Nat Commun*, 5(4693), 2014.

[26] Xihong Hao. A review on the dielectric materials for high energy-storage application. *Journal of Advanced Dielectrics*, 3(01):1330001, 2013.

[27] B. Heiler and B. Ploss. Dielectric nonlinearities of P(VDF-TrFE). *Proceedings of the 8th International Symposium on Electrets(ISE 8), 1994.*, pages 662–667, 1994.

[28] M. S. Hunter and P. Fowle. Factors Affecting the Formation of Anodic Oxide Coatings. *Journal of The Electrochemical Society*, 101(10):514–519, 1954.

[29] Kenji Ishikawa and Takatoshi Uemori. Surface relaxation in ferroelectric perovskites. *Phys. Rev. B*, 60:11841–11845, 1999.

[30] Hiroshi Ishiwara, Masanori Okuyama, and Yoshihiro Arimoto. *Ferroelectric Random Access Memories: Fundamentals and Applications*, volume 93. Springer Science & Business Media, 2004.

[31] Qing Jiang, Chun Cheng Yang, and Jian Chen Li. Size-Dependent Melting Temperature of Polymers. *Macromolecular Theory and Simulations*, 12(1):57–60, 2003.

[32] Basilio Jiménez and Julio Antonio Gonzalo. *Ferroelectricity: The Fundamentals Collection*. Wiley-VCH, 2005.

[33] Soon-Won Jung, Sung-Min Yoon, Seung Youl Kang, and Byoung-Gon Yu. Properties of ferroelectric P(VDF-TrFE) 70/30 copolymer films as a gate dielectric. *Integrated Ferroelectrics*, 100(1):198–205, 2008.

[34] F. Keller, M. S. Hunter, and D. L. Robinson. Structural Features of Oxide Coatings on Aluminum. *Journal of The Electrochemical Society*, 100(9):411–419, 1953.

[35] Jae Hyun Kim, Jyongsik Jang, and Wang-Cheol Zin. Thickness dependence of the melting temperature of thin polymer films. *Macromolecular Rapid Communications*, 22(6):386–389, 2001.

[36] N.M. Kocharyan and Kh.B. Pachadzhyan. The piezoelectric effect in polymers. *Polymer Mechanics*, 4(1):117–119, 1968.

[37] R. Kretschmer and K. Binder. Surface effects on phase transitions in ferroelectrics and dipolar magnets. *Phys. Rev. B*, 20:1065–1076, 1979.

[38] R Kretschmer and K Binder. Surface effects on phase transitions in ferroelectrics and dipolar magnets. *Physical Review B*, 20(3):1065, 1979.

[39] JB Lando and WW Doll. The polymorphism of poly (vinylidene fluoride). I. The effect of head-to-head structure. *Journal of Macromolecular Science, Part B: Physics*, 2(2):205–218, 1968.

[40] Gwang-Geun Lee, Yoshihisa Fujisaki, Hiroshi Ishiwara, and Eisuke Tokumitsu. Low-Voltage Operation of Ferroelectric Gate Thin Film Transistors Using Indium Gallium Zinc Oxide-Channel and Ferroelectric Polymer Poly (vinylidene fluoride–trifluoroethylene). *Applied Physics Express*, 4(9):091103, 2011.

[41] A. P. Levanyuk and D. G. Sannikov. Phenomenologic Theory of Dielectric Anomalies in Ferroelectric Materials with Several Phase Transitions at Temperatures Close Together. *Soviet Physics JETP*, 33:600, 1971.

[42] AP Levanyuk and Daniil G Sannikov. Improper ferroelectrics. *Soviet Physics Uspekhi*, 17(2):199, 1974.

[43] Weiping Li, Yuejin Zhu, Dayin Hua, Peiqing Wang, Xiaorong Chen, and Jie Shen. Crystalline morphologies of P (VDF-TrFE)(70/30) copolymer films above melting point. *Applied Surface Science*, 254(22):7321–7325, 2008.

[44] K-G Lim, K-H Chew, L-H Ong, and M Iwata. Electrostatic coupling and interface intermixing in ferroelectric superlattices. *EPL (Europhysics Letters)*, 99(4):46004, 2012.

[45] Malcolm E Lines and Alastair M Glass. *Principles and applications of ferroelectrics and related materials*. Clarendon press Oxford, 2001.

[46] SG Lu, B Rozic, QM Zhang, and Z Kutnjak. *Electrocaloric effect (ECE) in ferroelectric polymer films*. INTECH Open Access Publisher, 2010. Published in *Ferroelectrics*, Dr. Indrani Coondoo (Ed.).

[47] Y. Mabuchi, T. Nakajima, T. Furukawa, and et al. Electric-Field-Induced Polarization Enhancement of Vinylidene/Trifluoroethylene Copolymer Ultrathin Films. *Applied Physics Express*, 4:071501, 2011.

[48] Yuichiro Mabuchi, Takashi Nakajima, Takeo Furukawa, and Soichiro Okamura. Electric-Field-Induced Polarization Enhancement of Vinylidene Fluoride/Trifluoroethylene Copolymer Ultrathin Films. *Applied Physics Express*, 4(7):071501, 2011.

[49] D. Mandal. *Ultra-thin Films of a Ferroelectric Copolymer: P(VDF-TrFE)*. PhD thesis, Brandenburgische Technische Universität, Cottbus, 2008.

[50] D. Mandal, K. Henkel, K. Müller, and D. Schmeißer. Bandgap determination of P(VDF-TrFE) copolymer film by electron energy loss spectroscopy. *Bulletin of Materials Science*, 33(4):457–461, 2010.

[51] R. C. G. Naber, B. de Boer, P. W. M. Blom, and D. M. de Leeuw. Low-voltage polymer field-effect transistors for nonvolatile memories. *Applied Physics Letters*, 87(20), 2005.

[52] Ronald C. G. Naber, Kamal Asadi, Paul W. M. Blom, Dago M. de Leeuw, and Bert de Boer. Organic Nonvolatile Memory Devices Based on Ferroelectricity. *Advanced Materials*, 22(9):933–945, 2010.

[53] Hari Singh Nalwa, editor. *Ferroelectric Polymers-Chemnistry, Physics, and Applications*. Marcel Dekker, Inc., New York, 1995.

[54] Hari Singh Nalwa, editor. *Handbook of Low and High Dielectric Constant Materials and Their Applications, Two-Volume Set*. Academic Press, 1999.

[55] Akira Odajima. A statistical theory of ferroelectric phase transition of vinylidene fluoride and trifluoroethylene copolymers. *Ferroelectrics*, 57(1):159–170, 1984.

[56] M. Okuyama and Y. Ishibashi, editors. *Ferroelectric Thin Films: Basic Properties and Device Pysics for Memory Applications*. Springer-Verlag, Berlin Heidelberg, 2005.

[57] Lye-Hock Ong, Junaidah Osman, and D. R. Tilley. Landau theory of second-order phase transitions in ferroelectric films. *Phys. Rev. B*, 63:144109, Mar 2001.

[58] Gianfranco Pacchioni and Sergio Valeri. *Oxide Ultrathin Films: Science and Technology*. John Wiley & Sons, 2012. chapter 12.

[59] Youn Jung Park, Seok Ju Kang, Bernard Lotz, Martin Brinkmann, Annette Thierry, Kap Jin Kim, and Cheolmin Park. Ordered Ferroelectric PVDF-TrFE Thin Films by High Throughput Epitaxy for Nonvolatile Polymer Memory. *Macromolecules*, 41:8648, 2008.

[60] Youn Jung Park, Seok Ju Kang, Cheolmin Park, Kap Jin Kim, Han Sup Lee, Moon Sook Lee, U-In Chung, and In Jun Park. Irreversible extinction of ferro-

electric polarization in P (VDF-TrFE) thin films upon melting and recrystallization. *Applied physics letters*, 88(24):242908, 2006.

[61] Boyu Peng, Xiaochen Ren, Zongrong Wang, Xinyu Wang, Robert C Roberts, and Paddy KL Chan. High performance organic transistor active-matrix driver developed on paper substrate. *Scientific reports*, 4, 2014.

[62] Beatrix Ploss. *Nichtlineare dielektrische Eigenschaften der ferroelektrischen Kopolymere P(VDF—TrFE).* PhD thesis, Universität (TH) Karlsruhe, 4 1996.

[63] Beatrix Ploss. Influence of poling and annealing on the nonlinear dielectric permittivity of PVDF-TRFE copolymers. *IEEE Transactions on Dielectrics and Dlectrical Insulation*, 5(1):91–95, 1998.

[64] Bernd Ploss. Dielectric nonlinearity of PVDF–TrFE copolymer. *Polymer*, 41(16):6087–6093, 2000.

[65] Bao-Dong Qu, Wei-Lie Zhong, and Pei-Lin Zhang. A new type of first-order phase transition in ferroelectric thin films. *Journal of Physics: Condensed Matter*, 6(6):1207, 1994.

[66] Karin M Rabe, Charles H Ahn, and Jean-Marc Triscone. *Physics of Ferroelectrics: A Modern Perspective*, volume 105. Springer Science & Business Media, 2007.

[67] C.B. Sawyer and C.H. Tower. Rochelle salt as a dielectric. *Phys. Rev.*, 35:269, 1930.

[68] R. Schroeder, L. A. Majewski, and M. Grell. All-Organic Permanent Memory Transistor Using an Amorphous, Spin-Cast Ferroelectric-like Gate Insulator. *Advanced Materials*, 16(7):633–636, 2004.

[69] T. Schwieger, X. Liu, D. Olligs, M. Knupfer, and Th. Schmidt. Orientation and electronic properties of pentacene molecules on SiO2 and GeS(0001) studied using x-ray absorption spectroscopy. *Journal of Applied Physics*, 96(10):5596–5600, 2004.

[70] J F Scott. Ferroelectrics go bananas. *Journal of Physics: Condensed Matter*, 20(2):021001, 2008.

[71] D. Smykalla, S. Karnati, and B. Ploss. Polarisation profiles in VDF-TrFE copolymer bilayers of molar ratio 70/30 and 56/44. In *Book of Abstract, 16th International Symposium on Electrets, Leuven, Belgium*, page 167, 2017.

[72] S. M. Sze and Kwok K. Ng. *Physics of Semiconductor Devices, 3rd ed.* Wiley, New York, 2006.

[73] Alexander K Tagantsev. Landau expansion for ferroelectrics: Which variable to use? *Ferroelectrics*, 375(1):19–27, 2008.

[74] E.-K. Tan, J. Osman, and D.R. Tilley. First-order phase transitions in ferroelectric films. *Solid State Communications*, 116(2):61 – 65, 2000.

[75] K. Tashiro, K. Takano, M. Kobayashi, Y. Chatani, and H. Tadokoro. Structural study on ferroelectric phase transition of vinylidene fluoride-trifluoroethylene copolymers (III) dependence of transitional behavior on VDF molar content. *Ferroelectrics*, 57(1):297–326, 1984.

[76] D. R. Tilley and B. Zeks. Landau Theory of Phase Transitions in Thick Films. *Solid State Communications*, 49:823, 1984.

[77] J. Valasek. Piezo-Electric and Allied Phenomena in Rochelle Salt. *Phys. Rev.*, 17:475–481, Apr 1921.

[78] Albert van Breemen, Benjamin Kam, Brian Cobb, Francisco Gonzales Rodriguez, Gert van Heck, Kris Myny, Alessio Marrani, Vincenzo Vinciguerra, and Gerwin Gelinck. Ferroelectric transistor memory arrays on flexible foils. *Organic Electronics*, 14(8):1966–1971, 2013.

[79] Pham Van Thanh, Bui Nguyen Quoc Trinh, Takaaki Miyasako, Phan Trong Tue, Eisuke Tokumitsu, and Tatsuya Shimoda. Electric Properties and Interface Charge Trap Density of Ferroelectric Gate Thin Film Transistor Using (Bi, La) 4Ti3O12/Pb (Zr, Ti) O3 Stacked Gate Insulator. *Japanese Journal of Applied Physics*, 51(9S1):09LA09, 2012.

[80] JL Wang, XJ Meng, and JH Chu. New Properties and Applications of Polyvinylidene-Based Ferroelectric Polymer. *InTech*, 2015.

[81] Zuo-Guang Ye. *Handbook of advanced dielectric, piezoelectric and ferroelectric materials: Synthesis, properties and applications*. Elsevier, 2008.

[82] Tarek Zaki. *Short-Channel Organic Thin-Film Transistors*. Springer International Publishing, 2015.

[83] Guodong Zhu, Zhigang Zeng, Li Zhang, and Xuejian Yan. Polarization fatigue in ferroelectric vinylidene fluoride and trifluoroethylene copolymer films. *Applied Physics Letters*, 89:102905, 2006.

[84] Ute Zschieschang, Frederik Ante, Tatsuya Yamamoto, Kazuo Takimiya, Hirokazu Kuwabara, Masaaki Ikeda, Tsuyoshi Sekitani, Takao Someya, Klaus Kern, and Hagen Klauk. Flexible Low-Voltage Organic Transistors and Circuits Based on a High-Mobility Organic Semiconductor with Good Air Stability. *Advanced materials*, 22(9):982–985, 2010.

Contributions

[85] C. Möse, D. von Nordheim, M. Pittner, B.Y. Peng, X.C. Ren, Z.R. Wang, Chan P.K.L., B. Ploss, and C.W. Leung. Ferroelectric Copolymer as Memory Layer for Organic Thin Film Transistor-based Memory Devices. In *Advanced Program of The 3rd International Symposium on Next-Generation Electronics, Taoyuan, Taiwan*, page 41, 2014.

[86] D. v. Nordheim, S. Hahne, and B. Ploss. Nonlinear Dielectric Properties and Polarization in Ferroelectric P(VDF-TrFE) Copolymer Thin Films. In *Proceedings of The 14th International Symposium of Electrets, Montpellier, France. ISBN: 9781457710230*, page 57, 2011.

[87] D. v. Nordheim, S. Hahne, and B. Ploss. Nonlinear Dielectric Properties and Polarization in Thin Ferroelectric P(VDF-TrFE) Copolymer Films. *IEEE Transactions on Dielectrics and Electrical Insulation*, 19:1175, 2012.

[88] D. v. Nordheim, S. Hahne, and B. Ploss. Nonlinear Dielectric Properties and Polarization in Ferroelectric P(VDF-TrFE) Copolymer Thin Films. In *Verhandlungen DPG (IV), DPG-Frühjahrstagung, Berlin*, 47, 2012.

[89] D. v. Nordheim, S. Hahne, and B. Ploss. Polarisation Readout and Determination of Landau Parameters of VDF-TrFE Thin Films from Dielectric Nonlinearities. In *Abstracts Book of The 8th Asian Meeting on Ferroelectrics, Pattaya, Thailand*, page 62, 2012.

[90] D. v. Nordheim, S. Hahne, and B. Ploss. Polarization Readout and Determination of Landau Parameters of VDF-TrFE Thin Films from Dielectric Nonlinearities. *Ferroelectrics*, 453:122, 2013.

[91] D. v. Nordheim, S. Hahne, and B. Ploss. Retention of Ferroelectric VDF-TrFE Copolymer Thin Films Characterized by Nondestructive Polarization Readout. In *Verhandlungen DPG (IV), DPG-Frühjahrstagung, Regensburg*, 48, 2013.

[92] D. v. Nordheim, S. Hahne, and B. Ploss. Retention of Ferroelectric VDF-TrFE Copolymer Thin Films Characterized by Nondestructive Polarization Readout. In *Verhandlungen DPG (IV), DPG-Frühjahrstagung, Dresden*, 49, 2014.

[93] D. v. Nordheim, S. Koch, S. Okamura, and B. Ploss. Retention of Thin Ferroelectric VDF-TrFE Copolymer Films Evaluated from Dielectric Non-Linearities. In *Proceedings of the 2013 Joint UFFC, EFTF and PFM Symposium, Prague, Czech Republic. ISBN 978-1-4673-5994-8*, page 63, 2013.

[94] D. v. Nordheim, C. Möse, B. Peng, X. Ren, P.K.L Chan, and C.W. Leung. Organic Field Effect Transistors With Ferroelectric VDF-TrFE Copolymer Gate Dielectric. In *Proceedings 2014 Joint IEEE ISAF, IWATMD and PFM, State College, Pennsylvania, USA*, page 407, 2014.

[95] D. von Nordheim, A. Austin, B. Ploss, and K.H. Chew. Ferroelectric Properties of Polymeric Bilayer Systems. *IEEE Transactions on Dielectrics and Electrical Insulation*, 23(1):129–133, 2016.

[96] D. von Nordheim and B. Ploss. Change in the ferroelectric to paraelectric phase transition order in P(VDF-TrFE) copolymer ultra-thin films. In *Book of Abstract, 16th International Symposium on Electrets, Leuven, Belgium*, page 103, 2017.

[97] D. von Nordheim and B. Ploss. Change in the ferroelectric to paraelectric phase transition in P(VDF-TrFE) copolymer ultra-thin films. In *Book of Abstract, 16th International Symposium on Electrets, Leuven, Belgium*, page 103, 2017.

[98] Z.R. Wang, D. von Nordheim, X.C. Ren, Chan P.K.L., C.W. Leung, and B. Ploss. Thin film transistors with organic active and high-k dielectric layers. In *Abstracts Book of The 8th Asian Meeting on Ferroelectrics, Pattaya, Thailand*, page 159, 2012.

[99] Hon Fai Wong, Sheung Mei Ng, Wang Fai Cheng, Yukuai Liu, Xinxin Chen, Danny von Nordheim, Chee Leung Mak, Jiyan Dai, Bernd Ploss, and Chi Wah Leung. Enhanced tunability of electrical and magnetic properties in (La, Sr) MnO3 thin films via field-assisted oxygen vacancy modulation. *Solid-State Electronics*, 2017.

Acknowledgements

This page is devoted to persons who supported me during the last years.

First of all I want to thank Prof. Ploss who always had a sympathetic ear for questions and problems. It is always inspiring to discuss with him about physics and all the rest. I also want to thank Prof. Gerhard for giving me the opportunity to receive the PhD from the University of Potsdam.

Furthermore, I have to thank my colleagues in the laboratory, Steffen Hahne and David Smykalla. Both gave valuable suggestions and discussed with me about various questions for hours. I am indebted for their help and assistance.

I will not miss the chance to thank the German Academic Exchange Service (DAAD) for the grants received over the years. Without the founding it would have been difficult if not impossible to spend time researching abroad. The time spend in other countries has not only fostered my professional competence, but also changed me as whole.

Once more I thank my family and my friends, who supported me during the last years. And finally I wish to thank Carolin for her patience, for her tireless support and for being a part of my life.

Statement of Authorship

I hereby solemnly affirm that this thesis was written by myself and describes my own work, unless otherwise acknowledged in the text. The thesis has not been submitted for the award of any other degree in any other tertiary institution.

Date	Danny von Nordheim